DEVELOPMENT OF PROVABLY STABLE A-Φ FORMULATION TIME DOMAIN INTEGRAL EQUATIONS

BY

THOMAS E. ROTH

THESIS

Submitted in partial fulfillment of the requirements
for the degree of Master of Science in Electrical and Computer Engineering
in the Graduate College of the
University of Illinois at Urbana-Champaign, 2017

Urbana, Illinois

Adviser:

Professor Weng Cho Chew

ABSTRACT

Applications involving quantum physics are becoming an increasingly important area for electromagnetic engineering. To address practical problems in these emerging areas, appropriate numerical techniques must be utilized. However, the unique needs of many of these applications require the development of new computational electromagnetic solvers. The **A**-Φ formulation is a novel approach that can address many of these needs. This formulation utilizes equations developed in terms of the magnetic vector potential (**A**) and electric scalar potential (Φ). The resulting equations overcome many of the limitations of traditional solvers and are ideal for coupling to quantum mechanical calculations. The main novelty of this thesis is the extension of the **A**-Φ formulation to two sets of time domain integral equations. These integral equations are provably stable and constitute robust numerical techniques that can be utilized in many applications. To validate the proposed time domain integral equations, numerical results are presented which demonstrate the stability and accuracy of the developed methods.

To my parents, for their love and support.

ACKNOWLEDGMENTS

I thank Professor Chew for his advice and helpful insight throughout my research toward this thesis. I also thank Michael Wei and Tian Xia for useful discussions related to solving frequency domain integral equations, the **A**-Φ formulation, and the A-EFIE. Discussions with Carlos Salazar-Lazaro were also very helpful as I began to study the functional framework for the time domain EFIE. I am also grateful to all my other colleagues: Joseph Rutherford, Mert Hidayetoğlu, Aiyin Liu, Lingling Meng, Shu Chen, Hui Gan, and Qi Dai. Finally, I especially thank all of my friends and family who have supported me throughout my studies.

TABLE OF CONTENTS

CHAPTER 1

INTRODUCTION

Traditionally, electromagnetic theory has been mainly described in terms of electric and magnetic fields, along with the related flux densities. Termed the **E-H** formulation, the corresponding equations have been leveraged successfully for many years to develop a plethora of electromagnetic-related technologies that utilize classical physics phenomena [1].

Currently, the ever-improving understanding of quantum physics is leading to a new age of technology development. For many applications, electromagnetic theory already has, and will continue to play a key role in the creation of novel technologies that leverage quantum physics [1]. This includes development in areas obviously related to electromagnetics, such as quantum optics and atom-photon interactions [1–3]. However, electromagnetic theory is also necessary in less obvious physical applications, for instance, those requiring Casimir force or near-field heat transfer calculations [4–8]. For each application area, suitable computational electromagnetic solvers are needed to bridge the gap between analytically solvable systems and those desired to be numerically analyzed for problems of practical interest.

The diverse set of applications imposes a number of different requirements on computational electromagnetic solvers to be widely applicable. One major requirement for the solvers is to be multi-scale; allowing for an accurate and efficient solution to be calculated over a wide range of length scales with respect to the wavelength of the electromagnetic field [1]. Different applications also require different physical quantities to be calculated. For instance, in the interaction of a charged particle and an electromagnetic field, $\mathbf{A}$ and Φ are needed in the solution of the Schrödinger equation [9]. Other examples include: the Maxwell stress tensor in Casimir force calculations; and dyadic Green's functions for atom-photon interactions or stimulated emission rate calculations [1, 5–7, 10, 11].

To address the growing needs of these and other applications, the **A**-Φ

formulation has been developed [1]. This formulates the computational electromagnetic solvers in terms of the vector and scalar potentials, leading to equations that are well-posed from very long to short wavelengths. This is a unique and novel property of the equations, which is not typically realized in the discretized **E**-**H** counterparts [12]. Additionally, the **A**-Φ formulation has the benefit of typically being more easily integrated into quantum physics calculations, where these quantities are deemed more fundamental than **E** and **H** [1, 8]. These properties make computational electromagnetic solvers developed from the **A**-Φ formulation ideal candidates for meeting the needs of emerging applications that rely on quantum physics.

Past work has extended the **A**-Φ formulation to the following methods: finite-difference time-domain [9], frequency domain finite element method [13], and frequency domain integral equations [14]. The focus of this thesis is to continue this development by extending the **A**-Φ formulation to time domain integral equations (TDIEs). These methods are attractive because they combine the many benefits of time domain methods with those of integral equations. For instance, time domain methods can perform broadband simulations and can be applied to a wider class of problems (e.g., nonlinear problems). Integral equations automatically satisfy the radiation condition and allow for flexible geometric modeling that only requires surface discretizations, greatly reducing the number of unknowns. Combining these benefits of TDIEs with the anticipated properties of the **A**-Φ formulation is expected to lead to a computational electromagnetic solver that can be used in many of the mentioned applications.

Although there is great promise in using TDIEs, certain drawbacks still exist. The most important issue with TDIEs is a long history of instability. Decades of work have gone into developing methods which lead to stable TDIE systems. The current state of the art has largely overcome any issue with instability for TDIEs using the **E**-**H** formulation. However, when implementing a new set of equations that have never been studied before, the same approaches that worked do not necessarily apply anymore. The quickest way to overcome this difficulty is to adopt a rigorous mathematical framework developed for the electric field integral equation [15]. By extending these results, a set of provably stable **A**-Φ TDIEs may be derived.

The rest of this thesis is organized as follows. Chapter 2 discusses the basic process of formulating and solving TDIEs. Included is a detailed dis-

cussion on how to accurately evaluate the matrix elements for the various TDIEs. In Chapter 3, the discussion of solving TDIEs is extended to the low frequency regime. In this regime, the typical **E**-**H** formulation TDIEs become progressively less accurate and less efficient to solve. In addition to reviewing the common methods for overcoming the break down of the **E**-**H** formulation, in depth discussions on the state of the art for time domain augmented electric field integral equations are discussed. Chapter 4 continues the discussion of solving TDIEs at low frequencies by proposing a number of novel integral equations. Included is an initial attempt at implementing a stable **A**-Φ TDIE. After the failure of this approach, Chapter 5 adopts a rigorous mathematical approach to develop provably stable **A**-Φ TDIEs. Numerical results are presented which verify the theoretical contributions of this chapter. Finally, in Chapter 6 conclusions and suggestions for future work are discussed.

CHAPTER 2

SOLUTION OF TIME DOMAIN INTEGRAL EQUATIONS

In this chapter, the formulations of various TDIEs for calculating the scattering from PEC structures are reviewed. In particular, the time domain electric field integral equation (EFIE), magnetic field integral equation (MFIE), combined field integral equation (CFIE), and their differentiated counterparts are discussed. Following this, the marching-on-in-time (MOT) discretization and solution procedure are discussed in the context of the differentiated EFIE. The calculation of the matrix elements in the MOT method using a separable approximation to the temporal convolution in these integral equations is discussed in detail. Numerical results are presented which highlight the capability of these traditional TDIEs for the analysis of broadband transient scattering from PEC structures.

2.1 Mathematical Formulation

Two methods for deriving TDIEs are presented in this section. The first approach, which performs the entire formulation directly in the time domain is used to derive the EFIE. The second approach is used to derive the MFIE, which utilizes inverse Fourier/Laplace transform techniques on the appropriate frequency domain equations to find the corresponding time domain equations. Finally, the combination of these two equations in the CFIE is presented.

2.1.1 Time Domain EFIE Derivation

Consider a time-varying electric field incident upon a scattering surface, S. As an initial condition, it is assumed that the electric field on the surface of the scatterer is 0 for all $t < 0$. For a perfect electric conductor (PEC), the

boundary condition on S is

$$\hat{n}\times\mathbf{E}^{\text{total}}(\mathbf{r},t)=0,\quad \forall t,\ \mathbf{r}\in S, \tag{2.1}$$

where $\hat{n}$ is the outward pointing unit normal vector to S. The total electric field may be decomposed into a sum of two components, the incident field ($\mathbf{E}^{\text{inc}}$) and scattered field ($\mathbf{E}^{\text{sc}}$). The incident field is defined as the field that would be present if there were no scattering object, while the scattered field is the component of the total field due to the presence of the scattering object. Substituting this expansion into (2.1) gives

$$-\hat{n}\times\mathbf{E}^{\text{sc}}(\mathbf{r},t)=\hat{n}\times\mathbf{E}^{\text{inc}}(\mathbf{r},t),\quad \forall t,\ \mathbf{r}\in S. \tag{2.2}$$

To arrive at an integral equation formulation, it is necessary to express $\mathbf{E}^{\text{sc}}$ in terms of the scattered magnetic vector potential, $\mathbf{A}^{\text{sc}}$, and the scattered electric scalar potential, Φ^{sc}. This gives

$$\hat{n}\times\left[\dot{\mathbf{A}}^{\text{sc}}(\mathbf{r},t)+\nabla\Phi^{\text{sc}}(\mathbf{r},t)\right]=\hat{n}\times\mathbf{E}^{\text{inc}}(\mathbf{r},t), \tag{2.3}$$

where the dot over $\mathbf{A}^{\text{sc}}$ is used to denote a temporal derivative. To arrive at the desired integral equations, it is first useful to consider the wave equations for $\mathbf{A}^{\text{sc}}$ and Φ^{sc}. These are

$$\nabla^2\mathbf{A}^{\text{sc}}(\mathbf{r},t)-c^{-2}\ddot{\mathbf{A}}(\mathbf{r},t)=-\mu\mathbf{J}(\mathbf{r},t) \tag{2.4}$$

$$\nabla^2\Phi^{\text{sc}}(\mathbf{r},t)-c^{-2}\ddot{\Phi}(\mathbf{r},t)=-\epsilon^{-1}\rho(\mathbf{r},t) \tag{2.5}$$

when the Lorenz gauge is used [1]. In these equations, c is the speed of light, μ is the permeability, ϵ is the permittivity, $\mathbf{J}$ is the current density, and ρ is the charge density. Both of these wave equations have well-known solutions in terms of the time domain Green's function as

$$\mathbf{A}^{\text{sc}}(\mathbf{r},t)=\int_V \mu\frac{\delta\big(t-R/c\big)}{4\pi R}*\mathbf{J}(\mathbf{r}',t)dV' \tag{2.6}$$

$$\Phi^{\text{sc}}(\mathbf{r},t)=\int_V \epsilon^{-1}\frac{\delta\big(t-R/c\big)}{4\pi R}*\rho(\mathbf{r}',t)dV', \tag{2.7}$$

where V is the volume that the sources $\mathbf{J}$ and ρ are contained in and $*$ denotes a temporal convolution. Further, $R=|\mathbf{r}-\mathbf{r}'|$, where $\mathbf{r}$ and $\mathbf{r}'$ are the

observation and source points, respectively. The notation dV' means that the integration is performed over the primed variables. In future equations, the retarded time will be simply denoted as $\tau = t - R/c$.

Using (2.6) and (2.7), the potentials in (2.3) may be related to sources on S, giving

$$\hat{n}\times\int_S\left[\mu\frac{\delta(\tau)}{4\pi R}*\dot{\mathbf{J}}(\mathbf{r}',t)+\nabla\frac{\delta(\tau)}{4\pi R\epsilon}*\rho(\mathbf{r}',t)\right]dS'=\hat{n}\times\mathbf{E}^{\text{inc}}(\mathbf{r},t). \tag{2.8}$$

This now represents an integral equation, since the unknown functions to be solved for, $\mathbf{J}$ and ρ, are found inside of an integral. Currently, (2.8) cannot be solved since it is a single equation with two unknowns. This can be addressed by using the current continuity equation to reduce the equation to having only a single unknown, $\mathbf{J}$. Performing this gives the EFIE, which is

$$\hat{n}\times\int_S\left[\mu\frac{\dot{\mathbf{J}}(\mathbf{r}',\tau)}{4\pi R}-\nabla\int_{-\infty}^{\tau}\frac{\nabla'\cdot\mathbf{J}(\mathbf{r}',t')}{4\pi R\epsilon}dt'\right]dS'=\hat{n}\times\mathbf{E}^{\text{inc}}(\mathbf{r},t). \tag{2.9}$$

The temporal integral in (2.9) is complicated to discretize; so it is common practice to instead enforce the *differentiated EFIE*, which is

$$\hat{n}\times\int_S\left[\mu\frac{\ddot{\mathbf{J}}(\mathbf{r}',\tau)}{4\pi R}-\nabla\frac{\nabla'\cdot\mathbf{J}(\mathbf{r}',\tau)}{4\pi R\epsilon}\right]dS'=\hat{n}\times\dot{\mathbf{E}}^{\text{inc}}(\mathbf{r},t). \tag{2.10}$$

In Sections 2.4.2 and 2.4.3, the discretizations of (2.10) and (2.9) are considered, respectively.

2.1.2 Time Domain MFIE Derivation

The MFIE in the frequency domain is

$$\frac{1}{2}\mathbf{J}(\mathbf{r},\omega)+\hat{n}\times\text{P.V.}\int_S\mathbf{J}(\mathbf{r}',\omega)\times\nabla\frac{e^{-jkR}}{4\pi R}dS'=\hat{n}\times\mathbf{H}^{\text{inc}}(\mathbf{r},\omega), \tag{2.11}$$

where ω is the angular frequency and k is the wavenumber [16]. The integral in (2.11) is understood to be taken in the principal value sense. This may be rewritten as

$$\frac{1}{2}\mathbf{J}(\mathbf{r},\omega)-\hat{n}\times\text{P.V.}\int_S\nabla\times\left(\mathbf{J}(\mathbf{r}',\omega)\frac{e^{-jkR}}{4\pi R}\right)dS'=\hat{n}\times\mathbf{H}^{\text{inc}}(\mathbf{r},\omega). \tag{2.12}$$

The inverse Fourier/Laplace transform of this equation is

$$\frac{1}{2}\mathbf{J}(\mathbf{r},t) - \hat{n}\times\text{P.V.}\int_S \nabla\times\left(\frac{\mathbf{J}(\mathbf{r}',\tau)}{4\pi R}\right)dS' = \hat{n}\times\mathbf{H}^{\text{inc}}(\mathbf{r},t). \tag{2.13}$$

The curl operator may be applied to give the time domain MFIE as

$$\frac{1}{2}\mathbf{J}(\mathbf{r},t) - \hat{n}\times\text{P.V.}\int_S \left[\frac{\dot{\mathbf{J}}(\mathbf{r}',\tau)}{4\pi R^2 c} + \frac{\mathbf{J}(\mathbf{r}',\tau)}{4\pi R^3}\right]\times\boldsymbol{R}\,dS' = \hat{n}\times\mathbf{H}^{\text{inc}}(\mathbf{r},t). \tag{2.14}$$

Since it is common to use the differentiated EFIE, the differentiated MFIE is also needed so that a differentiated CFIE can be formed. This is easily calculated to be

$$\frac{1}{2}\dot{\mathbf{J}}(\mathbf{r},t) - \hat{n}\times\text{P.V.}\int_S \left[\frac{\ddot{\mathbf{J}}(\mathbf{r}',\tau)}{4\pi R^2 c} + \frac{\dot{\mathbf{J}}(\mathbf{r}',\tau)}{4\pi R^3}\right]\times\boldsymbol{R}\,dS' = \hat{n}\times\dot{\mathbf{H}}^{\text{inc}}(\mathbf{r},t). \tag{2.15}$$

2.1.3 Time Domain CFIE Derivation

The EFIE and MFIE are known to suffer from the problem of *interior resonance* [16]. At resonant frequencies of the scattering object, the integral operators have a non-trivial null space. If the spectrum of the incident pulse in the simulation contains one or more of these resonant frequencies, the simulation can be inaccurate and/or unstable. The well-known solution to this problem is to use the CFIE, which is a linear combination of the EFIE and MFIE, i.e.,

$$(1-\alpha)\text{MFIE} - \alpha\hat{n}\times\text{EFIE} = (1-\alpha)\hat{n}\times\mathbf{H}^{\text{inc}}(\mathbf{r},t) - \alpha\hat{n}\times\hat{n}\times\mathbf{E}^{\text{inc}}(\mathbf{r},t), \tag{2.16}$$

where $0 < \alpha < 1$, the MFIE is the LHS of (2.14) and the EFIE is the LHS of (2.9). Typically, $\alpha = 1/2$ to give equal weighting between the MFIE and EFIE. The same approach can be used to form the differentiated CFIE from the differentiated MFIE and EFIE.

2.2 Marching-on-in-Time Discretization

In order to solve the integral equations derived in Section 2.1, the equations must be converted into suitable matrix systems. For simplicity, the discretization of (2.10) is considered first to introduce the basic procedure, known as the MOT method. The full formulas for all the integral equations will be given in Section 2.4 after the procedure for evaluating the matrix elements is discussed.

The first step of the MOT method is to discretize S into a union of triangular patches. Next, the unknown current density is expanded with known temporal and spatial basis functions that have unknown expansion coefficients, i.e.,

$$\mathbf{J}(\mathbf{r}', t) = \sum_{n=1}^{N_s} \sum_{j=1}^{N_t} J_n^{(j)} T^{(j)}(t) \mathbf{f}_n(\mathbf{r}'). \tag{2.17}$$

In (2.17), $\mathbf{f}_n$ is the spatial basis function associated with the nth interior edge, $T^{(j)}(t) = T(t - j\Delta t)$ is the temporal basis function, and $J_n^{(j)}$ is the expansion coefficient to be solved for. Additionally, N_s is the total number of interior edges on S, N_t is the number of time steps the simulation will cover, and Δt is the width of each time step. Typically, the spatial basis functions are selected to be the Rao-Wilton-Glisson (RWG) functions [17]. More options exist for the temporal discretization, but the most common choices are third-order Lagrange interpolating functions or quadratic B-spline functions [18, 19]. As will be discussed Section 2.3 and Chapter 5 in this thesis, the proper choice of temporal basis function is critical to the stability of a TDIE.

To solve for the expansion coefficients in (2.17), a matrix system needs to be developed. This is done by testing (2.10) temporally and spatially to arrive at a set of equations. To yield a square matrix system, (2.10) is tested at each interior edge of S with an RWG function. This process is performed at each time step, which is equivalent to temporal test functions of the form $\delta(t - i\Delta t)$. The physical meaning of this process is to require that the incident electric field and all scattered fields "collected" at the mth RWG function cancel at each time step. This ensures that the correct boundary condition is maintained throughout the simulation.

The matrix system describing this process at an arbitrary time step is

$$[\mathbf{Z}^{(0)}]\{J^{(i)}\} = \{V^{(i)}\} - \sum_{j=i-j_{\max}}^{i-1} [\mathbf{Z}^{(i-j)}]\{J^{(j)}\}. \tag{2.18}$$

An element of the matrix $[\mathbf{Z}^{(i-j)}]$ may be calculated as

$$[\mathbf{Z}^{(i-j)}]_{mn} = \int_S \int_S \left[\mu \frac{\mathbf{f}_m(\mathbf{r}) \cdot \mathbf{f}_n(\mathbf{r}')}{4\pi R} \ddot{T}^{(i-j)} + \frac{\nabla \cdot \mathbf{f}_m(\mathbf{r}) \nabla' \cdot \mathbf{f}_n(\mathbf{r}')}{4\pi R \epsilon} T^{(i-j)} \right] dS' dS, \tag{2.19}$$

where $T^{(i-j)} = T\big((i-j)\Delta t - R/c\big)$. An excitation vector element is given as

$$\{V^{(i)}\}_m = \int_S \mathbf{f}_m(\mathbf{r}) \cdot \mathbf{E}^{\text{inc}}(\mathbf{r}, i\Delta t) dS. \tag{2.20}$$

Finally, $\{J^{(i)}\} = \{J_1^{(i)}, J_2^{(i)}, \ldots J_{N_s}^{(i)}\}^T$. By solving (2.18) at each time step, the expansion coefficients of (2.17) may be calculated.

A few comments are in order to understand (2.18). First, the matrix $[\mathbf{Z}^{(0)}]$ is extremely sparse and represents the immediate interactions that occur between nearby basis functions. Similarly, the rest of the matrices are also sparse and represent the interactions between basis functions after the scattered fields have propagated for a certain number of time steps. Although all of the matrices are sparse, collectively they still constitute all of the $O(N_s^2)$ interactions expected by an integral equation method. Importantly, the summation of matrix vector products in (2.18) has a maximum number of terms, determined by how many time steps it takes for a signal to propagate the distance corresponding to the maximum separation of any two points on S. This allows the expansion coefficients at each time step to be calculated based on the incident field and a finite number of past values of the current density. Performing this process at each time step constitutes the MOT procedure.

The computational complexity of this procedure is $O(N_t N_s^2)$. Similar to frequency domain methods, this is a prohibitively high computational complexity for problems of practical interest. Fortunately, fast algorithms have been developed which can lower this computational complexity. In particular, the multilevel plane wave time domain method (PWTD) has a computational complexity of $O(N_t N_s \log^2 N_s)$. Other fast algorithms exist, however, this is not the focus of this thesis so they will not be discussed further.

2.3 Stability of Time Domain Integral Equations

Before delving too deeply into the full details of how to solve TDIEs, it is useful to discuss the issue of stability. Historically, stability has been one of the major factors limiting the widespread application of TDIEs. In this section, a simplified model of the MOT system using linear systems theory is presented. The goal is to motivate why instability can occur in TDIEs; while also giving some clues as to what issues should be addressed to lead to stable systems. It is important to stress that this analysis is not intended to cover all possible reasons for instability or to be interpreted as a rigorous presentation.

To begin, consider the linear system block diagram for the MOT system of (2.18) in Fig. 2.1. Due to the feedback loop, it is clear that this system can be considered to be like an "infinite impulse response" filter. From linear system theory, it is immediately understood that stability of such a system will depend on a number of factors. However, assuming the derivation of the equations has been performed correctly, it is anticipated for physical reasons that the equivalent continuous system must be stable. The extension of the physical stability to the discrete model shown in Fig. 2.1 will then entirely depend on the calculation of the matrix representation of the different integral operators.

The calculation of the matrix representation of the integral operators depend on two factors. The first factor is how accurately each matrix element is calculated. This is a necessary condition for stability, as has been noted in [15, 20], and is considered in detail in Section 2.4. The second, and more subtle factor, is the functions used in the discretization of the integral operator (i.e., the basis and testing functions). If incorrect basis and testing functions are used, the matrix representation of the integral operators can no longer be expected to inherit the stability assumed for physical reasons of the continuous equations. In practice, it is usually the temporal basis and testing functions that will impact the stability the most. This is because the spatial basis and testing functions are almost always selected correctly in the literature; making it difficult to gauge how they impact the stability. Determining the correct basis and testing functions for a given integral operator is a difficult task, and is considered in detail in Chapter 5.

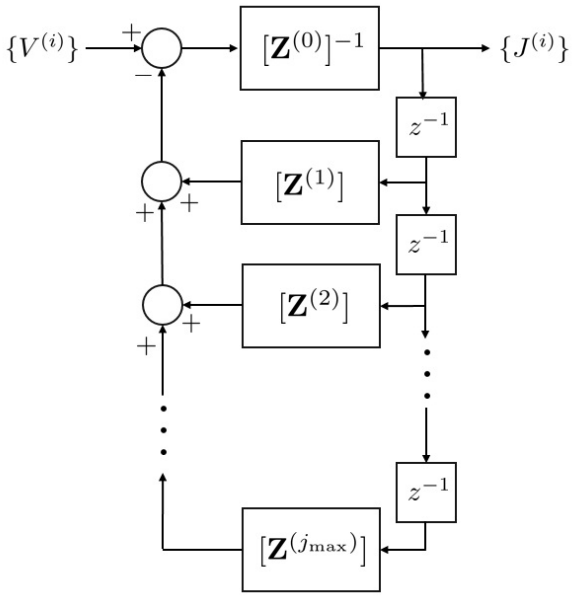

Figure 2.1: Block diagram for the MOT system.

2.4 Evaluation of Matrix Elements

One of the necessary (but *not* sufficient) conditions for a TDIE method to be stable is the accurate evaluation of the matrix elements [15, 20]. Standard numerical quadrature on integrals such as those contained in (2.19) is inaccurate. This is because the integrals often have discontinuities and shadowing effects that are a result of the finite velocity of the electromagnetic waves. This inaccuracy contributes to the instability of TDIEs; so alternative integration techniques are needed.

There are two main classes of techniques for calculating these integrals: analytical and numerical. The analytical techniques attempt to calculate as many of the integrals as is possible analytically. Due to the high complexity of this process, it is not currently possible to calculate all of the integrals in this way (and may not be possible). As a result, a number of them must still be approximated numerically. The most popular of the analytical techniques are those presented in [20, 21]. The numerical techniques attempt to accurately evaluate the matrix elements while being based purely on numerical techniques, i.e., no complex analytical expressions need to be computed. The most successful numerical technique is the one proposed in [22]. This technique approximates the temporal convolution with the time domain Green's

function using a separable expansion. This is a robust technique which may be used for any spatial basis function or surface discretization. It also benefits from an overall simplicity compared to the analytical methods, making this numerical method very attractive.

The method used for evaluating matrix elements in this thesis is the separable approximation to the temporal convolution developed in [22]. This method is a critical element of how TDIEs are solved in this thesis, so it is reviewed in detail. The basic concepts of the technique are presented in Section 2.4.1. Following this, the application of this technique to the differentiated EFIE and MFIE is discussed in Section 2.4.2. Finally, the modifications that are needed to discretize the EFIE are presented in Section 2.4.3.

2.4.1 Separable Expansion of the Time Domain Green's Function

The time domain Green's function can be found by taking the inverse Fourier transform of the appropriate frequency domain Green's function. In the case of a homogeneous medium, this gives the time domain Green's function to be

$$g(\mathbf{r}, \mathbf{r}', t) = \frac{\delta(t - R/c)}{4\pi R}, \tag{2.21}$$

which has been encountered previously in the solution to the wave equations presented in Section 2.1.1. In the context of an integral equation, this Green's function serves to tie the temporal and spatial variables together, leading to an overall complication in being able to accurately evaluate the necessary matrix elements of a MOT implementation.

This complication can be illustrated by considering the example of (2.19). In short, the time domain Green's function is extremely ill-posed when discretized in different ways. First, the instantaneous nature of the delta function gives rise to a technically infinite bandwidth pulse. This will be smoothed somewhat through the convolution process, but the end result is still not bandlimited. Further, when testing with delta functions in the time domain, as is done in the MOT method, various shadow regions can be formed over the spatial domains to be integrated. This leads to matrix elements which cannot be accurately evaluated using typical numerical

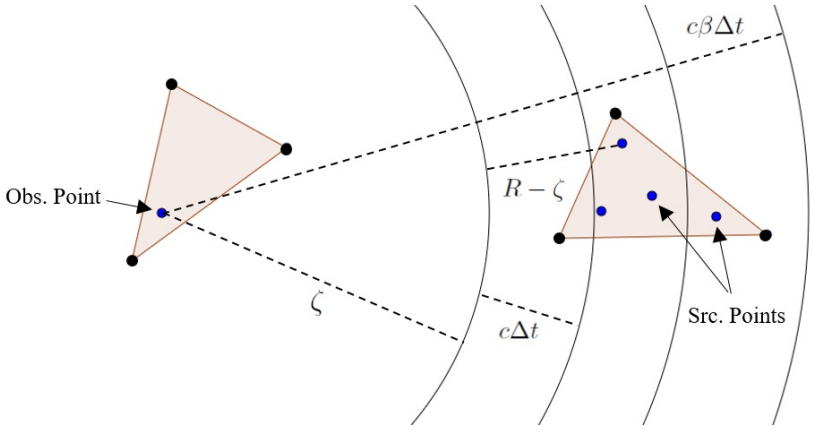

Figure 2.2: Geometry illustrating the origin of the various parameters in the separable expansion of the time domain Green's function (note: $\alpha = 0$).

quadrature methods. This lack of accuracy typically leads to numerical instability as the errors are fed back into the system at each time step and grow rapidly to overpower the desired signal (often called late-time instability, but can occur before "late"-time).

The key observation of the separable expansion method of [22] is that the completeness relation for any suitable set of orthogonal functions can be written in a general form as

$$\sum_{l=0}^{\infty} a_l F_l(x) F_l(x') = \delta(x - x'), \tag{2.22}$$

where F_l is the lth function of the orthogonal set, assumed here to be real-valued. The preferred orthogonal set for this application comprises Legendre polynomials, since they already have a convenient support for the expansion (i.e., they are nonzero for $-1 < x < 1$).

The important aspect is that the two variables that are intertwined in the delta function, x and x', are now separated into a product of two functions. In the context of TDIEs, one of the variables will depend on time while the other depends on space. When the delta function is expanded in this way, the factors that only depend on time can be factored out of the spatial integrals. This greatly simplifies the accurate numerical evaluation of the integrals, as will be seen briefly.

In the context of the time domain Green's function, this expansion gives

$$\begin{aligned} g(\mathbf{r},\mathbf{r}',t) &= \frac{1}{4\pi R}\delta(t-\zeta/c) * \delta(t-(R-\zeta)/c) \\ &= \frac{1}{4\pi R}\delta(t-\zeta/c) * \sum_{l=0}^{\infty} a_l P_l(k_1 t + k_2) P_l(k_1(R-\zeta)/c + k_2) \\ &\approx \frac{1}{4\pi R}\delta(t-\zeta/c) * \sum_{l=0}^{N_h} a_l P_l(k_1 t + k_2) P_l(k_1(R-\zeta)/c + k_2), \end{aligned} \tag{2.23}$$

where P_l is the lth-order Legendre polynomial. Physically, this can be considered to be filtering the time domain Green's functions. That is, the infinite bandwidth delta function has been smoothed so that it may be modeled better.

A number of comments are still required to explain the different pieces of (2.23), with the associated geometry shown in Fig. 2.2. First, the presence of the $\delta(t-\zeta/c)$ is used to limit the total support that the expansion is performed over. It does this since ζ is taken to be the largest multiple of $c\Delta t$ between an observation (testing) point and the source triangle that the expansion is desired to cover. Then, k_1 and k_2 are used to normalize the arguments of the Legendre polynomials so that

$$\begin{aligned} k_1\alpha + k_2 &= -1 \\ k_1\beta + k_2 &= 1. \end{aligned} \tag{2.24}$$

In (2.24), α and β denote the temporal support that is covered by the expansion so that the integrands will be smooth over the entire source triangle. In practice, α is typically set to zero. Then, β is the smallest integer such that a sphere with radius $\beta c\Delta t$ centered at the observation point will entirely enclose the source triangle. Further, $a_l = k_1(2l+1)/2$ and N_h is the total number of polynomials used in the expansion. Numerical experiments discussed in [22] suggest that it is suitable to choose $N_h = 3\beta$, which is done for all results presented in this thesis.

When this expansion of the delta function in the time domain Green's function is used, the space and time integrals are separated. This leads to spatial integrals that may be evaluated in a manner similar to frequency domain methods. For these integrals, the Legendre polynomial plays a similar role to the exponential in the frequency domain Green's function. This allows the

same types of singularity extraction and numerical quadrature techniques to be used. Additionally, the temporal integrals can be calculated analytically or through one-dimensional numerical quadrature (preferred method). Further details related to the implementation of this method in the context of a full MOT procedure will be discussed in Sections 2.4.2 and 2.4.3.

2.4.2 Discretization of the Differentiated EFIE and MFIE

To begin, it will be useful to adopt a simple operator notation so that the differentiated EFIE in (2.10) may be rewritten as

$$\hat{n}\times\dot{\mathcal{L}}\big\{\mathbf{J}\big\}(\mathbf{r},t) = \hat{n}\times\dot{\mathbf{E}}^{\text{inc}}(\mathbf{r},t), \tag{2.25}$$

where

$$\dot{\mathcal{L}}\big\{\mathbf{J}\big\}(\mathbf{r},t) = \int_S \left[\mu\frac{\ddot{\mathbf{J}}(\mathbf{r}',\tau)}{4\pi R} - \nabla\frac{\nabla'\cdot\mathbf{J}(\mathbf{r}',\tau)}{4\pi R\epsilon}\right]dS'. \tag{2.26}$$

To use the separable expansion for the convolution, it is desired to write this operator before the temporal convolution was evaluated, i.e.,

$$\dot{\mathcal{L}}\big\{\mathbf{J}\big\}(\mathbf{r},t) = \int_S \left[\mu\frac{\delta(\tau)*\ddot{\mathbf{J}}(\mathbf{r}',t)}{4\pi R} - \nabla\frac{\delta(\tau)*\nabla'\cdot\mathbf{J}(\mathbf{r}',t)}{4\pi R\epsilon}\right]dS'. \tag{2.27}$$

Using the expansion of the time domain Green's function presented in (2.23), the convolution in (2.27) may be expanded. Since the goal is to evaluate the matrix elements of the discretized operator, the expansion of the current density is also performed. Showing the results for only a single set of basis functions gives

$$\begin{aligned}
&\dot{\mathcal{L}}\big\{\mathbf{f}_n T^{(j)}(t)\big\}(\mathbf{r},t) \approx \\
&\int_S \sum_{l=0}^{N_h} \frac{a_l}{4\pi}\delta(t-\zeta/c) * P_l(k_1 t+k_2) * \left[\mu\ddot{T}^{(j)}(t)\frac{P_l\big(k_1(R-\zeta)/c+k_2\big)}{R}\mathbf{f}_n(\mathbf{r}')\right. \\
&\qquad\left. - \epsilon^{-1}T^{(j)}(t)\nabla\frac{P_l\big(k_1(R-\zeta)/c+k_2\big)}{R}\nabla'\cdot\mathbf{f}_n(\mathbf{r}')\right]dS'.
\end{aligned} \tag{2.28}$$

For simplicity, the $\approx$ sign will no longer be used since it is understood that the finite summation leads to only an approximate calculation of the resulting

matrix elements.

The next step in the MOT method is to test (2.28) spatially and temporally. The temporal test function is $\delta(t - i\Delta t)$ and the spatial test function is $\mathbf{f}_m(\mathbf{r})$. Using an inner product notation to denote a surface integral with respect to the unprimed variables, the testing process may be written as

$$\left\langle \mathbf{f}_m(\mathbf{r}), \dot{\mathcal{L}}\left\{\mathbf{f}_n T^{(j)}(t)\right\}(\mathbf{r}, i\Delta t)\right\rangle = \int_S \int_S \sum_{l=0}^{N_h} a_l \Bigg[\mu \ddot{\xi}_l^{(i-j)} \mathbf{f}_m(\mathbf{r}) \cdot \mathbf{f}_n(\mathbf{r}') + \epsilon^{-1} \xi_l^{(i-j)} \nabla \cdot \mathbf{f}_m(\mathbf{r}) \nabla' \cdot \mathbf{f}_n(\mathbf{r}')\Bigg] \frac{P_l(\hat{R})}{4\pi R} dS' dS, \quad (2.29)$$

where $\hat{R} = k_1(R - \zeta)/c + k_2$. The temporal convolutions are given by

$$\xi_l^{(i-j)} = \int_{-\infty}^{\infty} P_l(k_1 t' + k_2) T\big((i-j)\Delta t - \zeta/c - t'\big) dt' \quad (2.30)$$

$$\ddot{\xi}_l^{(i-j)} = \int_{-\infty}^{\infty} P_l(k_1 t' + k_2) \ddot{T}\big((i-j)\Delta t - \zeta/c - t'\big) dt'. \quad (2.31)$$

The expression in (2.29) is a single matrix element in (2.18).

There are a few important points to note related to (2.29). The most important point is that the spatial and temporal integrations have been separated, allowing each to be evaluated independently. The spatial integrals are now similar to those encountered in frequency domain integral equation methods. As a result, the same evaluation techniques and singularity extraction methods are applicable. For this thesis, singularities are extracted using the formulas in [23]. Another essential point is that all shadowing or discontinuous behavior has been absorbed into the one-dimensional temporal integrals. These types of integrals are simple to calculate using standard one-dimensional quadrature rules. Overall, this allows for the matrix elements in (2.18) to be calculated accurately, which is necessary for the discretized TDIEs to yield stable results. A final point is that for a given geometry all of the possible temporal integrals may be precomputed. This is substantially more efficient than recomputing all of the temporal integrals each time the values are needed.

Similar approaches to those just discussed may be used to discretize the differentiated MFIE. As with the differentiated EFIE, it will again be useful to introduce an operator notation. This allows the differentiated MFIE to

be written as

$$\hat{n}\times\dot{\mathcal{K}}\big\{\mathbf{J}\big\}(\mathbf{r},t) = \hat{n}\times\dot{\mathbf{H}}^{\text{inc}}(\mathbf{r},t), \tag{2.32}$$

where

$$\hat{n}\times\dot{\mathcal{K}}\big\{\mathbf{J}\big\}(\mathbf{r},t) = \frac{1}{2}\dot{\mathbf{J}}(\mathbf{r},t) - \hat{n}\times\int_S \left[\frac{\ddot{\mathbf{J}}(\mathbf{r}',\tau)}{4\pi R^2 c} + \frac{\dot{\mathbf{J}}(\mathbf{r}',\tau)}{4\pi R^3}\right]\times\boldsymbol{R}\,dS'. \tag{2.33}$$

Note that for brevity the explicit notation for the second integral to be evaluated in a principal value sense has been dropped. It is, of course, still meant to be evaluated in this sense.

This operator may alternatively be rewritten so that the temporal convolution has not yet been evaluated. This gives a more useful form for the separable expansion to the convolution to be applied. Following the same steps as shown for the differentiated EFIE leads to a discretized form of the $\hat{n}\times\dot{\mathcal{K}}$ operator as

$$\begin{aligned}\big\langle\mathbf{f}_m(\mathbf{r}), \hat{n}\times\dot{\mathcal{K}}\big\{\mathbf{f}_n T^{(j)}(t)\big\}(\mathbf{r},i\Delta t)\big\rangle &= \frac{1}{2}\int_S \dot{T}\big((i-j)\Delta t\big)\mathbf{f}_m(\mathbf{r})\cdot\mathbf{f}_n(\mathbf{r}')dS \\ -\int_S\int_S\sum_{l=0}^{N_h} a_l\left[\frac{\dot{\xi}_l^{(i-j)}}{4\pi R^3} + \frac{\ddot{\xi}_l^{(i-j)}}{4\pi R^2 c}\right]&P_l(\hat{R})\mathbf{f}_m(\mathbf{r})\cdot\hat{n}\times\mathbf{f}_n(\mathbf{r}')\times\boldsymbol{R}\,dS'dS,\end{aligned} \tag{2.34}$$

where

$$\dot{\xi}_l^{(i-j)} = \int_{-\infty}^{\infty} P_l(k_1 t' + k_2)\dot{T}\big((i-j)\Delta t - \zeta/c - t'\big)dt'. \tag{2.35}$$

With the appropriate matrix elements now derived, the full equations for the different MOT implementations of the various differentiated TDIEs may be given. The general form of the matrix system is

$$[\mathbf{Z}_A^{(0)}]\{J^{(i)}\} = \{V_A^{(i)}\} - \sum_{j=i-j_{\max}}^{i-1}[\mathbf{Z}_A^{(i-j)}]\{J^{(j)}\}, \tag{2.36}$$

where A can be either E, M, or C, which denote the differentiated EFIE,

MFIE, or CFIE, respectively. The matrix elements are then given by

$$[\mathbf{Z}_E^{(i-j)}]_{mn} = \big\langle \mathbf{f}_m(\mathbf{r}), \dot{\mathcal{L}}\big\{\mathbf{f}_n T^{(j)}(t)\big\}(\mathbf{r}, i\Delta t)\big\rangle \tag{2.37}$$

$$[\mathbf{Z}_M^{(i-j)}]_{mn} = \big\langle \mathbf{f}_m(\mathbf{r}), \hat{n}\times\dot{\mathcal{K}}\big\{\mathbf{f}_n T^{(j)}(t)\big\}(\mathbf{r}, i\Delta t)\big\rangle \tag{2.38}$$

$$[\mathbf{Z}_C^{(i-j)}]_{mn} = \alpha[\mathbf{Z}_E^{(i-j)}]_{mn} + (1-\alpha)[\mathbf{Z}_M^{(i-j)}]_{mn}, \tag{2.39}$$

while the excitation vectors are given by

$$\{V_E^{(i)}\}_m = \int_S \mathbf{f}_m(\mathbf{r}) \cdot \dot{\mathbf{E}}^{\text{inc}}(\mathbf{r}, i\Delta t) dS \tag{2.40}$$

$$\{V_M^{(i)}\}_m = \int_S \mathbf{f}_m(\mathbf{r}) \cdot \hat{n}\times\dot{\mathbf{H}}^{\text{inc}}(\mathbf{r}, i\Delta t) dS \tag{2.41}$$

$$\{V_C^{(i)}\}_m = \alpha\{V_E^{(i)}\}_m + (1-\alpha)\{V_M^{(i)}\}_m. \tag{2.42}$$

Note that $0 < \alpha < 1$, which is used to form the differentiated CFIE as a linear combination of the differentiated EFIE and MFIE.

2.4.3 Discretization of the EFIE

Much of the discretization of the EFIE follows directly from the examples shown in Section 2.4.2. The new concept that must be covered for discretizing the EFIE is how to handle the temporal integral present in (2.9).

As with the differentiated EFIE and MFIE, an operator notation can be adopted. This allows the EFIE to be written as

$$\hat{n}\times\mathcal{L}\big\{\mathbf{J}\big\}(\mathbf{r}, t) = \hat{n}\times\mathbf{E}^{\text{inc}}(\mathbf{r}, t), \tag{2.43}$$

where

$$\mathcal{L}\big\{\mathbf{J}\big\}(\mathbf{r}, t) = \mathcal{L}_{\text{V}}\big\{\mathbf{J}\big\}(\mathbf{r}, t) + \mathcal{L}_{\text{S}}\big\{\mathbf{J}\big\}(\mathbf{r}, t) \tag{2.44}$$

$$\mathcal{L}_{\text{V}}\big\{\mathbf{J}\big\}(\mathbf{r}, t) = \int_S \mu \frac{\dot{\mathbf{J}}(\mathbf{r}', \tau)}{4\pi R} dS' \tag{2.45}$$

$$\mathcal{L}_{\text{S}}\big\{\mathbf{J}\big\}(\mathbf{r}, t) = -\int_S \nabla \int_{-\infty}^{\tau} \frac{\nabla' \cdot \mathbf{J}(\mathbf{r}', t')}{4\pi R\epsilon} dt' dS'. \tag{2.46}$$

The $\mathcal{L}_{\text{V}}$ operator may be discretized easily using the methods shown in Section 2.4.2. However, the $\mathcal{L}_{\text{S}}$ operator is more challenging to discretize, so the process will be reviewed in detail.

A naive discretization of (2.46) will lead to a MOT implementation that has a higher computational complexity than the traditional $O(N_t N_s^2)$. This must be avoided for obvious practical reasons, so a recursive calculation procedure has been developed to calculate portions of the temporal integral in (2.46) [22].

A simplified example of this can be seen by considering a summation of integrals,

$$\sum_{j=1}^{N_t} \int_{-\infty}^{t} J_n^{(j)} T^{(j)}(t') dt'. \tag{2.47}$$

A similar summation is required for implementing a discretized version of the $\mathcal{L}_{\mathrm{S}}$ operator. For an arbitrary t, this summation can be separated into two sets. The first set is those integrals for which

$$\int_{-\infty}^{t} J_n^{(j)} T^{(j)}(t') dt' = \int_{-\infty}^{\infty} J_n^{(j)} T^{(j)}(t') dt', \tag{2.48}$$

while the second set is the integrals for which (2.48) does not apply. At later time steps, integrals in the first set contribute a constant amount to the full result. It is inefficient to recalculate the sum of these constant results for every time step. Instead, a recursive procedure should be used that only needs to be updated with the values of integrals that are transitioning from the second set to the first set.

In the context of the EFIE, this type of recursive procedure can be applied. Consider the tested $\mathcal{L}_{\mathrm{S}}$ operator with the temporal convolution written using the separable expansion, i.e.,

$$\begin{aligned} &\left\langle \mathbf{f}_m(\mathbf{r}), \mathcal{L}_{\mathrm{S}} \left\{ \mathbf{f}_n T^{(j)}(t) \right\} (\mathbf{r}, i\Delta t) \right\rangle \\ &\qquad = \int_S \int_S \sum_{l=0}^{N_h} a_l \hat{\xi}_l^{(i-j)} \frac{P_l(\hat{R})}{4\pi R \epsilon} \nabla \cdot \mathbf{f}_m(\mathbf{r}) \nabla' \cdot \mathbf{f}_n(\mathbf{r}') dS' dS. \end{aligned} \tag{2.49}$$

In (2.49), the temporal integrals are accounted for in

$$\hat{\xi}_l^{(i-j)} = \int_{-\infty}^{\infty} P_l(k_1 t' + k_2) \int_{-\infty}^{\kappa - t'} T(t'') dt'' dt', \tag{2.50}$$

where $\kappa = (i-j)\Delta t - \zeta/c$. Comparing the structure of (2.50) to other similar

terms, e.g. (2.30), suggests that the integral of the basis function in (2.50) may be treated similar to the derivatives of the basis function. That is, the integral of the basis function may be calculated analytically and then evaluated at the necessary points for the one-dimensional numerical quadrature used to expand the outer temporal integral. The difference with (2.50) is that the support of the integral of the basis function is unbounded. However, for sufficiently large values $\kappa - t'$, the result simply becomes constant. This suggests that a recursive procedure may be useful in simplifying the overall computation.

The procedure for calculating the temporal integral in (2.50) can now be discussed. This procedure will be broken into two parts: one that deals with the integral when the inner integral over the temporal basis function is changing and one when the inner integral gives a constant result. For the first part, the inner integral is still changing because $\kappa - t'$ is still within the support of T. In this region, $\hat{\xi}_l^{(i-j)}$ may be evaluated similar to $\xi_l^{(i-j)}$ and used accordingly in (2.49).

In the second part, the inner integral is constant because $\kappa - t'$ is greater than the support of T. In this situation, the integral becomes much simpler. This is because the Legendre polynomials are mutually orthogonal between different orders. As a result, once the inner integral is constant over the support of P_l, the only Legendre polynomial that needs to be considered is P_0.

To express these ideas mathematically, it will be useful to introduce more notation. First, it is noted that the support of T is $[-\Delta t, p\Delta t]$, where p is determined by the particular basis function used. Further, as has already been discussed, the support of P_l is $[0, \beta\Delta t]$. It is now useful to break $\hat{\xi}_l^{(i-j)}$ into two expressions,

$$\tilde{\xi}_l^{(i-j)} = \int_0^{\beta\Delta t} P_l(k_1 t' + k_2) \int_{-\infty}^{\kappa - t'} T(t'')dt''dt', \text{ for } \kappa - \beta\Delta t < p\Delta t \quad (2.51)$$

$$\bar{\xi}_l^{(i-j)} = \delta_{l0}\beta\Delta t, \text{ for } \kappa - \beta\Delta t \geq p\Delta t, \quad (2.52)$$

where δ_{l0} is a Kronecker delta function. Note that the second expression has not completely accounted for the temporal integral of the basis function. This will be accounted for separately so that the matrix elements may be defined appropriately. By separating $\hat{\xi}_l^{(i-j)}$ into two expressions, the $\mathcal{L}_S$ operator

must also be separated into two expressions. This is given as

$$\begin{aligned}\big\langle \mathbf{f}_m(\mathbf{r}), \mathcal{L}_{\mathrm{S}}\big\{\mathbf{f}_n T^{(j)}(t)\big\}(\mathbf{r}, i\Delta t)\big\rangle &= \big\langle \mathbf{f}_m(\mathbf{r}), \mathcal{L}_{\mathrm{S}'}\big\{\mathbf{f}_n T^{(j)}(t)\big\}(\mathbf{r}, i\Delta t)\big\rangle \\ &\quad + \big\langle \mathbf{f}_m(\mathbf{r}), \mathcal{L}_{\mathrm{T}}\big\{\mathbf{f}_n T^{(j)}(t)\big\}(\mathbf{r}, i\Delta t)\big\rangle \int_{-\infty}^{\infty} T(t'')dt'', \quad (2.53)\end{aligned}$$

where

$$\begin{aligned}&\big\langle \mathbf{f}_m(\mathbf{r}), \mathcal{L}_{\mathrm{S}'}\big\{\mathbf{f}_n T^{(j)}(t)\big\}(\mathbf{r}, i\Delta t)\big\rangle \\ &\qquad = \int_S \int_S \sum_{l=0}^{N_h} a_l \tilde{\xi}_l^{(i-j)} \frac{P_l(\hat{R})}{4\pi R\epsilon} \nabla \cdot \mathbf{f}_m(\mathbf{r}) \nabla' \cdot \mathbf{f}_n(\mathbf{r}') dS' dS \quad (2.54)\end{aligned}$$

$$\begin{aligned}&\big\langle \mathbf{f}_m(\mathbf{r}), \mathcal{L}_{\mathrm{T}}\big\{\mathbf{f}_n T^{(j)}(t)\big\}(\mathbf{r}, i\Delta t)\big\rangle \\ &\qquad = \int_S \int_S \sum_{l=0}^{N_h} a_l \bar{\xi}_l^{(i-j)} \frac{P_l(\hat{R})}{4\pi R\epsilon} \nabla \cdot \mathbf{f}_m(\mathbf{r}) \nabla' \cdot \mathbf{f}_n(\mathbf{r}') dS' dS. \quad (2.55)\end{aligned}$$

A modified MOT system for the EFIE may now be expressed that accounts for the recursive computation of the temporal integral. This is

$$[\mathbf{Z}_{E'}^{(0)}]\{J^{(i)}\} = \{V_{E'}^{(i)}\} - \sum_{j=i-j_{\max}}^{i-1} [\mathbf{Z}_{E'}^{(i-j)}]\{J^{(j)}\} - \sum_{j=i-j_{\max}-1}^{i-p-1} [\mathbf{Z}_{T}^{(i-j)}]\{C^{(j+1)}\}. \quad (2.56)$$

The matrix elements may be calculated to be

$$[\mathbf{Z}_{E'}^{(i-j)}]_{mn} = \big\langle \mathbf{f}_m(\mathbf{r}), \mathcal{L}_{\mathrm{V}}\big\{\mathbf{f}_n T^{(j)}(t)\big\}(\mathbf{r}, i\Delta t) + \mathcal{L}_{\mathrm{S}'}\big\{\mathbf{f}_n T^{(j)}(t)\big\}(\mathbf{r}, i\Delta t)\big\rangle \quad (2.57)$$

$$[\mathbf{Z}_{T}^{(i-j)}]_{mn} = \begin{cases} \big\langle \mathbf{f}_m(\mathbf{r}), \mathcal{L}_{\mathrm{T}}\big\{\mathbf{f}_n T^{(j)}(t)\big\}(\mathbf{r}, i\Delta t)\big\rangle, \ p \le \kappa/\Delta t - \beta \le (p+1) \\ 0, \ \text{otherwise}, \end{cases} \quad (2.58)$$

and the excitation vector elements are

$$\{V_{E'}^{(i)}\}_m = \int_S \mathbf{f}_m(\mathbf{r}) \cdot \mathbf{E}^{\mathrm{inc}}(\mathbf{r}, i\Delta t) dS. \quad (2.59)$$

A recursive calculation is used to compute $\{C^{(j+1)}\}$, which is given by

$$\{C^{(j+1)}\} = \{C^{(j)}\} + \{J^{(j)}\} \int_{-\infty}^{\infty} T(t'')dt'', \ \{C^{(1)}\} = \mathbf{0}. \tag{2.60}$$

Extensions of this approach to the MFIE and CFIE follow easily from the formulas already presented, and so are omitted here.

It is useful to discuss the reason for the definition of (2.58). This is to avoid calculating portions of the integrals too many times in the recursive process. The idea is as follows: due to the finite support of the temporal basis functions, the interaction between any pair of basis and testing functions will last for a finite amount of time. In the context of the matrix system, this means that the mn elements will only be filled for a subset of all of the matrices. If the last interaction between the mn elements for a set of triangles is given in the third matrix, for instance, than the fourth Z_T matrix is the only one that should be filled.

2.5 Numerical Results

Two simple numerical examples are presented in this section to demonstrate the validity of the formulations presented throughout this chapter. One example uses the differentiated CFIE and the other uses the EFIE.

For all simulations considered, the scatterer is a PEC sphere with a radius of 1 meter. The incident field is given by a plane wave with a temporal shape defined by a modulated Gaussian pulse,

$$\mathbf{F}^{\text{inc}}(\mathbf{r}, t) = \mathbf{F}_0 \text{exp}\left[-\left(\frac{t_r - t_p}{\sqrt{2}\sigma} \right)^2 \right] \cos(2\pi f_0 t_r). \tag{2.61}$$

In (2.61), $\mathbf{F}^{\text{inc}}$ should be picked appropriately for the integral equation being simulated (e.g., $\mathbf{E}^{\text{inc}}$ for the EFIE). The polarization direction and amplitude are set by $\mathbf{F}_0$, and $t_r = t - \mathbf{r} \cdot \hat{\mathbf{k}}/c$, where $\hat{\mathbf{k}}$ sets the propagation direction. The width of the pulse is set by $\sigma = 3/(2\pi f_{\text{bw}})$, where f_{bw} defines the bandwidth of the pulse. Finally, $t_p = 8\sigma$ and f_0 is the center frequency of the pulse. For all simulations, the polarization is in the $\hat{\mathbf{x}}$ direction and the propagation direction is in the $\hat{\mathbf{z}}$ direction.

For all simulations, the time step is typically selected to be some set

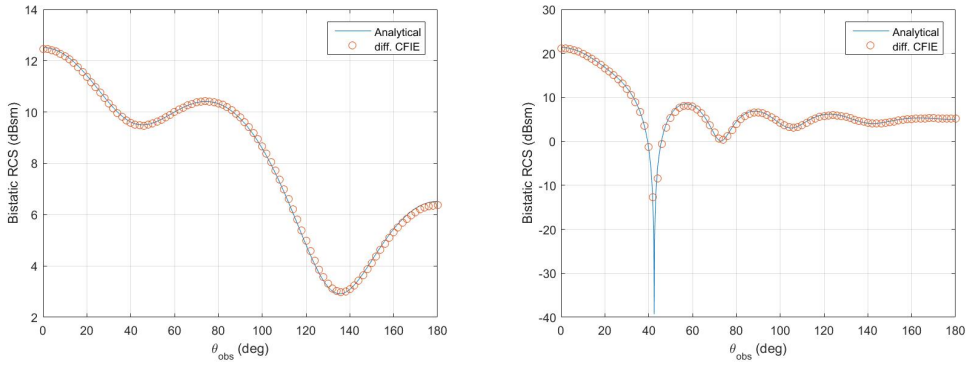

(a) (b)

Figure 2.3: E-plane bistatic RCS results for a 1 meter radius PEC sphere using the differentiated CFIE at (a) 100 MHz and (b) 300 MHz.

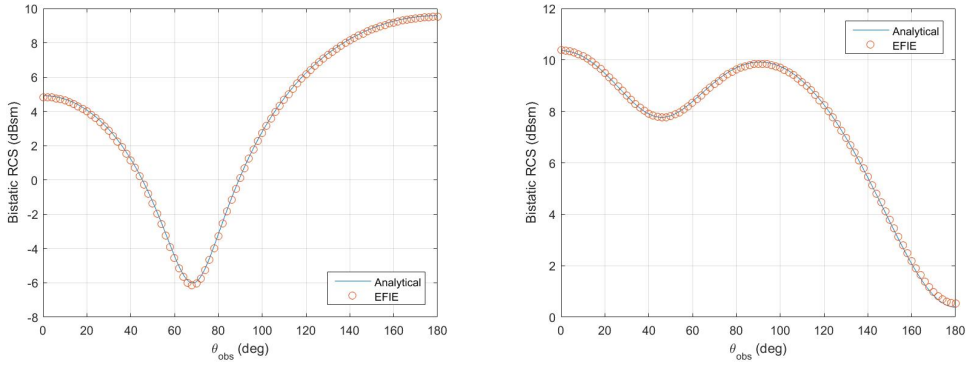

(a) (b)

Figure 2.4: E-plane bistatic RCS results for a 1 meter radius PEC sphere using the EFIE at (a) 40 MHz and (b) 80 MHz.

oversampling of the Nyquist frequency. This is typically given as $\Delta t = 1/\big(s(f_0 + f_{\text{bw}})\big)$, where s is usually set to 10 or 20.

The first simulation considered uses the differentiated CFIE. The temporal basis function used is the quadratic B-spline, which is the appropriate choice for this integral equation [15, 19]. The center frequency is 300 MHz, the bandwidth is 200 MHz, and the time step is 0.1 ns. The far-field scattering results are calculated by converting the solved for current densities to the frequency domain and then using standard methods. The bistatic RCS results for the sphere are calculated using the results from the differentiated CFIE and the Mie series (analytical solution). The plots of sample results at 100 and 300 MHz are included in Fig. 2.3.

The next simulation considered uses the EFIE. The temporal basis function is a triangle function, which is an appropriate choice for the EFIE [15]. The center frequency is 40 MHz, the bandwidth is 40 MHz, and the time step is 0.5 ns. The bistatic RCS results at 40 and 80 MHz are shown in Fig. 2.4. The EFIE has been calculated at a lower frequency than the previous example to avoid interior resonances of the sphere. It should also be noted that the EFIE is not accurate at all frequencies for this simulation. This is a consequence of the low frequency and dense mesh breakdowns of the EFIE, which will be discussed in detail in Chapter 3.

CHAPTER 3

SOLUTION OF TIME DOMAIN INTEGRAL EQUATIONS AT LOW FREQUENCIES

The issues related to solving TDIEs at low frequencies (equivalently, long wavelengths) are reviewed in this chapter. Additionally, the state of the art in resolving these issues in the frequency and time domains are discussed. Numerical examples are presented which demonstrate some of the extreme effects that can occur due to the time domain low frequency breakdown.

Following this, the time domain augmented electric field integral equation (A-EFIE) is reviewed in detail. This is one of the more modern approaches to overcoming the low frequency breakdown of the EFIE; and as will be demonstrated, there are still needed improvements. The interest in investigating this approach is that it is similar in some ways to the $\mathbf{A}$-Φ formulation. As such, it serves as a useful intermediary step to developing and implementing an $\mathbf{A}$-Φ TDIE.

Since methods in both the frequency domain and time domain will now be discussed, new abbreviations are needed to avoid confusion. In each case, the frequency domain EFIE will be abbreviated as FD-EFIE, while the time domain EFIE will be abbreviated as TD-EFIE. Similar abbreviations will be used for other integral equations as needed.

3.1 Electric Field Integral Equation at Low Frequencies

The state of the art in solving low frequency problems in the frequency domain and time domain is reviewed. Following this, a more detailed analysis on the origin of the low frequency and dense mesh breakdowns of the TD-EFIE is presented. The basics of performing an eigenvalue stability analysis for a MOT system are introduced before numerical experiments are performed to clearly show the effects of low frequency breakdown.

3.1.1 Frequency Domain Approaches

The low frequency and dense mesh breakdowns of the FD-EFIE have been extensively studied in the frequency domain [24–28]. The occurrence of the low frequency breakdown is attributed mainly to the disparity in size of the contributions due to the vector and scalar potential terms of the FD-EFIE operator [28]. This occurs at low frequencies due to the frequency dependent scaling of these contributions. A somewhat related phenomenon is the dense mesh breakdown. This occurs when a number of mesh elements are electrically small [12, 29, 30]. The end results of the low frequency and dense mesh breakdowns are a progressively ill-conditioned matrix system and loss of solution accuracy.

A number of techniques have been proposed to overcome these limitations of the FD-EFIE. One of the most popular approaches is to perform a quasi-Helmholtz decomposition. This separates the unknown current density into approximately solenoidal and non-solenoidal contributions, wich separately capture the quasi-magnetostatic and quasi-electrostatic physics. This is performed by calculating loop-star or loop-tree basis functions for a given geometry and then expanding and testing the unknown current appropriately with these bases [24–27]. This approach is more difficult to implement than a traditional FD-EFIE method because of the need to search for these bases. This can be difficult to perform on complicated geometries, and increases the complexity of the code. Further, this method does not capture the wave physics effects of higher frequencies well. This leads back to the original problem of poor convergence for the iterative solver, or failure to converge at all [28].

This issue of ill-conditioning for loop-tree decompositions has been addressed using hierarchical regularization techniques [29]. In this method, a coarse mesh is produced on the structure to be analyzed. The coarse mesh is then subdivided into a number of regions (typically using an oct-tree type subdivision). The different regions are then further subdivided, with finer and finer meshes created in each region until the structure finally reaches a mesh appropriate to yield the desired accuracy. The hierarchical regularization is then performed as a set of operations on these nested meshes and basis functions. The overall effect of these operations is to precondition the final matrix system to allow for the efficient convergence of iterative solvers for

very complicated geometries [29]. Although this approach has shown good results, the added complexity of generating the code for this method makes it not as appealing as a simpler solution to the low frequency or dense mesh breakdown of the EFIE for many cases.

Another approach to dealing with the dense mesh conditioning problems is to leverage Calderón identities [30]. These take advantage of the self-regularizing property of the different integral equation operators. These methods are not simple to discretize, and require a careful selection of basis functions to arrive at non-singular Gram matrices. A more detailed discussion of these methods in the context of TDIEs is presented in the next section.

A simpler solution that has been found to be widely effective for a number of complicated geometries is the FD-A-EFIE [28]. This approach uses the charge density as a second set of unknowns to supplement those of the current density. To arrive at a square matrix system, the continuity equation is added as an additional constraining set of equations. This approach is effective even when utilizing simple RWG and pulse basis functions for the current and charge, respectively. This makes it a very attractive technique that can be easily incorporated with fast algorithms such as the MLFMA. Additionally, due to the saddle point form of this matrix system, a wide amount of mathematical literature is available to guide the construction of simple constraint preconditioners [31]. These can improve the convergence of the iterative solver as the frequency goes to DC; allowing the method to be applied over a very wide frequency range.

Another approach that adopts a similar methodology to the FD-A-EFIE has also been formulated [32]. This method adds a number of other constraining equations and modifications to allow for an accurate solution at even lower frequencies than the FD-A-EFIE. However, this removes the simplicity of the original method that has been so appealing. In particular, the method of [32] uses the following constraints: it enforces the continuity equation with the Green's function as an integral kernel, constrains the normal component of the magnetic field, utilizes a more complicated BC testing function, requires solving for the charge density at DC, as well as implements an iterative diagonal matrix scaling procedure to further improve the conditioning. This leads to a more complicated discretization procedure and produces an over-determined matrix system. Instead of solving in a least-squares sense

(or some other appropriate method), the authors make the system square by adding equations that represent separate physical constraints together directly in the matrix generation process. Although successful in their general goals, the extra complications of the method to reach increasingly lower frequencies seems to make the applicability of this method only sensible for a small class of problems.

Recently, a number of integral equations that are based on the vector and scalar potentials have been proposed as another simple method to solve low frequency breakdown problems in the frequency domain [1, 14]. These share a very similar matrix structure to the FD-A-EFIE, but under appropriate preconditioning can achieve faster convergence than the FD-A-EFIE [14]. They have been shown to be both stable at fairly low frequencies and for dense meshes; and can be easily integrated with fast solvers like the MLFMA. This suggests that they could prove to be an effective tool after conducting further research into them for realistic engineering problems.

3.1.2 Time Domain Approaches

Similar to the frequency domain, the traditional TD-EFIE will break down due to low frequency and dense mesh phenomena [33]. This can be again seen as a problem partially related to the scaling of the matrix elements with respect to the time step size. Since the time step is selected as an oversampling of the Nyquist rate, as the frequency of the problem lowers the time step naturally becomes larger. Elements that involve temporal derivatives have an $O(1/\Delta t)$ or higher dependence on the time step, and quickly become smaller than other terms in the operator. Although the cause of the problem is similar to that in the frequency domain, the results of this problem in the time domain are more severe. In addition to resulting in a worsening condition number of the matrix system to be solved at each time step, the solution also becomes unstable with exponentially growing modes being excited. These modes can quickly overpower the important aspects of the solution and yield a set of current values that are unusable for calculating physical parameters of interest, such as the RCS.

To overcome these problems, many of the methods suggested in the frequency domain have been adapted to provide low frequency stable and well-

conditioned matrix systems in the time domain. One of the earliest approaches was to use a loop-tree decomposition which could effectively stabilize the matrix system for low frequency problems [33]. This type of decomposition placed a cap on the condition number of the matrix system. However, in practice, it was found to still be too high for complex meshes to yield efficient solutions [34]. A logical step was to adapt the hierarchical regularization process to the time domain, which was performed in [34]. However, this suffers from the same issues of complexity in implementation as its frequency domain counterpart, making it not attractive for practical use. Another more recent method has been proposed that performs the quasi-Helmholtz decomposition using a combination of projection matrices and various auxiliary unknowns to achieve stable scaling as the time step is changed [35]. This has the benefit of not requiring a global search for loop currents, but increases the coding complexity in other areas. Although the results appear promising, the results in the literature have not shown the accuracy of the method at very low frequencies. Further, a more straightforward method is always preferable.

Another interesting approach is to leverage time domain Calderón identities [36, 37]. These identities are rooted in the spectral properties of the different time domain integral operators that are traditionally used. It is shown in [36] how applying the $\mathcal{L}$ operator twice has a self-regularizing property (denoted as $\mathcal{L}^2$). This is seen by noting the projection properties of the radiation integrals that are typically used in the equivalence principle formulation of integral equations. This allows the spectral properties of the $\mathcal{L}^2$ operator to be associated with those of the $\mathcal{K}$ operator, which is known to produce better conditioned systems. Achieving these theoretical properties are not trivial, however, and require a finely tuned discretization procedure to yield the desired properties. The details are involved, and can be found in [36, 37].

In addition to the discussion of Calderón identities, [36] gives an excellent background discussion on the state of the art in TDIEs at the time of publication. Further, [37] makes the important point that the stability problems that are found with TDIEs at this point in time are usually no longer related to inaccurate evaluation of matrix elements. Instead, they argue that the issue lies in the spectral properties and null spaces (or approximate null spaces) of the operators. This suggests that the success of a particular method heav-

ily depends on the spectral properties of the operator. However, recent work shows that the proper choice of basis functions also plays an essential role in determining stability [15]. This will be discussed in great detail in Chapter 5.

In addition to the variety of techniques already discussed, a TD-A-EFIE has also been developed [38]. This work also implemented a temporal low pass filtering method to stabilize the solution. This is one of the earliest stabilization techniques developed in the history of TDIEs, and is typically no longer used. This technique is included in their work because, as will be demonstrated later, the TD-A-EFIE is more prone to instability than the TD-EFIE. The TD-A-EFIE was further developed in [39–41], with the main contribution being the extension of the preconditioner proposed in [28] to the time domain. A further development was performing a temporal integral of the continuity equation. This requires additional overhead and matrix storage, so other methods are still of practical interest.

3.2 Time Domain Electric Field Integral Equation Low Frequency and Dense Mesh Breakdowns

The focus of this section is to demonstrate with numerical examples the breakdown phenomenon of the TD-EFIE at low frequencies. An eigenvalue stability analysis will also be introduced to more rigorously demonstrate what kinds of instabilities are present in the MOT matrix system. Performing this stability analysis also allows for the presentation of the associated eigenvectors of the unstable modes of the marching system. This will be performed on the TD-EFIE to verify this analysis approach before it is applied to more novel integral operators in Chapter 4.

3.2.1 Origin of the Low Frequency and Dense Mesh Breakdowns

Before presenting the numerical results, the TD-EFIE operator is analyzed to highlight the origin of the low frequency breakdown. This analysis closely follows the approach and conclusions presented in [36]. To begin, consider

again the $\dot{\mathcal{L}}$ operator, reproduced here as

$$\dot{\mathcal{L}}\{\mathbf{J}\}(\mathbf{r},t) = \int_S \left[\mu \frac{\ddot{\mathbf{J}}(\mathbf{r}',\tau)}{4\pi R} - \nabla \frac{\nabla' \cdot \mathbf{J}(\mathbf{r}',\tau)}{4\pi R\epsilon}\right] dS'. \tag{3.1}$$

The onset of the low frequency breakdown can be understood by considering how the two terms of the operator scale as the time step for the discretized system changes. The two temporal derivatives on the first term (vector potential contribution) makes it scale as $O(1/\Delta t^2)$ while the second term (scalar potential contribution) scales as $O(1)$. As $\Delta t \to \infty$, implying low frequency dominance; the vector potential contribution will be swamped by the scalar potential contribution, leading to ill-conditioning.

Eventually, a full breakdown of the system occurs in the form of unstable current growth. This occurs due to a projection of the solution onto the null space of the operator, namely static and linear in time solenoidal currents (e.g., loop currents). At lower frequencies, these modes are not correctly modeled or constrained, leading to them becoming unstable. In the language of the eigenvalue stability analysis, to be introduced in Section 3.2.2, it is expected to see unstable eigenvalues associated with eigenvectors that are approximately solenoidal.

At this point, it is also useful to discuss the origin of the dense mesh breakdown for the TD-EFIE. This is related to the spectral properties of the continuous operator, as detailed in [36]. The issue is that the $\mathcal{L}$ operator has a discontinuous spectrum, but is compact on the space of solenoidal currents. This means that there will be two branches of singular values in the spectrum, one associated with solenoidal currents and one with the complement of this subspace. The singular values of the solenoidal currents approach zero; with spatially faster varying solenoidal currents associated with smaller singular values. Similarly, the singular values of the complement of the solenoidal current subspace are tending toward infinity; with larger singular values attributed to faster varying currents. This means that as the mesh is refined, the faster varying currents of the two subspaces may be modeled by the mesh. This leads to a progressive increase in the condition number as the mesh becomes smaller with respect to the wavelength. As pointed out in [36], this is a property of the operator and cannot be overcome simply by performing a loop-tree decomposition. Rather, the operator itself must be changed to overcome these limitations, e.g. through Calderón identities.

3.2.2 Eigenvalue Stability Analysis

For many years, the stability of TDIEs was proved in a non-rigorous manner. This was done by simply showing that the solved-for current densities did not have exponentially growing solutions for many time steps after the incident field had decayed. Although fine for many practical purposes, this lack of rigor made it difficult to gain better theoretical understanding of the types of instabilities and how to overcome them. To address this, an eigenvalue analysis of the marching system was devised in [42]. This analysis allows a rigorous test of whether any instability is theoretically possible in the system.

To perform this analysis, an appropriate matrix system must be devised that relates the past current densities to the future ones. For instance, the MOT system for (3.1) is given in (2.36). The updated current vector can be solved for by multiplying by $[\mathbf{Z}^{(0)}]^{-1}$. The summation of matrix-vector products with the past current vectors can be arranged into a single matrix describing this entire process. This can be easily assembled, and is

$$\begin{Bmatrix} U^{(i+1)} \\ U^{(i)} \\ U^{(i-1)} \\ \vdots \\ U^{(i-j_{\max}+3)} \\ U^{(i-j_{\max}+2)} \end{Bmatrix} = \begin{bmatrix} \mathbf{C}^{(1)} & \mathbf{C}^{(2)} & \dots & \mathbf{C}^{(j_{\max}-1)} & \mathbf{C}^{(j_{\max})} \\ \mathbf{I} & \mathbf{0} & \dots & \mathbf{0} & \mathbf{0} \\ \mathbf{0} & \mathbf{I} & \dots & \mathbf{0} & \mathbf{0} \\ \vdots & \vdots & \ddots & \vdots & \vdots \\ \mathbf{0} & \mathbf{0} & \dots & \mathbf{I} & \mathbf{0} \end{bmatrix} \begin{Bmatrix} U^{(i)} \\ U^{(i-1)} \\ U^{(i-2)} \\ \vdots \\ U^{(i-j_{\max}+2)} \\ U^{(i-j_{\max}+1)} \end{Bmatrix}, \tag{3.2}$$

where $U^{(i)}$ is a vector of coefficients for the basis functions appropriate to the matrix system being analyzed at the ith time step. Additionally, $\mathbf{C}^{(j)} = -[\mathbf{Z}^{(0)}]^{-1}[\mathbf{Z}^{(j)}]$, where $[\mathbf{Z}^{(j)}]$ should be the matrix from the integral equation being analyzed. The matrix in (3.2) is typically termed the *companion matrix*. By solving for the eigenvalues of the companion matrix, it can be determined whether the MOT system is stable. If any eigenvalues lie outside the unit circle on the complex plane, the method will be unstable with exponentially growing solutions. Further, if any eigenvalue lies on the unit circle, the method is considered to be marginally stable [37]. These solutions have polynomial growth, and so are still not technically stable. However, solutions can still be practical if the growth is slow enough. Naturally, this

is still undesirable, and so a totally stable system is obviously preferable.

It is also useful to note that because the eigenvalues are being solved for, the eigenvectors of the system can also be found. This is useful for diagnosing the kinds of spatial variations that lead to the instability in the marching system. This will be used in Chapter 4 to assist in determining the flaws of various integral operators.

3.2.3 Numerical Results

To demonstrate the low frequency breakdown of the differentiated TD-EFIE, a number of simulations are presented with the central frequency of the incident pulse progressively lowered. All simulations are performed on the same mesh of a 1 meter radius sphere. For each simulation, the average edge length as compared to the maximum frequency in the incident pulse is presented, along with the time step used. Additionally, the eigenvalues of the companion matrix are presented to highlight the growth of the instability in a more rigorous manner than just presenting the unstable current densities.

For each simulation, the changes to the center frequency and bandwidth change the companion matrix. For instance, each simulation will have different individual $[\mathbf{Z}^{(j)}]$ matrices. As a result, the first row of matrices in the companion matrix will be completely different for each simulation.

The first example is for a center frequency of 1 kHz and a bandwidth of 500 Hz. This is already in the low frequency breakdown regime, so it is expected to see eigenvalues outside of the unit circle. The relevant simulation parameters are presented in the caption of Fig. 3.1. The next set of results, shown in Fig. 3.2, are for a center frequency of 100 Hz and a bandwidth of 50 Hz. The eigenvalue spectrum shows that the low frequency instability is growing, with the eigenvalues now further outside of the unit circle near the $(1, 0i)$ point. The final example is for a center frequency of 10 Hz and a bandwidth of 5 Hz, with the results shown in Fig. 3.3. The eigenvalues are now clearly showing the instability of the method. Further, in the presented current density it is clear that no usable information can be extracted for post-processing.

It is important to note that these examples have been shown for some extreme cases on a very simple geometry. The onset of these effects can be

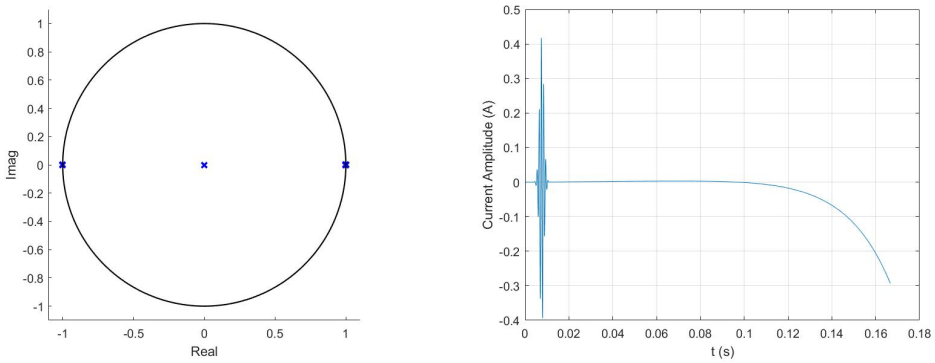

(a) (b)

Figure 3.1: Center frequency is 1 kHz and bandwidth is 500 Hz. Average edge length is $1.359 \times 10^{-6}\lambda$, $\Delta t = 33.3$ μs: (a) eigenvalues and (b) current.

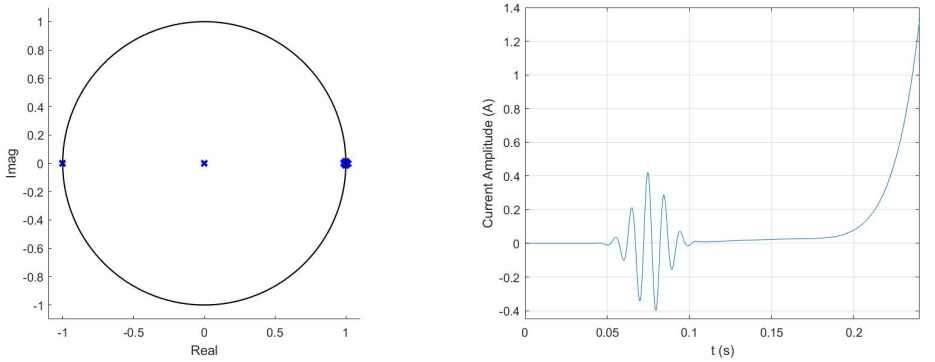

(a) (b)

Figure 3.2: Center frequency is 100 Hz and bandwidth is 50 Hz. Average edge length is $1.359 \times 10^{-7}\lambda$, $\Delta t = 0.333$ ms: (a) eigenvalues and (b) current.

much earlier on more complicated or multiscale structures [33]. Additionally, as previously discussed, the effects can also be more subtle. The increasingly ill-conditioned nature of the matrix system begins at higher frequencies than those presented here, and makes it impractical to solve for problems of engineering interest.

In addition to looking at the eigenvalues, it is of interest to determine the spatial structure of the eigenvectors associated with unstable modes. For the differentiated TD-EFIE, it is anticipated that the unstable eigenvectors will correspond to approximately solenoidal current densities. This is verified for a couple unstable modes, with one presented in Fig. 3.4. In addition to the unstable mode, a stable mode is also shown in Fig. 3.4. This mode can

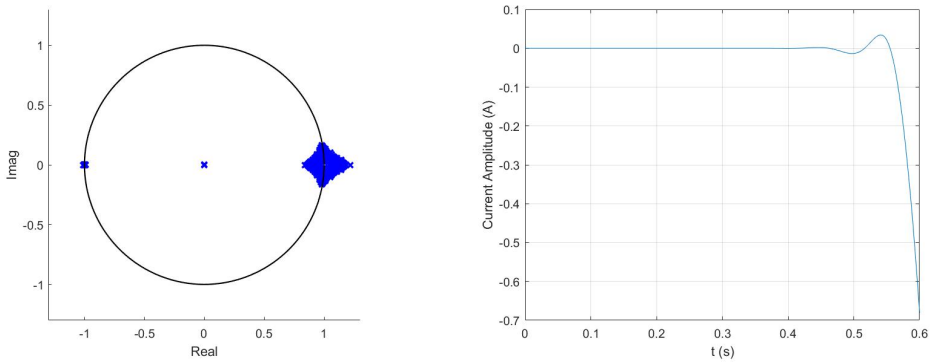

(a) (b)

Figure 3.3: Center frequency is 10 Hz and bandwidth is 5 Hz. Average edge length is $1.359 \times 10^{-8}\lambda$, $\Delta t = 3.33$ ms: (a) eigenvalues and (b) current.

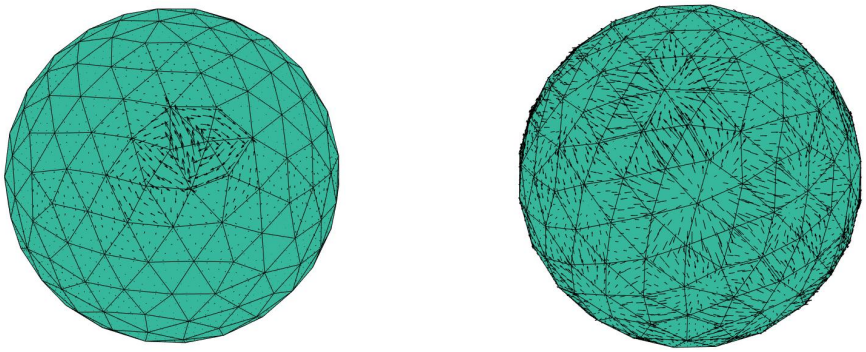

(a) (b)

Figure 3.4: Eigenvectors for center frequency of 1 kHz simulation: (a) unstable mode that is approximately solenoidal and (b) stable mode that is approximately in the complement of the solenoidal current subspace.

be seen to lie in the subspace of current densities that is approximately the complement of the solenoidal subspace, as expected.

3.3 Time Domain Augmented Electric Field Integral Equation

The formulation of the FD-A-EFIE and its corresponding constraint preconditioner is briefly reviewed. The formulation is then converted to the time domain with some basic results presented. From these results, it will be shown that there exists a stability problem with current implementations

of the TD-A-EFIE. A number of methods that have been developed to address this will be presented and analyzed for the robustness of the proposed method.

3.3.1 Frequency Domain A-EFIE Formulation

As has been previously mentioned, the A-EFIE has a very similar structure to the EFIE. The derivation is largely the same, however, the integral operator for the scalar potential contribution is written in terms of the charge density on the surface. This equation has two sets of unknowns, one for the current density and one for the charge density. This requires an additional constraint equation to lead to a solvable system, for which the continuity equation is used. This may be expressed in terms of a block matrix system as

$$\begin{bmatrix} \mathbf{V} & \mathbf{D}^T\mathbf{S} \\ \mathbf{D} & k_0^2\mathbf{I} \end{bmatrix} \begin{Bmatrix} ik_0\mathbf{j} \\ c_0\mathbf{q} \end{Bmatrix} = \begin{Bmatrix} \eta_0^{-1}\mathbf{b} \\ \mathbf{0} \end{Bmatrix}, \tag{3.3}$$

where $\mathbf{j}$ and $\mathbf{q}$ are vectors of the expansion coefficients for the current densities and charge densities, respectively. The scaling of the different coefficients is important to keep the matrix system stable as the frequency is brought closer to DC. The different subblock matrices that represent integral operators are given as

$$\mathbf{V}_{mn} = \mu_r \int_{S_m}\int_{S_n} \frac{e^{ikR}}{4\pi R}\, \mathbf{f}_m(\mathbf{r}) \cdot \mathbf{f}_n(\mathbf{r}')dS'dS \tag{3.4}$$

$$\mathbf{S}_{mn} = \epsilon_r^{-1} \int_{T_m}\int_{T_n} \frac{e^{ikR}}{4\pi R}\, h_m(\mathbf{r})h_n(\mathbf{r}')dS'dS, \tag{3.5}$$

where $\mathbf{f}_m$ is a normalized RWG function associated with the mth edge that has a spatial support over S_m [28]. Further, h_m is the pulse basis function (constant on a triangle) associated with the mth triangle, denoted as T_m. Finally, $k = \omega/c$ is the wavenumber. These integral operators correspond to the vector and scalar potential contributions to the scattered electric field, respectively (after appropriate modification for the scalar term). Additionally,

the excitation of the system is

$$\mathbf{b}_m = \int_{S_m} \mathbf{f}_m(\mathbf{r}) \cdot \mathbf{E}^{\text{inc}}(\mathbf{r})\, dS. \tag{3.6}$$

Since the testing function on the first equation is actually an RWG, some bookkeeping must be done to arrive at the appropriate contribution for the scalar potential term. This is done through the $\mathbf{D}$ matrix, which accounts for the divergence of the RWG functions. Explicitly, $\mathbf{D}$ is a $N_p \times N_e$ matrix where N_p is the number of triangles and N_e is the number of interior edges. The matrix is given by

$$\mathbf{D}_{mn} = \begin{cases} 1, & \text{patch of } h_m \text{ is the positive part of } \mathbf{f}_n \\ -1, & \text{patch of } h_m \text{ is the negative part of } \mathbf{f}_n \\ 0, & \text{otherwise.} \end{cases} \tag{3.7}$$

To enforce charge neutrality, one charge unknown can be dropped for each separated surface. This can be accounted for in the matrix system by defining two mapping matrices that map the reduced vector of charge unknowns to and from the total vector of charge unknowns. These are denoted as $\mathbf{F}$ (forward) and $\mathbf{B}$ (backwards), with more details given in [28]. Inserting these into the matrix system gives the final system as

$$\begin{bmatrix} \mathbf{V} & \mathbf{D}^T\mathbf{S}\,\mathbf{B} \\ \mathbf{F}\,\mathbf{D} & k_0^2\mathbf{I} \end{bmatrix} \begin{Bmatrix} ik_0\mathbf{j} \\ c_0\mathbf{q}_r \end{Bmatrix} = \begin{Bmatrix} \eta_0^{-1}\mathbf{b} \\ \mathbf{0} \end{Bmatrix}, \tag{3.8}$$

where $\mathbf{q}_r$ is the reduced vector of charge unknowns.

As is pointed out in [28], this type of matrix system may be classified as a saddle point problem [31]. This system can become ill-conditioned for problems as the frequency goes to DC; but the saddle point theory suggests an efficient way to form an effective preconditioner. The particular choice is to use a *constraint preconditioner* as a right preconditioner. The constraint preconditioner is picked to be an easier to invert saddle point problem that shares the same structure as the matrix system trying to be solved. Since the preconditioner matrix needs to be inverted, it is desirable to have as sparse

a matrix as possible. The particular matrix picked is

$$\mathbf{M} = \begin{bmatrix} \mathbf{V}_d & \left(\mathbf{F}\,\mathbf{D}\right)^T \left(\mathbf{F}\,\mathbf{S}_d\mathbf{F}^T\right) \\ \mathbf{F}\,\mathbf{D} & k_0^2\mathbf{I} \end{bmatrix}, \tag{3.9}$$

where a subscript d is used to denote that only the diagonal elements of the matrix are used. This matrix notation may be abbreviated to

$$\mathbf{M} = \begin{bmatrix} \mathbf{V}_d & \mathbf{D}_r^T\mathbf{S}_{rd} \\ \mathbf{D}_r & k_0^2\mathbf{I} \end{bmatrix}. \tag{3.10}$$

The inverse of this block matrix can be found in closed form to be

$$\mathbf{M}^{-1} = \begin{bmatrix} \mathbf{V}_d^{-1} & \mathbf{0} \\ \mathbf{0} & \mathbf{0} \end{bmatrix} + \begin{bmatrix} -\mathbf{V}_d^{-1}\mathbf{D}_r^T\mathbf{S}_{rd} \\ \mathbf{I} \end{bmatrix} \Delta^{-1} \begin{bmatrix} -\mathbf{D}_r\mathbf{V}_d^{-1} & \mathbf{I} \end{bmatrix}, \tag{3.11}$$

where the Schur complement is

$$\Delta = k_0^2\mathbf{I} - \mathbf{D}_r\mathbf{V}_d^{-1}\mathbf{D}_r^T\mathbf{S}_{rd}. \tag{3.12}$$

The benefit of this matrix inversion process is that instead of needing to numerically invert the full $\mathbf{M}$ matrix, only the smaller Schur complement must be inverted numerically. Additional details on the formulation of the FD-A-EFIE and extensive numerical examples for realistic structures can be found in [28].

3.3.2 Time Domain A-EFIE Formulation

The formulation of the A-EFIE can be easily extended to the time domain using the methods detailed in Chapter 2. Performing this, and using the separable approximation for the delta function of the time domain Green's

function, the matrix system to be solved is

$$\begin{bmatrix} \mathbf{V}^{(0)} & \mathbf{D}^T\mathbf{S}^{(0)}\mathbf{B} \\ d^{(0)}\mathbf{F}\,\mathbf{D} & \dot{\mathbf{I}}^{(0)} \end{bmatrix} \begin{Bmatrix} \big(c_0\Delta t\big)^{-1}\mathbf{j}^{(i)} \\ c_0\mathbf{q}_r^{(i)} \end{Bmatrix} = \begin{Bmatrix} \eta_0^{-1}\mathbf{b}^{(i)} \\ \mathbf{0} \end{Bmatrix} - \sum_{j=i-j_{max}}^{i-1} \begin{bmatrix} \mathbf{V}^{(i-j)} & \mathbf{D}^T\mathbf{S}^{(i-j)}\mathbf{B} \\ d^{(i-j)}\mathbf{F}\,\mathbf{D} & \dot{\mathbf{I}}^{(i-j)} \end{bmatrix} \begin{Bmatrix} \big(c_0\Delta t\big)^{-1}\mathbf{j}^{(j)} \\ c_0\mathbf{q}_r^{(j)} \end{Bmatrix}. \quad (3.13)$$

The core integral operator subblock matrices are

$$\mathbf{V}_{mn}^{(i-j)} = \frac{\mu_r\Delta t}{4\pi}\int_{S_m}\int_{S_n}\sum_{l=0}^{N_h} a_l\dot{\xi}_l^{(i-j)}\mathbf{f}_m(\mathbf{r})\cdot\mathbf{f}_n(\mathbf{r}')\frac{P_l(\hat{R})}{R}dS'dS \quad (3.14)$$

$$\mathbf{S}_{mn}^{(i-j)} = -\frac{1}{4\pi\epsilon_r}\int_{T_m}\int_{T_n}\sum_{l=0}^{N_h} a_l\xi_l^{(i-j)}h_m(\mathbf{r})h_n(\mathbf{r}')\frac{P_l(\hat{R})}{R}dS'dS. \quad (3.15)$$

The temporal convolutions have been accounted for in

$$\xi_l^{(i-j)} = \int_{-\infty}^{\infty} P_l(k_1t'+k_2)T\big((i-j)\Delta t-\zeta/c-t'\big)dt' \quad (3.16)$$

$$\dot{\xi}_l^{(i-j)} = \int_{-\infty}^{\infty} P_l(k_1t'+k_2)\dot{T}\big((i-j)\Delta t-\zeta/c-t'\big)dt', \quad (3.17)$$

and T is the temporal basis function. The remaining terms to be defined are

$$\dot{\mathbf{I}}_{mn}^{(i)} = \begin{cases} \dfrac{1}{c_0^2\Delta t}\dot{T}\big(i\Delta t\big), & m=n \\ 0, & \text{otherwise,} \end{cases} \quad (3.18)$$

$$\mathbf{b}_m^{(i)} = \int_{S_m}\mathbf{f}_m(\mathbf{r})\cdot\mathbf{E}^{\text{inc}}(\mathbf{r},i\Delta t)dS, \quad (3.19)$$

and $d^{(i)} = T(i\Delta t)$. Note that because of the temporal dependence of the continuity equation constraint, the bottom blocks of this matrix system are only non-zero for a very small number of matrices. More details on evaluating the different matrix elements can be found in Section 2.4.

The different scaling coefficients are arranged so that the scaling of the matrix elements are

$$\begin{bmatrix} O\big(1\big) & O\big(1\big) \\ O\big(1\big) & O\big((c_0\Delta t)^{-2}\big) \end{bmatrix}. \quad (3.20)$$

The reasons for this scaling can be understood by applying the Geršgorin circle theorem to this matrix to estimate its condition number [14, 34, 43]. In essence, the Geršgorin circle theorem says that for a $N \times N$ matrix with elements v_{ij} the eigenvalues lie in the union of disks defined by

$$\begin{cases} \text{centers: } v_{ii}, i = 1, \ldots, N \\ \text{radii: } \sum_{j \neq i}^{N} |v_{ij}|, i = 1, \ldots, N. \end{cases} \tag{3.21}$$

That is, all the eigenvalues of the matrix lie in the union of the disks with center defined by the diagonal element of the row and a radius equal to the sum of the absolute value of all other elements of the row. By applying this to the block matrix system, it is seen that there will be two distinct families of eigenvalues due to the upper and lower blocks of the matrix. Due to the scaling of the matrix, the eigenvalues associated with the upper part of the matrix should not change as the time step is adjusted and will lie at some finite value. Similarly, for the lower blocks of the matrix the centers of the disks will collapse to the origin as the time step is increased. Importantly, the radii of the disks will remain constant. This limits the locations of the eigenvalues, and will keep the condition number fairly flat *at low frequencies*, assuming no mesh dependent conditioning effects are occurring. In practice, for the simple sphere geometries tested it has been found that the condition number remains at $O\left(10^3\right)$ from very low frequencies up to the low MHz range. To further improve the convergence of iterative solvers, the preconditioner shown in (3.11) can be implemented in the time domain [39].

3.3.3 Time Domain A-EFIE Results at Low Frequencies

To highlight the utility of the TD-A-EFIE at low frequencies, a simple numerical example is presented. The results of this are shown in Fig. 3.5. This example shows the accuracy of the TD-A-EFIE when operating in the low frequency regime, where the differentiated TD-EFIE breaks down. For this example, the incident pulse has a center frequency of 100 kHz and a bandwidth of 50 kHz. The time step is 0.333 μs, and the average edge length is $1.359 \times 10^{-4}\lambda$ at 150 kHz.

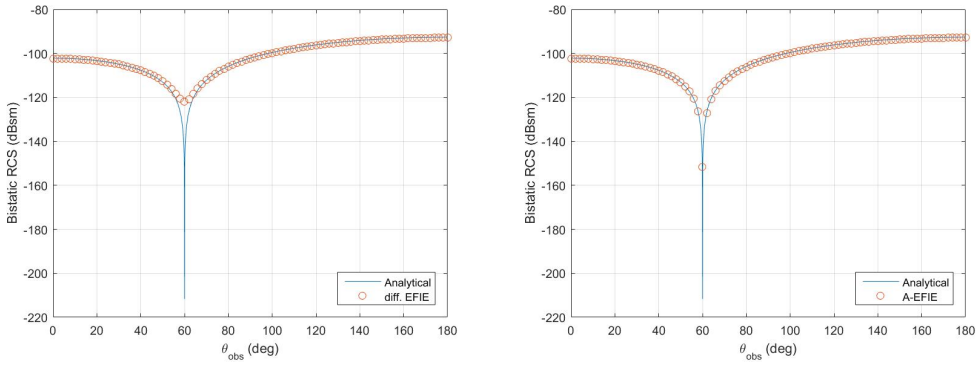

(a) (b)

Figure 3.5: RCS results for a 1 meter radius sphere at 100 kHz: (a) differentiated TD-EFIE and (b) TD A-EFIE.

3.4 Time Domain Augmented Electric Field Integral Equation Stability

The stability of the TD-A-EFIE is reviewed in this section. Numerical examples are presented which demonstrate that the TD-A-EFIE has worse stability than the differentiated TD-EFIE at middle frequencies. Following this, a number of stabilization approaches that have been proposed are reviewed.

3.4.1 Stability Analysis

Although the TD-A-EFIE is successful at producing accurate results at lower frequencies than the TD-EFIE, it is not free from issues. Unfortunately, it has been found that the TD-A-EFIE is not as stable as the TD-EFIE (or differentiated TD-EFIE) at middle frequencies. To demonstrate this, an eigenvalue analysis was performed for a simulation on a 1 meter radius sphere with a center frequency of 80 MHz and a bandwidth of 20 MHz. The time step is 0.9 ns and the average edge length at 100 MHz is 0.0906λ. The eigenvalues for the two systems are shown in Fig 3.6; where it is clearly seen that the TD-A-EFIE is substantially less stable than the differentiated TD-EFIE.

From the discussions in [37], it is expected that the TD-A-EFIE must have some type of null space (or approximate null space) at middle frequencies that is not present in the differentiated TD-EFIE. To further investigate this, a

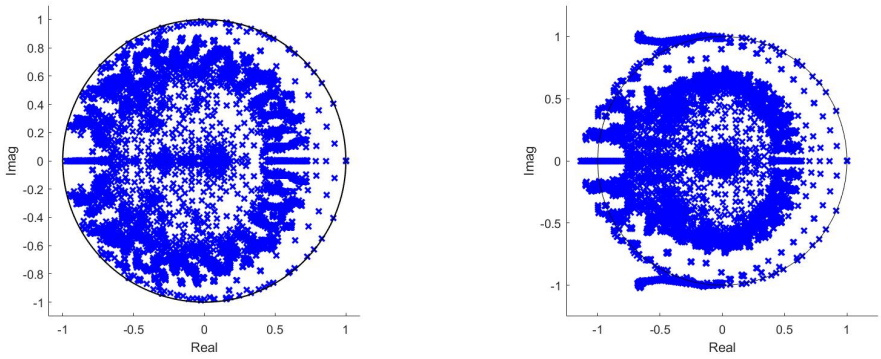

(a) (b)

Figure 3.6: Eigenvalues for a center frequency of 80 MHz and a bandwidth of 20 MHz: (a) differentiated TD-EFIE and (b) TD-A-EFIE.

few of the eigenvectors associated to the most unstable modes are shown in Fig. 3.7. There is not much structure to these unstable modes, however, it does appear that they may be related to a buildup of charge on some patches. It is anticipated that the strong form of the continuity equation is not acting as a good constraint for the additional unknowns at middle frequencies. This leads to the presence of unstable modes where the differentiated TD-EFIE has none, since the continuity equation is enforced by design.

Another simulation at slightly lower frequencies is prepared on the same mesh to further investigate the change in the unstable eigenvectors as the frequency is adjusted. In addition to this, the temporal basis function for the TD-A-EFIE is changed from a quadratic B-spline to a cubic Lagrange interpolator, which is more typically used in the literature [38]. For this simulation, the center frequency of the incident pulse is 30 MHz and the bandwidth is 20 MHz, making the time step 1 ns. The eigenvalues of the companion matrix are shown in Fig. 3.8. It is seen that the system is more stable for the larger time step and the higher-order temporal basis function. However, the system is still not stable, with a number of eigenvalues being found to lie outside the unit circle.

Once again, the eigenvectors of these unstable modes can be studied to gain more insight into the flaws of the approach. Sample eigenvectors of the most unstable modes are shown in Fig. 3.9. It is seen that at the slightly lower frequency, these eigenvectors have substantially more structure than the unstable modes at 80 MHz. These vector fields appear to be related to

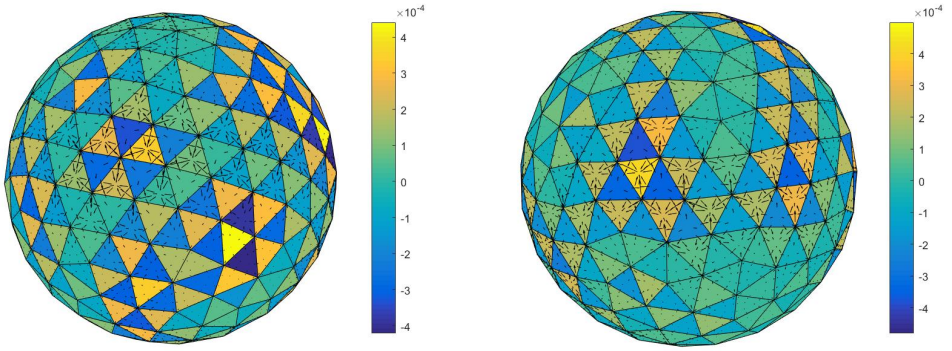

(a) (b)

Figure 3.7: Eigenvectors for sample unstable modes with a center frequency of 80 MHz and a bandwidth of 20 MHz.

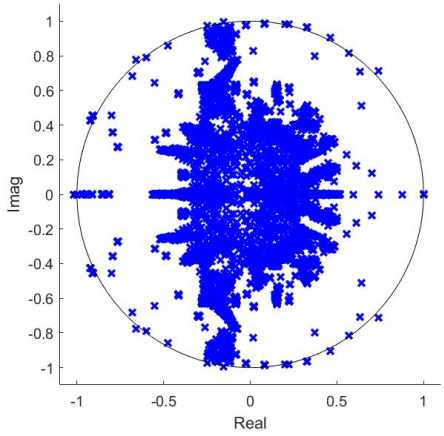

Figure 3.8: Eigenvalues for a center frequency of 30 MHz and a bandwidth of 20 MHz.

spherical harmonics that will have an approximately zero divergence over the surface of the sphere. Further unstable modes are investigated, and it is seen that they in general correspond to modes that will approximately live in the subspace of solenoidal currents. The conclusion is that the time derivative in the $\mathbf{V}^{(i)}$ operator and the divergence of the current in the continuity equation leads to a null space of static solenoidal currents. Through the discretization process, this null space will become larger to encompass approximately static and solenoidal currents. Since these reside in a null space, or an approximate null space of the operator, they are not well-constrained by the system and can lead to exponential growth. This same type of null space also affects the differentiated TD-EFIE. However, it appears that using the strong form of

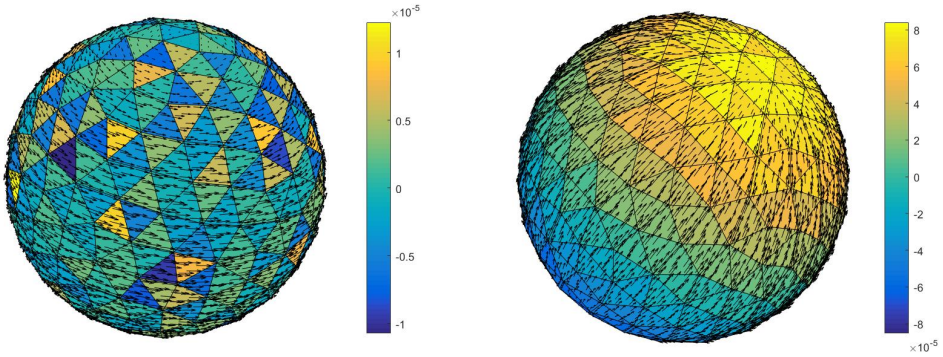

(a) (b)

Figure 3.9: Eigenvectors for sample unstable modes with a center frequency of 30 MHz and a bandwidth of 20 MHz.

the continuity equation is leading to a less stable system.

Through the analysis in Chapter 5, it will be shown that the major problem with the TD-A-EFIE is actually the temporal basis functions being used. Despite this, there is still a greater amount of numerical instability inherent to the TD-A-EFIE than the differentiated TD-EFIE or TD-EFIE. It is expected that the numerical method is more sensitive to stability issues when multiple unknown functions are used. The reason is that there is more room for numerical errors to become significant when multiple equations need to be enforced together.

3.4.2 Time Domain A-EFIE Stabilization Approaches

As was shown in Section 3.4.1, the TD-A-EFIE appears to have worse stability than the differentiated TD-EFIE at middle frequencies. This occurs even when using specially made integration techniques to accurately evaluate the matrix elements. In this section, a number of possible stabilization techniques that have been used in the literature are reviewed to determine their general applicability to the TD-A-EFIE.

Low-Pass Filtering

One of the original techniques to stabilize the high frequency instability in traditional TDIEs was to perform a low-pass filtering operation by averaging

a number of the current densities [44]. This methodology was adopted in [38] to aid in the stability of the TD-A-EFIE when using third-order Lagrange interpolating functions for the temporal basis functions. The averaged value that will be used in the time-marching procedure (once it is available) is

$$\tilde{U}^{(j)} = 0.25\tilde{U}^{(j-1)} + 0.5U^{(j)} + 0.25U^{(j+1)}, \tag{3.22}$$

where $\tilde{U}^{(j)}$ is the filtered basis coefficient for an arbitrary unknown and $U^{(j)}$ is the corresponding unfiltered coefficient. This approach is simple to implement, and can extend the range of the problems that may be evaluated, but does not solve the problem of instability in general. As such, it is not a preferable approach and has been largely dismissed by most of the more experienced research groups in the field [21, 22, 45].

Projection onto Stable Modes

In [46], a method was developed to make an explicit time domain FEM simulation unconditionally stable. The general concept was to solve an eigenvalue problem based on the system matrix, identify which eigenvectors corresponded to stable modes, and then project the solution procedure into the subspace spanned *only* by stable modes. In this way, stability could be ensured while also still being able to meet accuracy specifications.

In [47], the authors claim to have adapted this method to the TDIE framework. From the citations, it is not clear whether this method is being used for the results presented in [39–41]. However, upon inspection of the method it does not appear that the authors of [47] have actually accomplished the goal of replicating [46] for TDIEs. From the description, the proposed method of [47] actually calculates the expansion coefficients for the first M time steps. They then treat these vectors as the columns of a matrix, whose SVD they calculate. The marching system is then projected onto the right singular vectors from the SVD calculation. They claim that this can effectively ensure the late time stability of the solution, while also lowering the computational complexity.

From (personal) numerical experiments, it was found that this method is distinctly different from [46] in a number of ways. First, the proposed method using an SVD approach does not ensure stability or accuracy. If

the unstable modes have already been excited in the early time steps than the right singular vectors of the SVD can still cause this instability in the reduced order system. Further, there is no clear way defined by the authors to associate a singular value with whether the mode will be stable or not. This is in stark contrast with [46], where rigorous guidelines are given to determine whether an eigenvalue corresponds to a stable mode or not. Finally, it is not clear how many time steps need to be solved before being able to project onto the reduced order system to ensure the accuracy of the solution.

This method also does not really improve the computational complexity. For large systems, the PWTD will still have to be used to calculate the first M time steps of current. The computational complexity reduction is marginal, at best, since an SVD will also need to be calculated on a very tall matrix. This, along with the other flaws of the method, make it not a practical approach for stabilizing the TD-A-EFIE.

Preconditioning

Since many of the effects that lead to instability in the time domain present themselves as a progressively more ill-conditioned problem in the frequency domain, there is some question as to whether preconditioning in the time domain may help the stability of the system. In [39], the authors propose a preconditioner for the TD-A-EFIE and claim that the system is highly stable and accurate (note: they have also made another modification to the formulation that will be discussed next). The preconditioner used is just a time domain version of (3.11), which can be implemented easily for small geometries.

The clearest way to test whether the preconditioner can aid in the stability of the method is to modify the eigenvalue stability analysis of (3.2) to account for the preconditioning. For a right preconditioner, the solution to the system of equations $\mathbf{Zx} = \mathbf{b}$ is solved iteratively as

$$\mathbf{ZM}^{-1}\mathbf{y} = \mathbf{b}, \tag{3.23}$$

where $\mathbf{y} = \mathbf{Mx}$. To incorporate this into the eigenvalue analysis, denote $\mathbf{C}_{\mathbf{M}}^{(j)} = -\left([\mathbf{Z}^{(0)}]\mathbf{M}^{-1}\right)^{-1}[\mathbf{Z}^{(j)}]\mathbf{M}^{-1}$. Then, the companion matrix for the pre-

conditioned marching system is

$$\begin{Bmatrix} V^{(i+1)} \\ V^{(i)} \\ V^{(i-1)} \\ \vdots \\ V^{(i-j_{\max}+3)} \\ V^{(i-j_{\max}+2)} \end{Bmatrix} = \begin{bmatrix} \mathbf{C}_{\mathbf{M}}^{(1)} & \mathbf{C}_{\mathbf{M}}^{(2)} & \dots & \mathbf{C}_{\mathbf{M}}^{(j_{\max}-1)} & \mathbf{C}_{\mathbf{M}}^{(j_{\max})} \\ \mathbf{I} & 0 & \dots & 0 & 0 \\ 0 & \mathbf{I} & \dots & 0 & 0 \\ \vdots & \vdots & \ddots & \vdots & \vdots \\ 0 & 0 & \dots & \mathbf{I} & 0 \end{bmatrix} \begin{Bmatrix} V^{(i)} \\ V^{(i-1)} \\ V^{(i-2)} \\ \vdots \\ V^{(i-j_{\max}+2)} \\ V^{(i-j_{\max}+1)} \end{Bmatrix}, \tag{3.24}$$

where $V^{(i)} = \mathbf{M}U^{(i)}$, using the notation from (3.2). Solving for the eigenvalues of this system and comparing them to the system without preconditioning showed a negligible change in the locations of the eigenvalues. When the time step is made much smaller than is needed for traditional sampling choices, the eigenvalues near the center of the complex plane have been seen to move; however, the unstable eigenvalues remain unaffected. This is illustrated in Fig. 3.10 where the eigenvalues are presented for two different cases. Both simulations are performed for a center frequency of 1 MHz with a 500 kHz bandwidth; but the temporal basis functions and time step are selected differently. For Fig. 3.10(a) a quadratic B-spline basis function is used with a time step of 3.33 ns, while for Fig. 3.10(b) a triangle basis function (first-order B-spline) is used with a time step of 0.453 ns. This shows that the preconditioner, although necessary for improving convergence of the iterative solver, has no noticeable effect on the stability of the system.

Integrating the Continuity Equation

In [39, 41], the authors suggest that the continuity equation should not be enforced directly to improve the stability and accuracy of the TD-A-EFIE. The argument is related to the traditional basis functions used for TDIEs, which are Lagrange interpolating functions. These do not have continuous derivatives, so it is suggested that the derivative of the charge temporal basis function should be avoided. This is because the strong form of the continuity equation requires evaluating the derivative of the basis function at exactly the discontinuous point. To avoid this, it is instead suggested that the temporal integral of the continuity equation should be enforced.

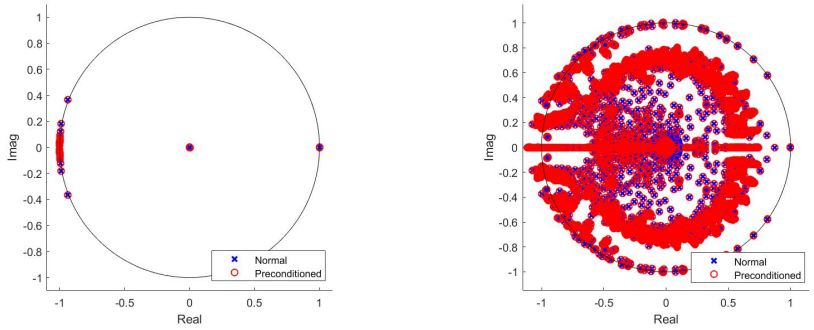

(a) (b)

Figure 3.10: Eigenvalue stability analysis with and without preconditioning: (a) quadratic B-spline basis function with $\Delta t = 3.33$ ns; and (b) triangle basis function with $\Delta t = 0.453$ ns.

In the traditional TD-A-EFIE, the continuity equation in its strong form only constraints a very small number of the matrices (i.e., the bottom blocks of the matrices are $\mathbf{0}$ for most matrices of the marching system). By enforcing the temporal integral of the continuity equation, the bottom-left block of the matrices never becomes $\mathbf{0}$, providing a stronger constraint on the solved-for current densities. However, because these matrices never become $\mathbf{0}$, the history of all past current basis coefficients must be used in the solution of every time step. A naive implementation of this would lead to an inefficient MOT system, however, a recursive procedure like that used in the TD-EFIE can be applied to avoid this.

Appropriate Temporal Basis Functions

From the work of [48], it is suggested that the temporal basis functions for the current and charge should be selected independently. They state that any discretization with a temporal basis function that is higher than order 1 for the charge will lead to an unstable result. This conclusion has not been verified yet, but the suggestion that different basis functions should be used is the correct approach. This will be discussed in more detail in Chapter 5.

CHAPTER 4

INITIAL DEVELOPMENT OF A-Φ TIME DOMAIN INTEGRAL EQUATIONS

As was demonstrated in Chapter 3, there appear to be unresolved stability problems with the TD-A-EFIE. In this chapter, two novel integral equations are proposed that attempt to address this. The two integral equations are an **A**-Φ TDIE and a modified TD-A-EFIE. The modified TD-A-EFIE is called the time domain weighted continuity EFIE (TD-WC-EFIE) for reasons that will be made clear in later sections. This integral equation is proposed based on physical insight from the **A**-Φ TDIE discussed.

The goals for both integral equations are to be accurate at low frequencies, while still maintaining stability at middle frequencies. As will be seen through the results, these goals are not achieved with these integral equations. However, the results and discussion are still useful in motivating the approach used in Chapter 5 to overcome these problems. Additionally, only a simple modification is needed to make the TD-WC-EFIE achieve low frequency accuracy and stability. After doing this, the other properties of the TD-WC-EFIE make it better to use than the TD-A-EFIE.

4.1 A-Φ Time Domain Integral Equation

Due to the stability issues present in the TD-A-EFIE, alternative integral equations have been considered. The goal is a method that can achieve accurate results at low frequencies and still be stable in the middle frequency regime. From the success of the **A**-Φ method in the frequency domain at this, it is anticipated that this formulation will be useful in the time domain [14].

This section briefly reviews the **A**-Φ formulation in the frequency domain before presenting the corresponding time domain equations. It is seen from the eigenvalue stability analysis of this system that the eigenvalues show a different structure as compared to the TD-A-EFIE system, but do not

correspond to a stable system themselves. Additionally, the eigenvectors of this system are inspected to determine what kinds of modes correspond to unstable ones.

4.1.1 Frequency Domain A-Φ Formulation

The **A**-Φ formulation for a PEC scatterer may be derived by considering the extinction theorem and the equivalence principle in the context of the vector potential wave equation presented in [1]. This yields the following integral equation,

$$\int_S \big[\mu g(\mathbf{r},\mathbf{r}',\omega)\mathbf{J}(\mathbf{r}',\omega) + \nabla' g(\mathbf{r},\mathbf{r}',\omega)\Sigma(\mathbf{r}',\omega)\big]\,dS' = -\mathbf{A}^{\text{inc}}(\mathbf{r},\omega), \tag{4.1}$$

where $\mathbf{A}^{\text{inc}}$ is the incident vector potential, $\mathbf{J}$ is the unknown current density, and Σ is another set of unknowns corresponding to $\hat{n}'\cdot\mathbf{A}$ [14]. Additionally, the homogeneous medium Green's function is

$$g(\mathbf{r},\mathbf{r}',\omega) = \frac{e^{ikR}}{4\pi R}, \tag{4.2}$$

where $k = \omega/c$.

Since two sets of unknowns are being used another constraint equation must be determined to arrive at a solvable system. This is done by taking the divergence of (4.1), invoking the Lorenz gauge, and using the defining equation of the scalar Green's function for the wave equation. This yields

$$\int_S \big[\mu g(\mathbf{r},\mathbf{r}',\omega)\nabla'\cdot\mathbf{J}(\mathbf{r}',\omega) + k^2 g(\mathbf{r},\mathbf{r}',\omega)\Sigma(\mathbf{r}',\omega)\big]\,dS' = -i\omega\mu\epsilon\Phi^{\text{inc}}(\mathbf{r},\omega), \tag{4.3}$$

where Φ^{inc} is the incident scalar potential. As is pointed out in [14], the physical meaning of (4.3) in conjunction with the scalar Huygens' principle integral equation is a weak form of the current continuity equation [49]. This weak form uses the Green's function as an integral kernel, and is explicitly written as

$$\int_S g(\mathbf{r},\mathbf{r}',\omega)\big[\nabla'\cdot\mathbf{J}(\mathbf{r}',\omega) - i\omega\rho(\mathbf{r}',\omega)\big]\,dS' = 0, \tag{4.4}$$

where ρ is the charge density. More details on the derivations of the governing differential and integral equations for the **A**-Φ formulation may be found in [1, 14].

With the necessary equations now derived, a matrix equation may be formed by expanding $\mathbf{J}$ with normalized RWG functions and Σ with pulse basis functions (constants on a triangle). Testing may be performed by using normalized RWG functions for (4.1), and pulse basis functions for (4.3) [28]. This leads to a block matrix system of the following form,

$$\begin{bmatrix} \mu_r \mathbf{V} & \mathbf{D}^T \mathbf{S} \\ \mathbf{S}\mathbf{D} & \epsilon_r k_0^2 \mathbf{S} \end{bmatrix} \begin{Bmatrix} c_0^{-1} \mathbf{j} \\ \eta_0^{-1} \boldsymbol{\psi} \end{Bmatrix} = \begin{Bmatrix} -\eta_0^{-1} \boldsymbol{\alpha} \\ -ik_0 \epsilon \boldsymbol{\phi} \end{Bmatrix}, \tag{4.5}$$

where $\mathbf{j}$ is a vector of expansion coefficients for the current density, and $\boldsymbol{\psi}$ is the same for Σ. The different matrix elements may be calculated as

$$\mathbf{V}_{mn} = \int_{S_m} \int_{S_n} g(\mathbf{r}, \mathbf{r}', \omega) \mathbf{f}_m(\mathbf{r}) \cdot \mathbf{f}_n(\mathbf{r}') dS' dS \tag{4.6}$$

$$\mathbf{S}_{mn} = \int_{T_m} \int_{T_n} g(\mathbf{r}, \mathbf{r}', \omega) h_m(\mathbf{r}) h_n(\mathbf{r}') dS' dS, \tag{4.7}$$

and $\mathbf{D}$ is the same connection matrix defined in (3.7) that accounts for the divergence of the normalized RWG functions. The excitation of the system is given as

$$\boldsymbol{\alpha}_m = \int_{S_m} \mathbf{f}_m(\mathbf{r}) \cdot \mathbf{A}^{\text{inc}}(\mathbf{r}) \, dS \tag{4.8}$$

$$\boldsymbol{\phi}_m = \int_{S_m} h_m(\mathbf{r}) \Phi^{\text{inc}}(\mathbf{r}) \, dS, \tag{4.9}$$

where definitions of the forms of $\mathbf{A}^{\text{inc}}$ and Φ^{inc} for different types of excitations (e.g., plane wave or NF dipole) can be found in [1, 14]. The development of a preconditioner and numerical results for this formulation may be found in [14].

4.1.2 Time Domain A-Φ Formulation

The equations presented in Section 4.1.1 can be easily converted to the time domain. This yields the two equations to be solved together as

$$\int_S \left[\mu \frac{\delta(\tau)}{4\pi R} * \mathbf{J}(\mathbf{r}',t) - \nabla\left(\frac{\delta(\tau)}{4\pi R} * \Sigma(\mathbf{r}',t)\right)\right] dS' = -\mathbf{A}^{\text{inc}}(\mathbf{r},t) \tag{4.10}$$

$$\int_S \frac{\delta(\tau)}{4\pi R} * \left[\nabla' \cdot \mathbf{J}(\mathbf{r}',t) - \epsilon \ddot{\Sigma}(\mathbf{r}',t)\right] dS' = \epsilon \dot{\Phi}^{\text{inc}}(\mathbf{r},t), \tag{4.11}$$

where $\tau = t - R/c$. After using the separable approximation to the delta function of the time domain Green's function, the matrix system to be solved becomes

$$\begin{bmatrix} \mu_r \mathbf{V}^{(0)} & \mathbf{D}^T \mathbf{S}^{(0)} \\ \mathbf{S}^{(0)} \mathbf{D} & -\epsilon_r c_0^{-2} \ddot{\mathbf{S}}^{(0)} \end{bmatrix} \begin{Bmatrix} c_0^{-1} \mathbf{j}^{(i)} \\ \eta_0^{-1} \boldsymbol{\psi}^{(i)} \end{Bmatrix} = \begin{Bmatrix} -\eta_0^{-1} \boldsymbol{\alpha}^{(i)} \\ \epsilon c_0^{-1} \dot{\boldsymbol{\phi}}^{(i)} \end{Bmatrix}$$
$$- \sum_{j=i-j_{max}}^{i-1} \begin{bmatrix} \mu_r \mathbf{V}^{(i-j)} & \mathbf{D}^T \mathbf{S}^{(i-j)} \\ \mathbf{S}^{(i-j)} \mathbf{D} & -\epsilon_r c_0^{-2} \ddot{\mathbf{S}}^{(i-j)} \end{bmatrix} \begin{Bmatrix} c_0^{-1} \mathbf{j}^{(j)} \\ \eta_0^{-1} \boldsymbol{\psi}^{(j)} \end{Bmatrix}. \tag{4.12}$$

The different matrix elements are defined as

$$\mathbf{V}_{mn}^{(i-j)} = \int_{S_m} \int_{S_n} \sum_{l=0}^{N_h} a_l \xi_l^{(i-j)} \mathbf{f}_m(\mathbf{r}) \cdot \mathbf{f}_n(\mathbf{r}') \frac{P_l(\hat{R})}{4\pi R} dS' dS \tag{4.13}$$

$$\mathbf{S}_{mn}^{(i-j)} = \int_{T_m} \int_{T_n} \sum_{l=0}^{N_h} a_l \xi_l^{(i-j)} h_m(\mathbf{r}) h_n(\mathbf{r}') \frac{P_l(\hat{R})}{4\pi R} dS' dS \tag{4.14}$$

$$\ddot{\mathbf{S}}_{mn}^{(i-j)} = \int_{T_m} \int_{T_n} \sum_{l=0}^{N_h} a_l \ddot{\xi}_l^{(i-j)} h_m(\mathbf{r}) h_n(\mathbf{r}') \frac{P_l(\hat{R})}{4\pi R} dS' dS, \tag{4.15}$$

where the temporal integrals are given by

$$\xi_l^{(i-j)} = \int_{-\infty}^{\infty} P_l(k_1 t' + k_2) T\big((i-j)\Delta t - \zeta/c - t'\big) dt' \tag{4.16}$$

$$\ddot{\xi}_l^{(i-j)} = \int_{-\infty}^{\infty} P_l(k_1 t' + k_2) \ddot{T}\big((i-j)\Delta t - \zeta/c - t'\big) dt', \tag{4.17}$$

with T being the temporal basis function used to expand the unknowns. For more details on the calculation of these matrix elements, consult Section 2.4.

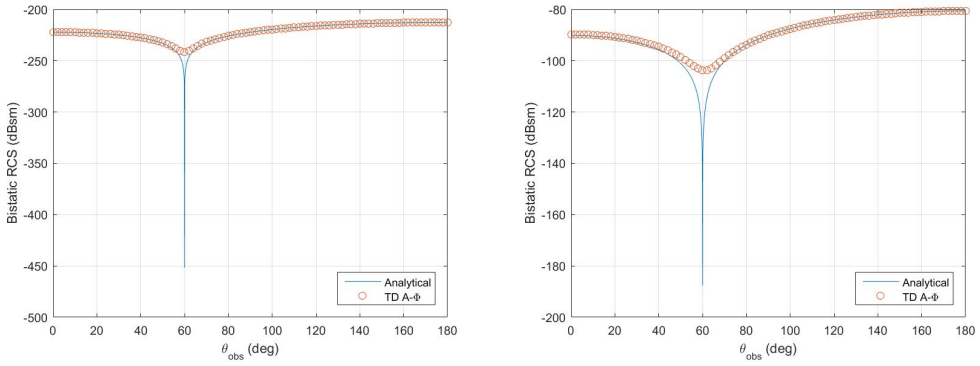

Figure 4.1: RCS results for a 1 meter radius sphere using the TD A-Φ at: (a) 100 Hz and (b) 200 kHz.

Finally, the excitations may be calculated as

$$\boldsymbol{\alpha}_m^{(i)} = \int_{S_m} \mathbf{f}_m(\mathbf{r}) \cdot \mathbf{A}^{\text{inc}}(\mathrm{r}, i\Delta t) dS \tag{4.18}$$

$$\dot{\boldsymbol{\phi}}_m^{(i)} = \int_{T_m} h_m(\mathbf{r}) \dot{\Phi}^{\text{inc}}(\mathbf{r}, i\Delta t) dS. \tag{4.19}$$

4.1.3 Time Domain A-Φ Results

The matrix system of (4.12) has been tested by simulating the scattering from a sphere for a number of different incident pulse definitions. In each case, the incident scalar potential has been set to 0 [14]. The temporal basis function used for all examples is the quadratic B-spline.

From the numerical tests, it is seen that the method is not exhibiting good accuracy or stability. The problem of accuracy is shown in Fig. 4.1, where the RCS results from two different simulations are shown. One of the simulations is for an incident pulse with a center frequency of 100 Hz, a bandwidth of 50 Hz, and with a corresponding time step of 0.333 ms. The second simulation is for an incident pulse with a center frequency of 200 kHz, a bandwidth of 100 kHz, and with a time step of 0.333 μs. This second simulation was not stable at late-time after the incident field had effectively decayed to zero. The RCS results presented were calculated from a Fourier transform of the current density only over stable time steps. It is evident from Fig. 4.1, that the approach currently being used is not able to capture the null in the RCS

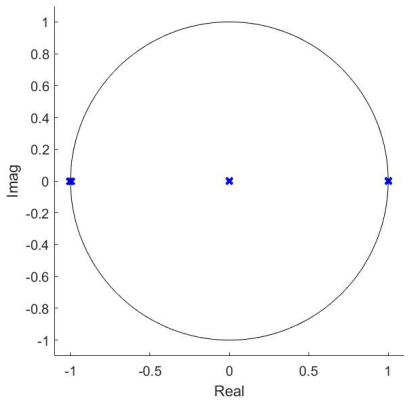

Figure 4.2: Eigenvalues stability analysis for the 200 kHz simulation.

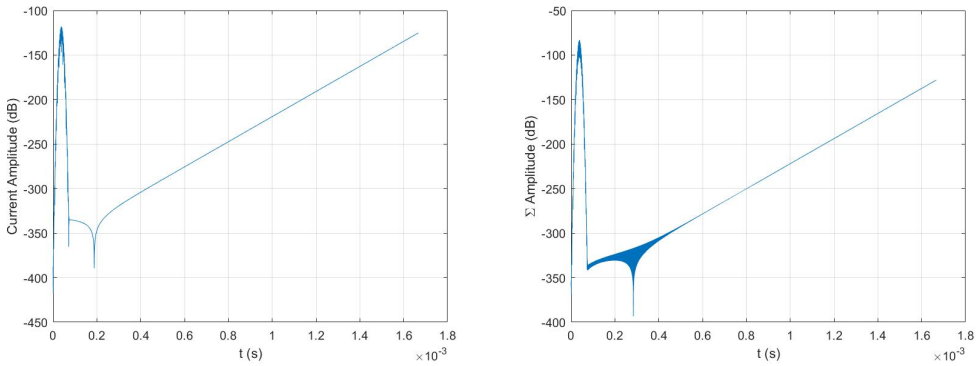

(a) (b)

Figure 4.3: Basis coefficients results for a 1 meter radius sphere using the TD A-Φ for the 200 kHz center frequency simulation: (a) current expansion coefficient and (b) normal component of the vector potential coefficient.

properly.

The problem of stability is illustrated for the simulation with a center frequency of 200 kHz and a bandwidth of 100 kHz. The eigenvalues from the stability analysis are plotted in Fig. 4.2, where it is seen that a number of eigenvalues lie outside of the unit circle near $(-1, 0i)$. To further investigate the nature of the instability, sample coefficients for the current and normal component of the vector potential unknowns are plotted in Fig. 4.3 for the 200 kHz simulation. It is seen that both unknowns are unstable, however, the normal component of the vector potential shows the classic high frequency oscillations where the coefficient varies rapidly between each time step.

To further examine the source of the instability for the **A**-Φ formulation,

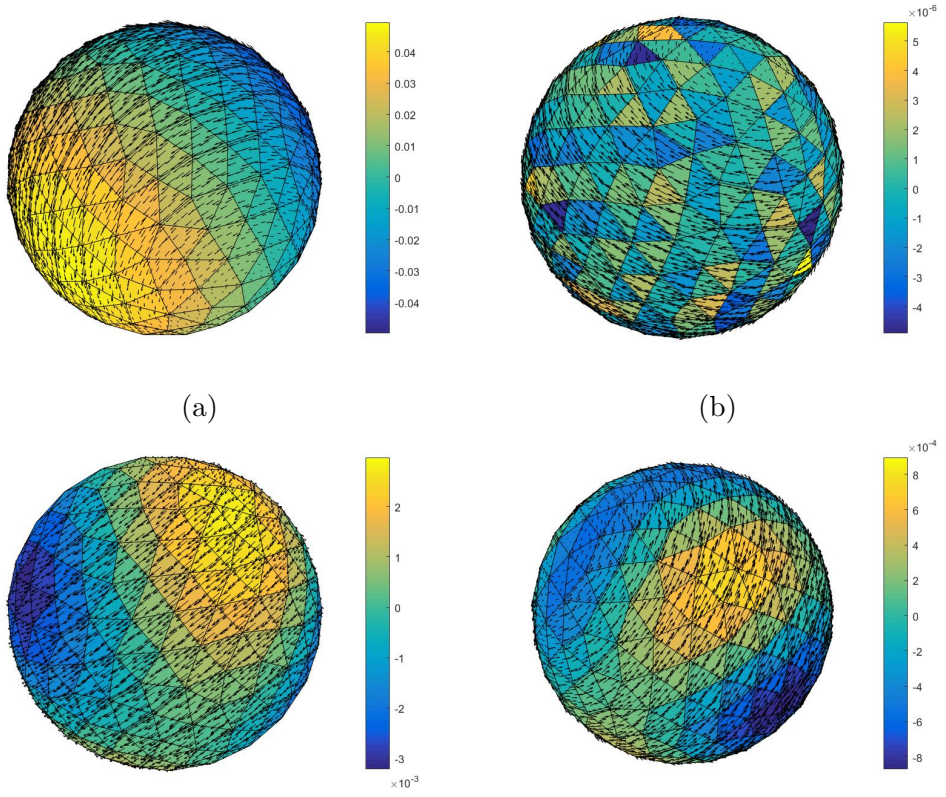

Figure 4.4: Sample eigenvectors of unstable modes for a 1 meter radius sphere using the TD A-Φ for the 200 kHz center frequency simulation with $\Delta t = 0.333$ μs: order is from most unstable to less unstable (a)-(d).

the eigenvectors of a few sample unstable modes are plotted in Fig. 4.4. The current density is represented by the vector arrows over the sphere, while the color of the patches corresponds to the value of the normal component of the vector potential. It is seen that the unstable modes are highly structured, suggesting that there may be a fundamental problem with the physics of the formulation. This concept will be further discussed in Chapter 5.

By recalling that the normal component of the vector potential can be related to a contribution to the charge, it is seen that the currents are flowing between points of charge buildup on the surface of the sphere. In contrast to the TD-EFIE and TD-A-EFIE, the current density for the **A**-Φ formulation does not show any obvious null space. This is a result of no time derivatives being applied to the integrals in the **V** matrix; making the static null space of solenoidal currents for the TD-EFIE and TD-A-EFIE disappear. However,

the two time derivatives on the Σ unknowns in the second equation could produce a null space for static and linearly varying/growing Σ. This would occur if the Σ unknowns are arranged to produce no contribution from the $\mathbf{S}^{(i)}$ matrix. It is difficult to know physically what the Σ unknowns should be doing, since they only contribute to a physical quantity such as the charge in conjunction with the scalar potential, which is not modeled explicitly in this formulation. As a result, no actions can be currently taken to "fix" the formulation. The question of how to fix the $\mathbf{A}$-Φ TDIE is considered in Chapter 5, where a rigorous mathematical framework is used to analyze the system of equations.

4.2 Weighted Continuity Electric Field Integral Equation

This section examines a modification to the A-EFIE based on the physical meaning of (4.3) proposed in [14]. That is, a Green's function weighted form of the continuity equation. The idea is that the strong form of the continuity equation in the time domain may have been a poor constraining equation. By modifying the continuity equation into an integral form, better stability properties may be achieved. This new formulation is examined in the frequency domain and the time domain. It is compared to the original A-EFIE to determine the benefits, if any, of this new approach. For brevity, the weighted continuity electric field integral equation will be referred to as the WC-EFIE. When explicit reference is made to a frequency domain or time domain implementation, FD-WC-EFIE and TD-WC-EFIE will be used, respectively.

4.2.1 Frequency Domain WC-EFIE Formulation

The formulation for the WC-EFIE can be performed easily in the frequency domain. The first equation that represents the traditional $\mathcal{L}$-operator remains the same, while the second equation is modified to be

$$\int_S g(\mathbf{r}, \mathbf{r}', \omega) \Big[\nabla' \cdot \mathbf{J}(\mathbf{r}', \omega) - i\omega\rho(\mathbf{r}', \omega) \Big] dS' = 0. \tag{4.20}$$

This second equation can be discretized by expanding the current with normalized RWG functions, the charge with pulse basis functions, and then testing with pulse basis functions. Performing this gives the following matrix system to be solved after accounting for the charge neutrality constraint,

$$\begin{bmatrix} \mu_r \mathbf{V} & \epsilon_r^{-1} \mathbf{D}^T \mathbf{S} \mathbf{B} \\ \mathbf{F} \mathbf{S} \mathbf{D} & k_0^2 \mathbf{F} \mathbf{S} \mathbf{B} \end{bmatrix} \begin{Bmatrix} ik_0 \mathbf{j} \\ c_0 \mathbf{q}_r \end{Bmatrix} = \begin{Bmatrix} \eta_0^{-1} \mathbf{b} \\ \mathbf{0} \end{Bmatrix}. \tag{4.21}$$

The connection $\mathbf{D}$, forward $\mathbf{F}$, and backward $\mathbf{B}$ matrices all have the same definitions as in the FD-A-EFIE. Similarly, nothing has changed the excitation vector so this may be evaluated in the same way as the FD-A-EFIE. The integral operator matrices have been adjusted to separate the physical scaling constants from their definitions. Explicitly, they are

$$\mathbf{V}_{mn} = \int_{S_m} \int_{S_n} g(\mathbf{r}, \mathbf{r}', \omega)\, \mathbf{f}_m(\mathbf{r}) \cdot \mathbf{f}_n(\mathbf{r}') dS' dS \tag{4.22}$$

$$\mathbf{S}_{mn} = \int_{T_m} \int_{T_n} g(\mathbf{r}, \mathbf{r}', \omega)\, h_m(\mathbf{r}) h_n(\mathbf{r}') dS' dS. \tag{4.23}$$

It is to be noted that if the charge neutrality mapping matrices were not to be used, this method could be easily made to produce a symmetric matrix. This is done by scaling the second constraining equation with ϵ_r^{-1}. This does not change the physics of the equation, but simply opens the formulation to potentially more efficient matrix storage and specialized symmetric matrix solution methods. In fact, numerical experiments have shown that using a constraint preconditioner removes the need for the charge neutrality constraint. As a result, the FD-WC-EFIE may lead to more efficient algorithms if the symmetry is exploited. This is not investigated further here, and so all results and equations are for a system using the charge neutrality constraint.

A constraint preconditioner similar to that used in [14] can be easily developed for this formulation. The easier to invert matrix with a similar saddle point form is defined to be

$$\mathbf{P}_c = \begin{bmatrix} \mu_r \mathbf{V}_d & \epsilon_r^{-1} \mathbf{D}^T \mathbf{S}_d \mathbf{B} \\ \mathbf{F} \mathbf{S}_d \mathbf{D} & k_0^2 \mathbf{F} \mathbf{S}_d \mathbf{B} \end{bmatrix}, \tag{4.24}$$

where a subscript of d represents only taking the diagonal elements of the dense integral operator matrices. This matrix may be inverted using the

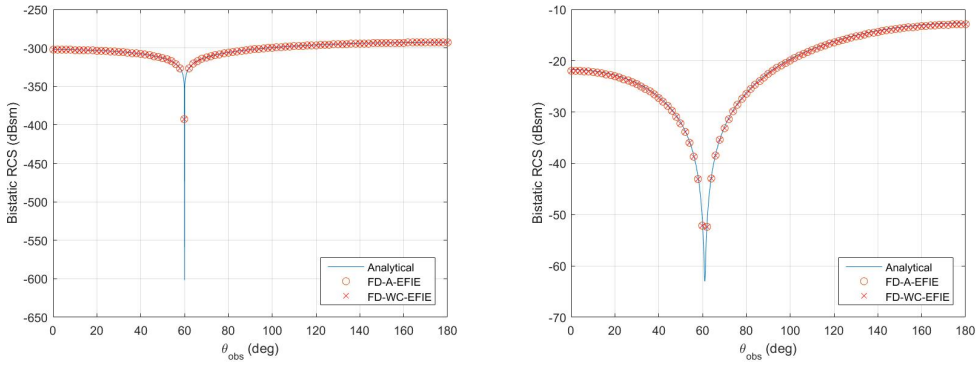

Figure 4.5: Accuracy comparison for the FD-A-EFIE and the FD-WC-EFIE for a 1 m radius PEC sphere at: (a) 1 Hz and (b) 10 MHz.

same approach illustrated in (3.11), therefore only requiring the numerical inversion of the smaller Schur complement matrix. Note that this preconditioner is used as a left preconditioner, while the one in (3.11) is used as a right preconditioner.

4.2.2 Frequency Domain WC-EFIE Numerical Results

Simulations of a 1 meter radius PEC sphere were conducted at a number of frequencies using the FD-A-EFIE and the proposed FD-WC-EFIE. Due to the frequency scaling of the matrix elements, the condition number for both methods was found to remain approximately constant from 1 Hz to 10 MHz. The condition number for each method was also found to be identical to the other, staying at an average value of 2028.49 with the deviation from this mean on $O(1)$ as the frequency was raised.

Two examples at opposite ends of the frequencies tested are shown in Fig. 4.5. Clearly, similar levels of accuracy are seen for the two methods. These solutions used an LU decomposition to solve the matrix system, with iterative solvers discussed next. Both simulations are for the same mesh of a 1 meter radius PEC sphere with an average edge length of 0.2718 m. This corresponds to an average edge length of $9.067 \times 10^{-3}\lambda$ at 10 MHz and $9.067 \times 10^{-10}\lambda$ at 1 Hz.

Preliminary results using a GMRES-30 (i.e., it restarts at 30 inner iterations) with a residual of 10^{-8} have been promising. Using the preconditioners

has shown similar results for both methods, although the FD-WC-EFIE has been seen to converge to a slightly lower residual in $O(1)$ less iterations. More study into the difference of the two methods on a more complicated scatterer is warranted to see if the FD-WC-EFIE can produce a large enough improvement in convergence to be considered a better alternative to the FD-A-EFIE.

4.2.3 Time Domain WC-EFIE Formulation

The promising results in the frequency domain warrant implementing this method in the time domain to see if it will have better stability than the TD-A-EFIE. The equations for this approach are presented before discussing numerical results.

The matrix system of the TD-WC-EFIE shares great similarity with that of the TD-A-EFIE. The first equation that represents the radiation of the scattered field through the $\mathcal{L}$ operator remains unchanged, while the second equation is adjusted to the Green's function weighted form of the continuity equation. The matrix system to be solved for this approach becomes

$$\begin{bmatrix} \Delta t \mu_r \mathbf{V}^{(0)} & -\epsilon_r^{-1}\mathbf{D}^T\mathbf{S}^{(0)}\mathbf{B} \\ \mathbf{F}\mathbf{S}^{(0)}\mathbf{D} & \left(\Delta t c_0^2\right)^{-1}\mathbf{F}\dot{\mathbf{S}}^{(0)}\mathbf{B} \end{bmatrix} \begin{Bmatrix} \left(c_0\Delta t\right)^{-1}\mathbf{j}^{(i)} \\ c_0\mathbf{q}_r^{(i)} \end{Bmatrix} = \begin{Bmatrix} \eta_0^{-1}\mathbf{b}^{(i)} \\ \mathbf{0} \end{Bmatrix} - \sum_{j=i-j_{max}}^{i-1} \begin{bmatrix} \Delta t \mu_r \mathbf{V}^{(i-j)} & -\epsilon_r^{-1}\mathbf{D}^T\mathbf{S}^{(i-j)}\mathbf{B} \\ \mathbf{F}\mathbf{S}^{(i-j)}\mathbf{D} & \left(\Delta t c_0^2\right)^{-1}\mathbf{F}\dot{\mathbf{S}}^{(i-j)}\mathbf{B} \end{bmatrix} \begin{Bmatrix} \left(c_0\Delta t\right)^{-1}\mathbf{j}^{(j)} \\ c_0\mathbf{q}_r^{(j)} \end{Bmatrix}. \quad (4.25)$$

The integral operators are defined as

$$\mathbf{V}_{mn}^{(i-j)} = \int_{S_m}\int_{S_n}\sum_{l=0}^{N_h} a_l \dot{\xi}_l^{(i-j)} \mathbf{f}_m(\mathbf{r})\cdot\mathbf{f}_n(\mathbf{r}')\frac{P_l(\hat{R})}{4\pi R}dS'dS \quad (4.26)$$

$$\mathbf{S}_{mn}^{(i-j)} = \int_{T_m}\int_{T_n}\sum_{l=0}^{N_h} a_l \xi_l^{(i-j)} h_m(\mathbf{r})h_n(\mathbf{r}')\frac{P_l(\hat{R})}{4\pi R}dS'dS \quad (4.27)$$

$$\dot{\mathbf{S}}_{mn}^{(i-j)} = \int_{T_m}\int_{T_n}\sum_{l=0}^{N_h} a_l \dot{\xi}_l^{(i-j)} h_m(\mathbf{r})h_n(\mathbf{r}')\frac{P_l(\hat{R})}{4\pi R}dS'dS, \quad (4.28)$$

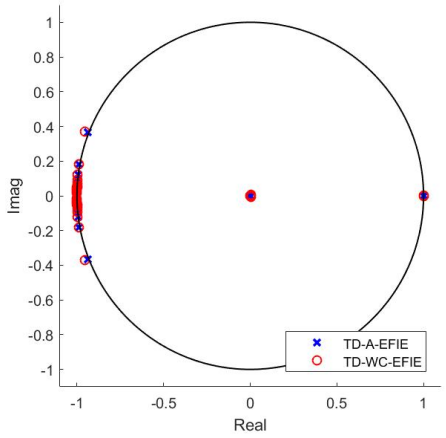

Figure 4.6: Eigenvalues for the TD-A-EFIE and TD-WC-EFIE.

where the temporal convolutions have been accounted for in

$$\xi_l^{(i-j)} = \int_{-\infty}^{\infty} P_l(k_1 t' + k_2) T\big((i-j)\Delta t - \zeta/c - t'\big) dt' \tag{4.29}$$

$$\dot{\xi}_l^{(i-j)} = \int_{-\infty}^{\infty} P_l(k_1 t' + k_2) \dot{T}\big((i-j)\Delta t - \zeta/c - t'\big) dt'. \tag{4.30}$$

All other matrices and vectors in (4.25) are defined in the same way as before for the TD-A-EFIE in Section 3.3. More details on evaluating the matrix elements may be found in Section 2.4.

4.2.4 Time Domain WC-EFIE Numerical Results

Numerical results are only presented to compare the stability of the TD-WC-EFIE and TD-A-EFIE. The accuracy for both methods is good, with similar results achieved as those in Fig. 4.5. The presented results are for a simulation with a center frequency of 1 MHz, a bandwidth of 500 kHz, and a time step of 33.33 ns. The simulations used a quadratic B-spline temporal basis function.

An eigenvalue stability analysis of the two methods was performed. The eigenvalues from the stability analysis are shown in Fig. 4.6. It is seen that the TD-WC-EFIE approach has shifted a number of the eigenvalues further out of the unit circle, slightly increasing the instability of the method.

Although these results appear to show the TD-WC-EFIE is not useful,

there are a number of benefits that the TD-WC-EFIE has which the TD-A-EFIE does not. First, as with the FD-WC-EFIE, the TD-WC-EFIE can be changed to a symmetric form. Second, there are many temporal basis functions where the TD-WC-EFIE is easier to implement than the TD-A-EFIE. As an example, the Lagrange interpolating functions only are piecewise-continuous, making the derivatives piecewise-discontinuous. However, the TD-A-EFIE requires the evaluation of the derivative of these basis functions exactly at the discontinuous point. This is ambiguous and can lead to a loss of accuracy if a correct implementation is not found. The TD-WC-EFIE has no such complication, since this integral form of the continuity equation allows the piecewise-discontinuous basis functions to be easily used. This is also simpler than the approach proposed in [41] that integrates the continuity equation in time. That approach requires a recursive calculation of these integrals to not increase the computational complexity of the method. However, using the Green's function weighting handles this in an intuitive and simple manner using matrices that must already be calculated for the $\mathcal{L}$ operator equation.

Through the analysis in Chapter 5, it will be shown how a stable implementation of the TD-A-EFIE and TD-WC-EFIE can be achieved. Combining the stability with the other benefits of the TD-WC-EFIE, this method is likely better than the TD-A-EFIE.

CHAPTER 5

PROVABLY STABLE A-Φ TIME DOMAIN INTEGRAL EQUATIONS

The failure of the heuristic methods used for developing the integral equations in Chapter 4 suggests that a new approach needs to be used. The approach adopted in this chapter is to use a rigorous functional framework that was developed to analyze the TD-EFIE. This functional framework may be extended to develop provably stable **A**-Φ TDIEs.

In this chapter, the historical context and motivations of the mathematical framework are discussed. Following this, a number of preliminary concepts are reviewed before introducing the function spaces that are the subject of the functional framework. The use of this rigorous mathematical analysis is then introduced in the context of the TD-EFIE. With all of the necessary concepts introduced, the extension of the functional framework to a variety of **A**-Φ TDIEs is discussed in detail. Following a discussion of how to discretize these equations, numerical results are presented which highlight the stability and accuracy of the developed **A**-Φ TDIEs.

5.1 Stability Proofs of Time Domain Integral Equations

Throughout the early development of time domain integral equations, it was quickly realized that many implementations had issues with stability. Substantial work was done in various communities to try and alleviate these problems, with varying degrees of success achieved. Common to all of these methods was an engineering mentality, i.e., attempting to solve the problem with ad hoc methods without necessarily requiring a complete understanding of the underlying problem. As pointed out in [50], each of these methods had an absence of mathematical analysis of the underlying integral equations. This led to the thought that, perhaps, the problem with these methods was

the omission of some essential feature. The lack of this essential feature could then make the proposed techniques not well-grounded, leading to the various problems encountered in practice.

The author of [50] further points out that the problem with the mathematical basis for these integral equations can be seen immediately by looking at the operators. All the different integral equations involve surface integrals of terms where the function and some degree of time derivative is required. Further, the arguments of these functions depend on a mixture of the space and time variables. This invalidates the consideration of these integrals in a traditional Fredholm sense; and so invalidates the typical mathematical framework for determining whether the equations admit a unique solution that is continuous with respect to the data. This is a fundamental question that must be answered to be able to properly analyze numerical schemes that attempt to solve the given equations.

In the interest of answering this, and related questions for the analysis of TDIEs, a particularly successful mathematical framework was developed. This functional framework is reviewed in [50] for acoustic problems, with small discussions related to the extension to electromagnetics. Unfortunately most of this work is published exclusively in French, and often only in theses that do not appear to be easily accessible online [51]. The work that is accessible is still often in French, and is written for the mathematical community rather than engineering readers [52]. Some authors in the engineering community for electromagnetic TDIEs have invoked the results of this mathematical framework. However, the discussion of the concepts are extremely limited and are largely hearsay since the works being cited are not accessible to be reviewed [45, 48, 53, 54].

Recently, [15] has given a more thorough discussion of the important results of [51]. It also presents a methodology for extending these results to other model equations without requiring a new and full mathematical analysis to be developed. This approach will be followed in this thesis, where it will be shown that the results of [15, 51] can be extended to suggest a number of provably stable A-Φ formulation TDIEs.

Due to the highly mathematical nature of the discussions in this chapter, it is useful to first recall the simple discussion on the stability of TDIEs in Section 2.3. There, an analogy was drawn between an "infinite impulse response" system and the MOT system. It was mentioned that to have a

stable system, the matrix representation of the continuous integral operators must be accurately calculated. This encompassed the simple observation that the integrals must be calculated accurately numerically, which was covered in detail in Section 2.4. It was also mentioned that for the matrix representation to inherit the stability of the continuous system required using appropriate basis and testing functions. In particular, the basis functions need to be in the domain of the integral operator, while the testing functions need to be in the dual space of the range of the integral operator [15, 55]. The focus of this chapter is to rigorously determine the correct integral operators to use in an **A**-Φ formulation TDIE, as well as the associated domains and ranges of the integral operators.

5.2 Functional Framework

The focus of this section is to review the important definitions of the functional framework developed in [51] and reported in [15]. To begin, the statement of the problem and the model equations are briefly recalled to introduce the notation used throughout this section, which is adapted from that presented in [15].

5.2.1 Problem Statement

Consider a bounded domain $\Omega^i \subset \mathbb{R}^3$ which represents the scatterer of interest, with its closure defined as $\overline{\Omega^i}$. The exterior region is defined as $\Omega^e = \mathbb{R}^3 \setminus \overline{\Omega^i}$, which is assumed to be a homogeneous region for the current purposes. The unit normal vector, $\hat{n}$, is defined on the interface $S = \partial\Omega^i = \partial\Omega^e$ and is assumed to point from Ω^i to Ω^e. For a PEC scatterer, the jump condition requires the tangential component of the electric field to vanish on the interface with free space. As an initial condition, it is required that the incident field has not yet reached the scatterer so that the induced current density $\mathbf{J}(\mathbf{r}, t)$ is zero $\forall t < 0$. Provided these conditions are met, the exterior scattering problem can be formulated as a boundary integral equation, given

for the TD-EFIE as

$$-\hat{n}\times\hat{n}\times\int_S\left[\mu\frac{\dot{\mathbf{J}}(\mathbf{r}',\tau)}{4\pi R}-\epsilon^{-1}\nabla\int_{-\infty}^{\tau}\frac{\nabla'\cdot\mathbf{J}(\mathbf{r}',t')}{4\pi R}dt'\right]dS'=-\hat{n}\times\hat{n}\times\mathbf{E}^{\text{inc}}(\mathbf{r},t), \tag{5.1}$$

for $(\mathbf{r},t)\in S\times\mathbb{R}_+$ ($\mathbb{R}_+$ means $\mathbb{R}\geq 0$). Further, $\tau=t-R/c$ is the retarded time where $R=|\mathbf{r}-\mathbf{r}'|$ and c is the speed of light in the external medium. As has been discussed previously, the integral in time is challenging to discretize efficiently so it is common practice in the engineering literature to instead enforce the time derivative of (5.1), yielding

$$-\hat{n}\times\hat{n}\times\int_S\left[\mu\frac{\ddot{\mathbf{J}}(\mathbf{r}',\tau)}{4\pi R}-\epsilon^{-1}\nabla\frac{\nabla'\cdot\mathbf{J}(\mathbf{r}',\tau)}{4\pi R}\right]dS'=-\hat{n}\times\hat{n}\times\dot{\mathbf{E}}^{\text{inc}}(\mathbf{r},t). \tag{5.2}$$

5.2.2 Relevant Sobolev Spaces

To properly investigate the mathematical properties of these integral equations, the problem must be recast into a variational framework with functions defined in appropriate function spaces. The function space developed in [51] is denoted as $\mathscr{H}^s$, and will be defined in more detail at the end of this section. It will be seen in later sections that this function space will not be able to cover all the needed functions; however, it does provide most of the foundation.

Due to the complexity of the problem in the time domain, most of the analysis is performed by taking a Fourier-Laplace transform of the model equations. The results found in the Laplace domain can then be related back to the time domain equations through the use of an inverse transform and the Paley-Wiener theorem [50]. Further, invoking a form of Parseval's theorem for appropriately defined Sobolev spaces allows for finite norms to be found which are related to the electromagnetic energy, demonstrating the stability for appropriately selected basis and testing functions. With this in mind, it is now possible to define the necessary properties of this functional framework before stating the variational problem to be solved.

To begin, it is useful to review the spatial properties of typical Sobolev spaces for electromagnetics, as these are needed concepts in defining $\mathscr{H}^s$. The details of these spatial Sobolev spaces are not rigorously defined in [15],

but discussion related to it may be found in [52, 56]. Following this, the needed definitions related to the Fourier-Laplace transform can be presented within the context of TDIEs. Finally, with all the constituent pieces properly defined, $\mathscr{H}^s$ can be introduced.

Spatial Sobolev Spaces

The original interest in defining Sobolev spaces in the context of integral equations was to rigorously define the function spaces that acted as the domain and range for different integral operators. Although the most familiar function space in many areas of physics is the Hilbert space L^2, it is quickly seen that this is not quite the concept needed for the present analysis. This led to the introduction of Sobolev spaces, which capture the notion that physical solutions should produce finite energy in any bounded domain. The core complication is that to calculate the energy of a solution often requires that the function and its gradient be square integrable (for scalar fields). This is obviously more restrictive of a space than L^2, so the concept of a Sobolev space is used to explicitly state the formal requirements needed of any solution to have the desired physical properties.

For the definitions of these function spaces in the external and interior domains of a scatterer, the concept is a simple integer order Sobolev space. This requires a function and its derivatives up to order ℓ be square integrable, where ℓ is an integer. This space is denoted as $H^\ell(\cdot)$, where the argument of the function space can be either Ω^i or Ω^e. This is a special notation for Sobolev spaces, which implies that the space is also a Hilbert space and that the inner product used in any norms is to be the L^2 one. For a typical problem, this becomes H^1 in these regions so that the solution will have finite energy, as desired.

The complication for integral equations comes from determining how to characterize the boundary values of these functions on S. This was handled using *trace theorems*, which result in the creation of a new space known as $H^{\frac{1}{2}}(S)$. The need for this space can be understood by considering a simple example, for instance, L^2. It is well known that L^2 "functions" are not really functions at all, i.e., they do not take on a definite value at each point. Instead, "functions" in L^2 are considered to be equivalence classes of functions. That is, functions which differ from one another in a special way

are considered to be the same L^2 function. In the case of L^2, all properties are defined in terms of integrals. In a crude sense, functions are then considered to be in the same equivalence class if they only differ by values that *do not change the result of the integral locally*. For instance, a function that is zero almost everywhere, but takes on finite values at isolated spikes (i.e., only has a value at a single point) is considered to be equivalent to the zero function in an L^2 sense.

In the case of $H^{\frac{1}{2}}(S)$, the same type of problem that occurred for L^2 functions occurs when trying to extend definitions of functions in $H^1(\Omega^i)$ and $H^1(\Omega^e)$ to a surface. This is because a two-dimensional surface in $\mathbb{R}^3$ is similar to isolated points on a one-dimensional line (i.e., it has a measure of zero). This is a simplified perspective of what the trace theorems are needed to address [56]. Although an important part of the development of functional analysis for integral equations, the details of this theory are not needed for the present purposes. As such, the details will not be discussed any further.

As already alluded to, the space $H^{\frac{1}{2}}(S)$ is made up of the boundary values of the functions in $H^1(\Omega^i)$ and $H^1(\Omega^e)$. The space $H^{\frac{1}{2}}(S)$ is a Hilbert space, and is seen to be smaller than L^2, since not all functions in L^2 can be extended into the regions Ω^i or Ω^e in a way that the necessary components are all square integrable. The inner product for this space is given in [56]; and has the feature that in addition to the standard L^2 inner product it also requires the functions to be integrated over a singular kernel of order R^{-3}. This concept is also extended to the normal derivatives (for scalar fields) of functions in $H^1(\cdot)$, and produces the space $H^{-\frac{1}{2}}(S)$. This is actually the dual space to $H^{\frac{1}{2}}$ and has a more complicated norm, which is discussed in [56].

These concepts may be extended to electromagnetic fields, which, for the energy to be bounded, requires that the function and its curl be square integrable. This leads to the following definitions of function spaces that will be of interest for electromagnetic fields.

Definition 1. *For a bounded domain D, the spaces $H(\mathrm{curl}, D)$ and $H(\mathrm{div}, D)$ are*

$$H(\mathrm{curl}, D) \coloneqq \left\{ \mathbf{v} \in L^2(D)^3, \nabla \times \mathbf{v} \in L^2(D)^3 \right\} \tag{5.3}$$

$$H(\mathrm{div}, D) \coloneqq \left\{ \mathbf{v} \in L^2(D)^3, \nabla \cdot \mathbf{v} \in L^2(D) \right\}, \tag{5.4}$$

with norms defined respectively as

$$||\mathbf{v}||_{\text{curl}} \coloneqq \left(||\mathbf{v}||^2 + ||\nabla \times \mathbf{v}||^2 \right)^{\frac{1}{2}} \tag{5.5}$$

$$||\mathbf{v}||_{\text{div}} \coloneqq \left(||\mathbf{v}||^2 + ||\nabla \cdot \mathbf{v}||^2 \right)^{\frac{1}{2}}, \tag{5.6}$$

where the unindexed norms refer to an L^2 norm.

Note that the notation $L^2(D)^3$ is shorthand for $L^2(D) \times L^2(D) \times L^2(D)$, i.e., all of the components of the vector function $\mathbf{v}$ reside in $L^2(D)$. Further, this is a definition that deals only with the spatial aspects of the functions. As a result, it can be used in either the frequency or time domain.

In source-free regions, the electromagnetic fields are divergence free, which implies that the appropriate energy space for the fields will be the intersection of $H(\text{curl}, D)$ and $H(\text{div}, D)$. The boundary values of these spaces are

$$\mathbf{v} \in H(\text{curl}, D) \implies \hat{n} \times \mathbf{v}|_S \in H^{-\frac{1}{2}}(S)^3 \tag{5.7}$$

$$\mathbf{v} \in H(\text{div}, D) \implies \hat{n} \cdot \mathbf{v}|_S \in H^{-\frac{1}{2}}(S), \tag{5.8}$$

where S is still used to denote the interface that the boundary values are being defined on. Integral equations are mainly concerned with the tangential fields to a surface (to define the equivalent currents). These tangential fields also obey Maxwell's equations, so an additional property can be found. This is that a surface divergence of tangential fields does not change the spatial order of smoothness of the fields [56]. This suggests the following definition of a space that will be used in the definition of $\mathscr{H}^s$ at the end of this section.

Definition 2. *The boundary values of electromagnetic fields on the interface S between the external and internal regions of a scatterer reside in*

$$H^{-\frac{1}{2}}(\text{div}, S) \coloneqq \left\{ \mathbf{v} \in H^{-\frac{1}{2}}(S)^3, \hat{n} \cdot \mathbf{v} = 0, \nabla_S \cdot \mathbf{v} \in H^{-\frac{1}{2}}(S) \right\}, \tag{5.9}$$

where $\nabla_S \cdot$ is explicitly noting that the divergence is a surface divergence on S.The norm for this space is given in [56].

A similar definition may also be made for a curl space [52, 56], but this is not needed here and so will not be presented. Of particular importance for

the discretization of the integral operators is that the RWG functions are members of the space $H^{-\frac{1}{2}}(\text{div}, S)$.

Fourier-Laplace Transform Definitions

Before discussing the temporal properties of the function space that will be used in the variational framework of the TDIEs, it is prudent to recall some relevant definitions for Fourier-Laplace transforms. This is because the overall complexity of the integral operators makes it easier to derive properties in the Laplace domain. These results can then be used to bound the time domain results through Parseval's theorem. All of these definitions are taken explicitly from [15] with only minor changes to keep notation consistent throughout this thesis.

Definition 3. *[15] For E a Hilbert space, $\mathcal{D}'_+(E)$ denotes the space of distributions in $\mathbb{R}$ with values in E and zero for all $t < 0$, and $\mathcal{S}'_+(E)$ denotes the space of tempered distributions in $\mathcal{D}'_+(E)$. The space of Laplace transformable functions $LT(\sigma, E)$ is defined for $\sigma \in \mathbb{R}$ with $\sigma > 0$ as*

$$LT(\sigma, E) \coloneqq \left\{ \mathbf{g} \in \mathcal{D}'_+(E),\, e^{-\sigma t}\mathbf{g} \in \mathcal{S}'_+(E) \right\} \tag{5.10}$$

where $\mathbf{g}(\mathbf{r}, t)$ is a vector function depending on space and time. Similar definitions are applicable to scalar functions.

This definition is rigorous, but somewhat obstructive to simple understanding. It is saying the following: vector functions will be defined later which depend on both space and time. The temporal dependence is always considered to only matter for $t > 0$. The spatial components of the vector function will reside in a Hilbert space, denoted as E in this definition. For many functions, the Fourier transform may not exist due to convergence problems. The Fourier-Laplace transform defines a constant damping parameter, σ, which is required to make the Fourier-Laplace transform integral converge.

The Fourier-Laplace transform is given in the next definition.

Definition 4. *[15] For $\mathbf{g} \in LT(\sigma, E)$, the Fourier-Laplace transform is*

defined as

$$\hat{\mathbf{g}}(\mathbf{r},\gamma) \coloneqq \int_{-\infty}^{\infty} e^{i\gamma t}\mathbf{g}(\mathbf{r},t)dt \tag{5.11}$$

for $\gamma = \eta + i\sigma$, where i is the imaginary unit: $i^2 = -1$. Similar definitions are applicable to scalar functions.

The key idea behind these definitions is that because the functions to be considered are causal, useful analytic properties can be found for the functions in the Laplace domain. This helps to guarantee that the integral over the Laplace space for Parseval's theorem will be finite. There are more complications related to the proper form of Parseval's theorem in the Laplace domain, but these details are extraneous to the current discussion [52].

Spatiotemporal Function Spaces

Having covered the necessary concepts of both spatial and temporal properties independently, the full spatiotemporal function spaces may now be defined.

Definition 5. *[15] The function space $\mathscr{H}^s$ for $s \in \mathbb{R}$ is defined as*

$$\begin{aligned}\mathscr{H}^s &\coloneqq H^s_\sigma\big(\mathbb{R}_+, H^{-\frac{1}{2}}(\mathrm{div}, S)\big) \\ &\coloneqq \left\{\mathbf{g} \in LT\left(\sigma, H^{-\frac{1}{2}}(\mathrm{div}, S)\right), ||\mathbf{g}||^2_{s,\sigma,H^{-\frac{1}{2}}(\mathrm{div},S)} < \infty\right\}\end{aligned} \tag{5.12}$$

where

$$||\mathbf{g}||^2_{s,\sigma,H^{-\frac{1}{2}}(\mathrm{div},S)} \coloneqq \frac{1}{2\pi}\int_{-\infty+i\sigma}^{\infty+i\sigma} |\gamma|^{2s}||\hat{\mathbf{g}}(\cdot,\gamma)||^2_{H^{-\frac{1}{2}}(\mathrm{div},S)}d\gamma \tag{5.13}$$

for $\sigma \in \mathbb{R}_+ : \sigma > 0$.

This definition requires some further discussion to better elucidate its meaning. It is first recognized that the s index is related to differentiability in the time domain. The σ parameter is required for the Fourier-Laplace transform to be well defined (i.e., it determines the damping that will make the integrals converge). It is further seen that $\mathscr{H}^s$ is composed only of causal functions (due to the $\mathbb{R}_+$). The spatial component of the functions resides

in $H^{-\frac{1}{2}}(\text{div}, S)$, which makes them meaningful functions from the electromagnetics point of view. The norm of these functions that is required to be finite is calculated in the Laplace domain, with Parseval's theorem allowing the finiteness to also be valid in the temporal domain. The exact form of the norm is to actually integrate the spatial Sobolev space norm over all frequency. This is, in effect, requiring that the energy from the electromagnetic boundary values be finite at all frequencies in such a way that the combination of all frequencies together is still finite.

Although the definition is complicated, it is seen that the physical meaning is reasonable. For the purposes of this thesis, the full power of these definitions is not required. The review of their meaning is important, however, to better understand the implications on the solution process for the TDIEs of interest to be studied.

One final point is related to the inner product for $\mathscr{H}^s$.

Definition 6. *[15] The Hilbert space $\mathscr{H}^s$ is equipped with a space-time inner product given by*

$$\langle \mathbf{g}(\mathbf{r},t), \mathbf{h}(\mathbf{r},t) \rangle_\sigma \coloneqq \int_{\mathbb{R}} e^{-2\sigma t} \int_S \mathbf{g}(\mathbf{r},t) \cdot \mathbf{h}(\mathbf{r},t) dS dt \tag{5.14}$$

for $\mathbf{g} \in \mathscr{H}^s$ and $\mathbf{h} \in \mathscr{H}^{-s}$.

This inner product will be useful in defining the bilinear forms that describe the variational problem to be solved. Further, it will be instrumental in understanding the properties of the equations derived in the next sections. In particular, it allows one to quickly determine the range of the different integral operators to be discussed in the next sections.

These definitions are appropriate for many of the vector functions that will be encountered throughout this chapter. However, it is also necessary for this thesis to have similar definitions for scalar quantities.

Definition 7. *The function space $\mathcal{H}^s$ for $s \in \mathbb{R}$ is defined as*

$$\begin{aligned} \mathcal{H}^s &\coloneqq H^s_\sigma\big(\mathbb{R}_+, H^{-\frac{1}{2}}(S)\big) \\ &\coloneqq \left\{ g \in LT\left(\sigma, H^{-\frac{1}{2}}(S)\right), ||g||^2_{s,\sigma,H^{-\frac{1}{2}}(S)} < \infty \right\} \end{aligned} \tag{5.15}$$

where

$$||g||^2_{s,\sigma,H^{-\frac{1}{2}}(S)} \coloneqq \frac{1}{2\pi}\int_{-\infty+i\sigma}^{\infty+i\sigma} |\gamma|^{2s}||\hat{g}(\cdot,\gamma)||^2_{H^{-\frac{1}{2}}(S)}d\gamma \tag{5.16}$$

for $\sigma \in \mathbb{R}_+ : \sigma > 0$.

Definition 8. *The Hilbert space* $\mathcal{H}^s$ *is equipped with a space-time inner product given by*

$$\langle g(\mathbf{r},t), h(\mathbf{r},t)\rangle_\sigma \coloneqq \int_{\mathbb{R}} e^{-2\sigma t}\int_S g(\mathbf{r},t)h(\mathbf{r},t)dSdt \tag{5.17}$$

for $g \in \mathcal{H}^s$ *and* $h \in \mathcal{H}^{-s}$.

These definitions follow the same form as those for $\mathscr{H}^s$, and have the same type of physical meaning.

5.3 Electric Field Integral Equation Variational Formulation

With the basic structure of the appropriate function space defined, the variational problem can now be developed. In [51], the original problem is formulated in terms of the surface current and charge density as unknowns. This is modified to only use the current density as the unknowns in [15], since this work was interested in solving the differentiated EFIE at middle frequencies. For the current purposes of this thesis, it is more useful to have a formulation that lies somewhere in between these two approaches to better reflect the actual discretization procedure that will be used. To make this point clear, the original formulation from [51] will be recalled before making modifications similar to those proposed in [15] to arrive at a form that will be useful for the present purposes.

As was alluded to in the last paragraph, the original function space actually used in [51] considers the current density and charge density as separate unknowns. This requires a slight modification to the function space presented in Section 5.2.2.

Definition 9. *[15] For $s \in \mathbb{R}$ and $\sigma > 0$,*

$$\mathscr{H}^s_{\rho,\mathbf{J}} \coloneqq \left\{ \big(\rho, \mathbf{J}\big) \in \mathcal{H}^s \times \mathscr{H}^s,\, \nabla \cdot \mathbf{J} + \dot{\rho} = 0 \right\}. \tag{5.18}$$

Note that in this definition, the $\times$ symbol is denoting a Cartesian product between the two function spaces, which are both defined on a two-dimensional manifold S. A subtle property of this definition that will be useful later is the relationship between spatial derivatives and the temporal regularity of a function (i.e., what temporal function space something is in after a spatial derivative is applied).

Lemma 1. *Electromagnetic functions have the property that spatial derivatives such as the gradient, divergence, and curl lower the regularity of the functions temporally by one degree. That is, if a function is in a temporal function space of H^s_σ then the spatial derivative of it is in H^{s-1}_σ.*

Proof. The proof for the divergence follows easily from the continuity equation in Definition 9. Both the charge and current are in the same temporal function space, so for the continuity equation to make sense requires $\nabla \cdot \mathbf{J}$ to have one degree lower temporal regularity than $\mathbf{J}$. Similarly, for Maxwell's equations to hold requires that the curl has the same property.

This property for the gradient can be illustrated by considering it in the context of inner products in $\mathscr{H}^s$ and $\mathcal{H}^s$. Consider $\nabla f \in \mathscr{H}^s$ and $\mathbf{J}' \in \mathscr{H}^{-s}_{\rho,\mathbf{J}}$. The inner product of these two functions is

$$\langle \nabla f, \mathbf{J}' \rangle_\sigma = -\langle f, \nabla \cdot \mathbf{J}' \rangle_\sigma = \langle f, \dot{\rho}' \rangle_\sigma \tag{5.19}$$

In going from the first equation to the second, Gauss' theorem is applied and the integral of the boundary term is seen to be zero. For the final equality to hold requires that $f \in \mathcal{H}^{s+1}$. This means, that at least in the context of these inner products, the gradient also affects the temporal regularity of functions. □

The following theorems may now be stated for the TD-EFIE, as given by [51] and reproduced in [15].

Theorem 1. *[15, 51] The EFIE admits the following variation formulation.* $\forall(\mathbf{E}^{\text{inc}}\times\hat{n}) \in \mathscr{H}^{\frac{3}{2}}$ *search for* $(\rho, \mathbf{J}) \in \mathscr{H}^{\frac{1}{2}}_{\rho,\mathbf{J}}$ *such that* $\forall(\rho', \mathbf{J}') \in \mathscr{H}^{\frac{1}{2}}_{\rho,\mathbf{J}}$:

$$b\big((\rho, \mathbf{J}), (\rho', \mathbf{J}')\big) = \int_{\mathbb{R}} e^{-2\sigma t} \int_S \big(\hat{n}\times(\mathbf{E}^{\text{inc}}\times\hat{n})\big) \cdot \ddot{\mathbf{J}}'(\mathbf{r}, t)\, dSdt, \tag{5.20}$$

with the bilinear form b defined as

$$b\big((\rho, \mathbf{J}), (\rho', \mathbf{J}')\big) = \int_{\mathbb{R}} e^{-2\sigma t} \Bigg\{ \int_S \int_S \Bigg[\mu \frac{1}{4\pi R} \dot{\mathbf{J}}(\mathbf{r}', \tau) \cdot \ddot{\mathbf{J}}'(\mathbf{r}, t) + \epsilon^{-1} \frac{1}{4\pi R} \rho(\mathbf{r}', \tau) \dddot{\rho}'(\mathbf{r}, t) \Bigg] dS'dS \Bigg\} dt. \tag{5.21}$$

Theorem 2. *(Uniqueness, [15, 51]) If* $(\mathbf{E}^{\text{inc}}\times\hat{n}) \in \mathscr{H}^{\frac{3}{2}}$*, then the variational formulation admits a unique solution* $(\rho, \mathbf{J}) \in \mathscr{H}^{\frac{1}{2}}_{\rho,\mathbf{J}}$.

Theorem 3. *(Stability, [15, 51]) The following bounds on the solution* $(\rho, \mathbf{J})$ *hold:*

$$||\rho||_{\frac{1}{2},\sigma,H^{-\frac{1}{2}}(S)} \leq C(S)\sigma^{-1} ||\mathbf{E}^{\text{inc}}\times\hat{n}||_{\frac{3}{2},\sigma,H^{-\frac{1}{2}}(\text{div},S)} \tag{5.22}$$

$$||\mathbf{J}||_{\frac{1}{2},\sigma,H^{-\frac{1}{2}}(\text{div},S)} \leq C(S)\sigma^{-1} ||\mathbf{E}^{\text{inc}}\times\hat{n}||_{\frac{3}{2},\sigma,H^{-\frac{1}{2}}(\text{div},S)}. \tag{5.23}$$

The proofs for these theorems should be in [51]. In simple terms, Theorem 2 gives the physical requirements for an incident field to lead to a unique solution to the variational problem. The important point for Theorem 3 is that the bounds that hold for the solution are related to the electromagnetic energy, so that the stability is achieved in a meaningful way. Further, the requirement on the incident field is not very restrictive. This is because of physical reasons the incident field is typically smooth, and decays appropriately for the simulation to be conducted over a finite time interval.

It is now desired to rewrite the variational form of the EFIE in a more suggestive way. This is done to make the discretization choices more explicit.

Lemma 2. *The variational formulation of Theorem 1 is equivalent to the following formulation.*

$\forall(\mathbf{E}^{\text{inc}}\times\hat{n})\in\mathscr{H}^{\frac{3}{2}}$ *search for* $(\rho,\mathbf{J})\in\mathscr{H}^{\frac{1}{2}}_{\rho,\mathbf{J}}$ *such that* $\forall\mathbf{J}'\in\mathscr{H}^{\frac{1}{2}}$:

$$d\big((\rho,\mathbf{J}),\mathbf{J}'\big)=\int_{\mathbb{R}}e^{-2\sigma t}\int_{S}\big(\hat{n}\times(\mathbf{E}^{\text{inc}}(\mathbf{r},t)\times\hat{n})\big)\cdot\ddot{\mathbf{J}}'(\mathbf{r},t)\,dSdt \tag{5.24}$$

with the bilinear form d *defined as*

$$\begin{aligned}d\big((\rho,\mathbf{J}),\mathbf{J}'\big)=\int_{\mathbb{R}}e^{-2\sigma t}\Bigg\{\int_{S}\int_{S}\Bigg[&\mu\frac{1}{4\pi R}\dot{\mathbf{J}}(\mathbf{r}',\tau)\cdot\ddot{\mathbf{J}}'(\mathbf{r},t)\\&-\epsilon^{-1}\frac{1}{4\pi R}\rho(\mathbf{r}',\tau)\nabla\cdot\ddot{\mathbf{J}}'(\mathbf{r},t)\Bigg]dS'dS\Bigg\}dt.\end{aligned} \tag{5.25}$$

Proof. As was previously noted $(\rho',\mathbf{J}')\in\mathscr{H}^{s}_{\rho,\mathbf{J}}$ requires the continuity equation to hold between ρ' and $\mathbf{J}'$. This allows the bilinear form b to be rewritten by eliminating the testing function ρ' through the continuity equation. □

The bilinear form d is more preferable for the later derivations. This is because the testing function being written exclusively in terms of the current is how engineering discretizations of the equation are actually performed. That is, by multiplying an equation by an RWG testing function which can have a gradient then transferred onto it.

Finally, it is useful to rewrite the bilinear form d as a bounded inner product that is equivalent to the EFIE variational problem.

Lemma 3. *The bilinear form* d *may be expressed as an inner product. The equivalence is*

$$d\big((\rho,\mathbf{J}),\mathbf{J}'\big)=\left\langle\int_{S}\left[\mu\frac{\dot{\mathbf{J}}(\mathbf{r}',\tau)}{4\pi R}+\epsilon^{-1}\nabla\frac{\rho(\mathbf{r}',\tau)}{4\pi R}\right]dS',\ddot{\mathbf{J}}'(\mathbf{r},t)\right\rangle_{\sigma} \tag{5.26}$$

with $(\rho,\mathbf{J})\in\mathscr{H}^{\frac{1}{2}}_{\rho,\mathbf{J}}$ *and* $\mathbf{J}'\in\mathscr{H}^{\frac{1}{2}}$. *Similarly, the excitation of the variational problem of Lemma 2 may be written as*

$$\begin{aligned}\int_{\mathbb{R}}e^{-2\sigma t}\int_{S}\big(\hat{n}\times(\mathbf{E}^{\text{inc}}(\mathbf{r},t)\times\hat{n})\big)\cdot\ddot{\mathbf{J}}'(\mathbf{r},t)\,dSdt&\\=\big\langle\big(\hat{n}\times(\mathbf{E}^{\text{inc}}(\mathbf{r},t)\times\hat{n})\big),\ddot{\mathbf{J}}'(\mathbf{r},t)\big\rangle_{\sigma}&\end{aligned} \tag{5.27}$$

for $(\mathbf{E}^{\text{inc}}\times\hat{n})\in\mathscr{H}^{\frac{3}{2}}$.

Proof. The first inner product is found by applying the identity $\nabla \cdot \big(\psi \mathbf{F}\big) = \psi\big(\nabla \cdot \mathbf{F}\big) + \mathbf{F} \cdot \big(\nabla \psi\big)$ to transfer the divergence of the test function to a gradient of the charge density term. The additional term, which is the divergence of both quantities, is zero by applying Gauss' theorem. The second inner product follows immediately from the definition given in (5.14). □

5.4 A-Φ Variational Formulations

The focus of this section is to take the variational formulation of Lemma 3, and modify it to imply different sets of variational problems that are possible choices of A-Φ systems. The importance of this is that the existence and stability properties of solutions to the EFIE can then be applied to the A-Φ systems. As will be seen by the results, the equations and appropriate basis and test spaces are not obvious from a simple inverse Fourier-Laplace transform of the equations presented in [1, 14], highlighting the necessity of this analysis.

5.4.1 Provably Stable A-Φ Formulations

From the discussions in Chapter 4, it is clear that the EFIE will need to be separated into two equations to derive **A**-Φ TDIEs. This requires separating the equation in Lemma 3 into two equations. By properly adjusting the Sobolev spaces for the different unknowns, the stability theorem of the EFIE will be able to be extended to the **A**-Φ equations *individually*. First, another definition of a spatial Sobolev space is required to properly express the variational problems to follow.

Definition 10. *The spatial function space of boundary values of scalar potentials on the interface S between the external and internal regions of a scatterer reside in*

$$H^{-\frac{1}{2}}(\nabla^2, S) \coloneqq \left\{ \Phi \in H^{-\frac{1}{2}}(S), \nabla^2 \Phi \in H^{-\frac{1}{2}}(S) \right\}. \tag{5.28}$$

With this definition, the EFIE may now be separated into two equations that are in terms of **A** and Φ.

Theorem 4. *The variational problem given in Lemma 3 is equivalent to the following two variational problems being enforced together.*

Differentiated Vector Potential Equivalence Principle:

$\forall(\dot{\mathbf{A}}^{\text{inc}} \times \hat{n}) \in \mathscr{H}^{\frac{3}{2}}$ *search for* $(\Pi, \mathbf{J}) \in \mathcal{H}^{\frac{1}{2}} \times \mathscr{H}^{\frac{1}{2}}$ *such that* $\forall \mathbf{J}' \in \mathscr{H}^{\frac{1}{2}}$:

$$\left\langle \int_S \left[\mu \frac{\dot{\mathbf{J}}(\mathbf{r}', \tau)}{4\pi R} - \nabla \frac{\Pi(\mathbf{r}', \tau)}{4\pi R} \right] dS', \ddot{\mathbf{J}}'(\mathbf{r}, t) \right\rangle_\sigma = \left\langle -\big(\hat{n} \times (\dot{\mathbf{A}}^{\text{inc}}(\mathbf{r}, t) \times \hat{n})\big), \ddot{\mathbf{J}}'(\mathbf{r}, t) \right\rangle_\sigma , \quad (5.29)$$

where $\Pi = \hat{n}' \cdot \dot{\mathbf{A}}$.

Scalar Huygens' Principle:

$\forall \Phi^{\text{inc}} \in H_\sigma^{\frac{5}{2}}\big(\mathbb{R}_+, H^{-\frac{1}{2}}(\nabla^2, S)\big)$ *search for* $\hat{n}' \cdot \nabla' \Phi \in \mathcal{H}^{\frac{1}{2}}$ *such that* $\forall \mathbf{J}' \in \mathscr{H}^{\frac{1}{2}}$:

$$\left\langle \int_S \frac{\hat{n}' \cdot \nabla' \Phi(\mathbf{r}', \tau)}{4\pi R} dS', \nabla \cdot \ddot{\mathbf{J}}'(\mathbf{r}, t) \right\rangle_\sigma = \left\langle \Phi^{\text{inc}}(\mathbf{r}, t), \nabla \cdot \ddot{\mathbf{J}}'(\mathbf{r}, t) \right\rangle_\sigma . \quad (5.30)$$

Proof. To begin, note that the due to Lemma 3 the full EFIE can be written as

$$\left\langle \int_S \left[\mu \frac{\dot{\mathbf{J}}(\mathbf{r}', \tau)}{4\pi R} + \epsilon^{-1} \nabla \frac{\rho(\mathbf{r}', \tau)}{4\pi R} \right] dS', \ddot{\mathbf{J}}'(\mathbf{r}, t) \right\rangle_\sigma = \left\langle \big(\hat{n} \times (\mathbf{E}^{\text{inc}}(\mathbf{r}, t) \times \hat{n})\big), \ddot{\mathbf{J}}'(\mathbf{r}, t) \right\rangle_\sigma . \quad (5.31)$$

A well-known definition from electromagnetic theory of a surface charge density in terms of the vector and scalar potentials is

$$\rho(\mathbf{r}', t) = -\epsilon\big[\Pi(\mathbf{r}', t) + \hat{n}' \cdot \nabla' \Phi(\mathbf{r}', t)\big]. \quad (5.32)$$

It is noted that because $\rho \in \mathcal{H}^{\frac{1}{2}}$, for (5.32) to be true in general requires $\Pi, \hat{n}' \cdot \nabla' \Phi \in \mathcal{H}^{\frac{1}{2}}$. Expanding the charge unknown in (5.31) gives

$$\left\langle \int_S \left[\mu \frac{\dot{\mathbf{J}}(\mathbf{r}', \tau)}{4\pi R} - \nabla \left(\frac{\Pi(\mathbf{r}', \tau)}{4\pi R} + \frac{\hat{n}' \cdot \nabla' \Phi(\mathbf{r}', \tau)}{4\pi R} \right) \right] dS', \ddot{\mathbf{J}}'(\mathbf{r}, t) \right\rangle_\sigma = \left\langle \big(\hat{n} \times (\mathbf{E}^{\text{inc}}(\mathbf{r}, t) \times \hat{n})\big), \ddot{\mathbf{J}}'(\mathbf{r}, t) \right\rangle_\sigma . \quad (5.33)$$

It is useful to expand the LHS into two inner products so that

$$\left\langle \int_S \left[\mu \frac{\dot{\mathbf{J}}(\mathbf{r}', \tau)}{4\pi R} - \nabla \frac{\Pi(\mathbf{r}', \tau)}{4\pi R} \right] dS', \ddot{\mathbf{J}}'(\mathbf{r}, t) \right\rangle_\sigma - \left\langle \int_S \nabla \frac{\hat{n}' \cdot \nabla' \Phi(\mathbf{r}', \tau)}{4\pi R} dS', \ddot{\mathbf{J}}'(\mathbf{r}, t) \right\rangle_\sigma = \left\langle \big(\hat{n} \times (\mathbf{E}^{\text{inc}}(\mathbf{r}, t) \times \hat{n}) \big), \ddot{\mathbf{J}}'(\mathbf{r}, t) \right\rangle_\sigma . \tag{5.34}$$

By recalling that the electric field may be defined through the vector and scalar potentials as

$$\mathbf{E}(\mathbf{r}, t) = -\dot{\mathbf{A}}(\mathbf{r}, t) - \nabla \Phi(\mathbf{r}, t), \tag{5.35}$$

the inner product on the RHS of (5.34) may be expanded. This gives

$$\begin{aligned} &\left\langle \int_S \left[\mu \frac{\dot{\mathbf{J}}(\mathbf{r}', \tau)}{4\pi R} - \nabla \frac{\Pi(\mathbf{r}', \tau)}{4\pi R} \right] dS', \ddot{\mathbf{J}}'(\mathbf{r}, t) \right\rangle_\sigma \\ &- \left\langle \int_S \nabla \frac{\hat{n}' \cdot \nabla' \Phi(\mathbf{r}', \tau)}{4\pi R} dS', \ddot{\mathbf{J}}'(\mathbf{r}, t) \right\rangle_\sigma = \left\langle - \big(\hat{n} \times (\dot{\mathbf{A}}^{\text{inc}}(\mathbf{r}, t) \times \hat{n}) \big), \ddot{\mathbf{J}}'(\mathbf{r}, t) \right\rangle_\sigma \\ &\qquad + \left\langle - \big(\hat{n} \times (\nabla \Phi^{\text{inc}}(\mathbf{r}, t) \times \hat{n}) \big), \ddot{\mathbf{J}}'(\mathbf{r}, t) \right\rangle_\sigma . \end{aligned} \tag{5.36}$$

The second inner product on the RHS and the second inner product on the LHS may be rewritten by transferring the gradient onto the testing function, applying Guass' theorem, and then noting that the integrals of the boundary terms are zero. Performing this gives

$$\begin{aligned} &\left\langle \int_S \left[\mu \frac{\dot{\mathbf{J}}(\mathbf{r}', \tau)}{4\pi R} - \nabla \frac{\Pi(\mathbf{r}', \tau)}{4\pi R} \right] dS', \ddot{\mathbf{J}}'(\mathbf{r}, t) \right\rangle_\sigma \\ &+ \left\langle \int_S \frac{\hat{n}' \cdot \nabla' \Phi(\mathbf{r}', \tau)}{4\pi R} dS', \nabla \cdot \ddot{\mathbf{J}}'(\mathbf{r}, t) \right\rangle_\sigma = \left\langle - \big(\hat{n} \times (\dot{\mathbf{A}}^{\text{inc}}(\mathbf{r}, t) \times \hat{n}) \big), \ddot{\mathbf{J}}'(\mathbf{r}, t) \right\rangle_\sigma \\ &\qquad + \left\langle \Phi^{\text{inc}}(\mathbf{r}, t), \nabla \cdot \ddot{\mathbf{J}}'(\mathbf{r}, t) \right\rangle_\sigma . \end{aligned} \tag{5.37}$$

At this point, by physical arguments it is possible to separate (5.37) into two equations as

$$\begin{aligned} &\left\langle \int_S \left[\mu \frac{\dot{\mathbf{J}}(\mathbf{r}', \tau)}{4\pi R} - \nabla \frac{\Pi(\mathbf{r}', \tau)}{4\pi R} \right] dS', \ddot{\mathbf{J}}'(\mathbf{r}, t) \right\rangle_\sigma \\ &\qquad = \left\langle - \big(\hat{n} \times (\dot{\mathbf{A}}^{\text{inc}}(\mathbf{r}, t) \times \hat{n}) \big), \ddot{\mathbf{J}}'(\mathbf{r}, t) \right\rangle_\sigma \end{aligned} \tag{5.38}$$

$$\left\langle \int_S \frac{\hat{n}' \cdot \nabla' \Phi(\mathbf{r}', \tau)}{4\pi R} dS', \nabla \cdot \ddot{\mathbf{J}}'(\mathbf{r}, t) \right\rangle_\sigma = \left\langle \Phi^{\text{inc}}(\mathbf{r}, t), \nabla \cdot \ddot{\mathbf{J}}'(\mathbf{r}, t) \right\rangle_\sigma . \quad (5.39)$$

This is possible since (5.39) is the scalar Huygens' principle integral equation, and so these two inner products must equal each other [49].

To conclude the proof, it only remains to explain the Sobolev space that Φ^{inc} is defined in. This is a simple modification, since $\mathbf{E}^{\text{inc}} \in \mathscr{H}^{\frac{3}{2}}$ implies that $\nabla \Phi^{\text{inc}}$ should be selected so that $\nabla \Phi^{\text{inc}} \in \mathscr{H}^{\frac{3}{2}}$. The definition of $\mathscr{H}^{\frac{3}{2}}$ requires $\nabla \Phi^{\text{inc}}$ to have a divergence that is still in $H^{-\frac{1}{2}}(S)$, i.e. $\nabla^2 \Phi^{\text{inc}} \in H^{-\frac{1}{2}}(S)$. However, from Definition 10 it is seen that requiring $\nabla \Phi^{\text{inc}} \in \mathscr{H}^{\frac{3}{2}} \iff \Phi^{\text{inc}} \in H_\sigma^{\frac{5}{2}}\big(\mathbb{R}_+, H^{-\frac{1}{2}}(\nabla^2, S)\big)$. The change in the order of the temporal function space is a result of Lemma 1. This showed the link between spatial derivatives and the temporal order of differentiability of an electromagnetic function. □

Theorem 5. *The variational problems given in Theorem 4 correspond to stable systems individually.*

Proof. This is deduced by exploiting the linearity of integration and the inner product. First, it is noted that the LHS of (5.31) may be written as

$$\left\langle \int_S \mu \frac{\dot{\mathbf{J}}(\mathbf{r}', \tau)}{4\pi R} dS', \ddot{\mathbf{J}}'(\mathbf{r}, t) \right\rangle_\sigma + \left\langle \int_S \epsilon^{-1} \nabla \frac{\rho(\mathbf{r}', \tau)}{4\pi R} dS', \ddot{\mathbf{J}}'(\mathbf{r}, t) \right\rangle_\sigma . \quad (5.40)$$

The importance is that both inner products must independently produce bounded results to equal the bounded RHS of (5.31). By expanding the charge density in terms of Π and $\hat{n}' \cdot \nabla' \Phi$, similar conclusions can be reached for the corresponding separated inner products. That is,

$$\left\langle \int_S \epsilon^{-1} \nabla \frac{\Pi(\mathbf{r}', \tau)}{4\pi R} dS', \ddot{\mathbf{J}}'(\mathbf{r}, t) \right\rangle_\sigma < \infty \quad (5.41)$$

$$\left\langle \int_S \epsilon^{-1} \nabla \frac{\hat{n}' \cdot \nabla' \Phi(\mathbf{r}', \tau)}{4\pi R} dS', \ddot{\mathbf{J}}'(\mathbf{r}, t) \right\rangle_\sigma < \infty, \quad (5.42)$$

given that Π and $\hat{n}' \cdot \nabla' \Phi$ are selected from the appropriate Sobolev spaces stated in Theorem 4. The same arguments can be applied for expanding the inner product on the RHS of (5.31). As a result, as long as the different functions are selected in the appropriate Sobolev spaces, the stability theorem of the EFIE will still apply to the separated problems. □

Although the derived variational formulations and stability theorem are a

useful step forward, inspection of the equations shows that there are three unknowns (i.e., $\mathbf{J}$, Π, and $\hat{n}' \cdot \nabla' \Phi$) with only two equations. However, the scalar Huygens' principle equation of (5.39) can be rewritten to use the same unknowns as the first equation.

Theorem 6. *The variational problems of Theorem 4 are equivalent to the following two variational problems which only require* $\mathbf{J}$ *and* Π *to be solved for.*

Differentiated Vector Potential Equivalence Principle:
$\forall(\dot{\mathbf{A}}^{\text{inc}} \times \hat{n}) \in \mathscr{H}^{\frac{3}{2}}$ *search for* $(\Pi, \mathbf{J}) \in \mathcal{H}^{\frac{1}{2}} \times \mathscr{H}^{\frac{1}{2}}$ *such that* $\forall \mathbf{J}' \in \mathscr{H}^{\frac{1}{2}}$:

$$\left\langle \int_S \left[\mu \frac{\dot{\mathbf{J}}(\mathbf{r}', \tau)}{4\pi R} - \nabla \frac{\Pi(\mathbf{r}', \tau)}{4\pi R} \right] dS', \ddot{\mathbf{J}}'(\mathbf{r}, t) \right\rangle_\sigma = \left\langle -\big(\hat{n} \times (\dot{\mathbf{A}}^{\text{inc}}(\mathbf{r}, t) \times \hat{n})\big), \ddot{\mathbf{J}}'(\mathbf{r}, t) \right\rangle_\sigma . \quad (5.43)$$

Scalar Potential Equivalence Principle:
$\forall \Phi^{\text{inc}} \in H_\sigma^{\frac{5}{2}}\big(\mathbb{R}_+, H^{-\frac{1}{2}}(\nabla^2, S)\big)$ *search for* $(\Pi, \mathbf{J}) \in \mathcal{H}^{\frac{1}{2}} \times \mathscr{H}^{\frac{1}{2}}$ *such that* $\forall \mathbf{J}' \in \mathscr{H}^{\frac{1}{2}}$:

$$\left\langle \int_S \left[\epsilon^{-1} \int_{-\infty}^{\tau} \frac{\nabla' \cdot \mathbf{J}(\mathbf{r}', t')}{4\pi R} dt' - \frac{\Pi(\mathbf{r}', \tau)}{4\pi R} \right] dS', \nabla \cdot \ddot{\mathbf{J}}'(\mathbf{r}, t) \right\rangle_\sigma = \left\langle \Phi^{\text{inc}}(\mathbf{r}, t), \nabla \cdot \ddot{\mathbf{J}}'(\mathbf{r}, t) \right\rangle_\sigma . \quad (5.44)$$

Proof. The first variational problem is identical to that in Theorem 4 so no changes are needed. The second variational problem may be derived by making the following changes to the first argument of the first inner product of (5.39).

$$\begin{aligned} \int_S \frac{\hat{n}' \cdot \nabla' \Phi(\mathbf{r}', \tau)}{4\pi R} dS' &= \int_S \frac{1}{4\pi R} \Big[\Pi(\mathbf{r}', \tau) + \hat{n}' \cdot \nabla' \Phi(\mathbf{r}', \tau) - \Pi(\mathbf{r}', \tau) \Big] dS' \\ &= \int_S \frac{1}{4\pi R} \Big[-\epsilon^{-1} \rho(\mathbf{r}, \tau) - \Pi(\mathbf{r}', \tau) \Big] dS' \qquad (5.45) \\ &= \int_S \left[\epsilon^{-1} \int_{-\infty}^{\tau} \frac{\nabla' \cdot \mathbf{J}(\mathbf{r}', t')}{4\pi R} dt' - \frac{\Pi(\mathbf{r}', \tau)}{4\pi R} \right] dS' \end{aligned}$$

Substituting this back into (5.39) gives the desired result. □

Theorem 7. *The variational problems given in Theorem 6 correspond to stable systems individually.*

Proof. The argument follows the same approach as that for Theorem 5. □

The variational problems of Theorem 6 are useful since they represent a solvable system. However, it is seen that the temporal test spaces of the two problems are different. The temporal test space of (5.43) is $H_\sigma^{-\frac{3}{2}}$ while that of (5.44) is $H_\sigma^{-\frac{5}{2}}$. This is seen by noting that $\mathbf{J}'(\mathbf{r},t) \in \mathscr{H}^{\frac{1}{2}}$; it then follows that $\ddot{\mathbf{J}}'(\mathbf{r},t) \in \mathscr{H}^{-\frac{3}{2}}$ and $\nabla \cdot \ddot{\mathbf{J}}'(\mathbf{r},t) \in \mathcal{H}^{-\frac{5}{2}}$. Unfortunately, this makes the *consistent discretization* of these two equations not possible. A consistent discretization would involve using the same set of temporal basis and testing functions in a MOT scheme for each equation. More details related to this concept are discussed in Section 5.5. Since a consistent discretization is not possible, another set of equations is needed which use the same temporal test space for both equations.

Before modifying the equations of Theorem 6 to ones that can be discretized consistently, discussion of how to integrate by parts temporally is required. This is discussed in more detail in [15], with only the key concepts reviewed here. The weighting function in the temporal integrals of the inner products in $\mathscr{H}^s$ and $\mathcal{H}^s$ complicates integrating by parts, but the end results are still what would be expected. Transferring a derivative from the equations onto the testing function requires that a testing function from one degree lower function space be used in the subsequent discretization process. Similarly, when transferring a derivative from the testing function onto the integral equations, the use of a testing function from one degree higher function space will be required in the discretization. Subtleties related to the extra term that arises by differentiating the weighting term can be resolved in the frequency domain, and are of little interest for actually discretizing the equations. More details related to this will be discussed in Section 5.5.

The first modifications to the equations of Theorem 6 results in the differentiated time domain A-Φ integral equation (abbreviated differentiated TD-APIE). From these equations, stability theorems may be extended to the TD-WC-EFIE discussed in Section 4.2.3.

Theorem 8. *(Differentiated TD-APIE) The variational problems of Theorem 6 can be modified to utilize the same temporal test space for both equations.*

Differentiated Vector Potential Equivalence Principle:
$\forall(\dot{\mathbf{A}}^{\text{inc}} \times \hat{n}) \in \mathscr{H}^{\frac{3}{2}}$ *search for* $(\Pi, \mathbf{J}) \in \mathcal{H}^{\frac{1}{2}} \times \mathscr{H}^{\frac{1}{2}}$ *such that* $\forall \mathbf{J}' \in \mathscr{H}^{\frac{1}{2}}$:

$$\left\langle \int_S \left[\mu \frac{\dot{\mathbf{J}}(\mathbf{r}', \tau)}{4\pi R} - \nabla \frac{\Pi(\mathbf{r}', \tau)}{4\pi R} \right] dS', \ddot{\mathbf{J}}'(\mathbf{r}, t) \right\rangle_\sigma = \left\langle -\big(\hat{n} \times (\dot{\mathbf{A}}^{\text{inc}}(\mathbf{r}, t) \times \hat{n})\big), \ddot{\mathbf{J}}'(\mathbf{r}, t) \right\rangle_\sigma . \quad (5.46)$$

Differentiated Scalar Potential Equivalence Principle:
$\forall \dot{\Phi}^{\text{inc}} \in H_\sigma^{\frac{3}{2}}\big(\mathbb{R}_+, H^{-\frac{1}{2}}(\nabla^2, S)\big)$ *search for* $(\Pi, \mathbf{J}) \in \mathcal{H}^{\frac{1}{2}} \times \mathscr{H}^{\frac{1}{2}}$ *such that* $\forall \mathbf{J}' \in \mathscr{H}^{\frac{1}{2}}$:

$$\left\langle \int_S \left[\epsilon^{-1} \frac{\nabla' \cdot \mathbf{J}(\mathbf{r}', \tau)}{4\pi R} - \frac{\dot{\Pi}(\mathbf{r}', \tau)}{4\pi R} \right] dS', \nabla \cdot \dot{\mathbf{J}}'(\mathbf{r}, t) \right\rangle_\sigma = \left\langle \dot{\Phi}^{\text{inc}}(\mathbf{r}, t), \nabla \cdot \dot{\mathbf{J}}'(\mathbf{r}, t) \right\rangle_\sigma . \quad (5.47)$$

Proof. The first variational problem is the same as in Theorem 6, so no changes are needed. The second variational problem is found by integrating by parts to transfer one of the time derivatives of the test function onto the integral equation. As was discussed, this results in the natural change to the degree of the temporal function space of the excitation. No higher degree of temporal derivative is required on the expansion functions than was already acceptable in the original EFIE, making this a valid set of equations. By recalling the relationship between spatial derivatives and the temporal regularity of functions, it is seen that the temporal test space for both equations is $H_\sigma^{-\frac{3}{2}}$, as desired. □

Theorem 9. *The variational problems of Theorem 8 correspond to stable systems individually.*

Proof. The first variational problem has not changed, so nothing is needed to be proved. As was mentioned in the proof of Theorem 8, the time derivatives required in (5.47) are still acceptable for the function spaces defined for all basis functions. Further, the function spaces for the incident scalar potential and testing functions have been adjusted according to the discussions on integrating by parts in [15]. □

At this point, it is possible to prove that the TD-WC-EFIE introduced in Section 4.2.3 is a stable system. The reason for the previously seen instability

was that an incorrect temporal basis and testing scheme was being used. This will be made more clear when the details of discretizing the variational problems are discussed in Section 5.5.

Corollary 1. *(TD-WC-EFIE) A combination of stable TDIEs can yield the TD-WC-EFIE; extending the stability theorems to this formulation.*
Electric Field Integral Equation:
$\forall(\mathbf{E}^{\text{inc}}\times\hat{n}) \in \mathscr{H}^{\frac{3}{2}}$ *search for* $(\rho, \mathbf{J}) \in \mathcal{H}^{\frac{1}{2}} \times \mathscr{H}^{\frac{1}{2}}$ *such that* $\forall \mathbf{J}' \in \mathscr{H}^{\frac{1}{2}}$:

$$\left\langle \int_S \left[\mu \frac{\dot{\mathbf{J}}(\mathbf{r}', \tau)}{4\pi R} + \epsilon^{-1} \nabla \frac{\rho(\mathbf{r}', \tau)}{4\pi R} \right] dS', \ddot{\mathbf{J}}'(\mathbf{r}, t) \right\rangle_\sigma = \left\langle \left(\hat{n} \times (\mathbf{E}^{\text{inc}}(\mathbf{r}, t) \times \hat{n}) \right), \ddot{\mathbf{J}}'(\mathbf{r}, t) \right\rangle_\sigma . \quad (5.48)$$

Weighted Continuity Equation:
Search for $(\rho, \mathbf{J}) \in \mathcal{H}^{\frac{1}{2}} \times \mathscr{H}^{\frac{1}{2}}$ *such that* $\forall \mathbf{J}' \in \mathscr{H}^{\frac{1}{2}}$:

$$\left\langle \int_S \left[\frac{\nabla' \cdot \mathbf{J}(\mathbf{r}', \tau)}{4\pi R} + \frac{\dot{\rho}(\mathbf{r}', \tau)}{4\pi R} \right] dS', \nabla \cdot \dot{\mathbf{J}}'(\mathbf{r}, t) \right\rangle_\sigma = 0. \quad (5.49)$$

The two equations may be discretized in a consistent manner, allowing for a well-functioning integral equation system to be implemented.

Proof. The first variational problem is the original EFIE which is known to be stable. It can be recovered by adding the scalar Huygens' principle integral equation of (5.39) to (5.46). This gives

$$\begin{aligned} &\left\langle \int_S \left[\mu \frac{\dot{\mathbf{J}}(\mathbf{r}', \tau)}{4\pi R} - \nabla \frac{\Pi(\mathbf{r}', \tau)}{4\pi R} \right] dS', \ddot{\mathbf{J}}'(\mathbf{r}, t) \right\rangle_\sigma + \\ &\left\langle \int_S \frac{\hat{n}' \cdot \nabla' \Phi(\mathbf{r}', \tau)}{4\pi R} dS', \nabla \cdot \ddot{\mathbf{J}}'(\mathbf{r}, t) \right\rangle_\sigma = \left\langle -\left(\hat{n} \times (\dot{\mathbf{A}}^{\text{inc}}(\mathbf{r}, t) \times \hat{n}) \right), \ddot{\mathbf{J}}'(\mathbf{r}, t) \right\rangle_\sigma \\ &\qquad + \left\langle \Phi^{\text{inc}}(\mathbf{r}, t), \nabla \cdot \ddot{\mathbf{J}}'(\mathbf{r}, t) \right\rangle_\sigma . \quad (5.50) \end{aligned}$$

The divergence of the testing function in the inner products from the scalar Huygens' principle integral equation can be transferred to a gradient of the other arguments. This allows the inner products to be combined, yielding

$$\left\langle \int_S \left[\mu \frac{\dot{\mathbf{J}}(\mathbf{r}', \tau)}{4\pi R} - \nabla \frac{1}{4\pi R} \left\{ \Pi(\mathbf{r}', \tau) + \hat{n}' \cdot \nabla' \Phi(\mathbf{r}', \tau) \right\} \right] dS', \ddot{\mathbf{J}}'(\mathbf{r}, t) \right\rangle_\sigma = \left\langle -\left(\hat{n} \times \left[\dot{\mathbf{A}}^{\text{inc}}(\mathbf{r}, t) + \nabla \Phi^{\text{inc}}(\mathbf{r}, t) \right] \times \hat{n} \right), \ddot{\mathbf{J}}'(\mathbf{r}, t) \right\rangle_\sigma . \quad (5.51)$$

Finally, recovery of (5.48) is possible by using the definitions of the surface charge density and electric field in terms of the vector and scalar potentials, (5.32) and (5.35), respectively.

The weighted continuity equation can be derived by integrating by parts temporally in the scalar Huygens' principle integral equation of (5.39). This gives

$$\left\langle \int_S \frac{\hat{n}' \cdot \nabla' \dot{\Phi}(\mathbf{r}', \tau)}{4\pi R} dS', \nabla \cdot \dot{\mathbf{J}}'(\mathbf{r}, t) \right\rangle_\sigma = \left\langle \dot{\Phi}^{\text{inc}}(\mathbf{r}, t), \nabla \cdot \dot{\mathbf{J}}'(\mathbf{r}, t) \right\rangle_\sigma . \quad (5.52)$$

The inner products on the RHS of (5.52) and (5.47) are now the same. Substituting the expression on the LHS of (5.52) into (5.47) gives

$$\left\langle \int_S \left[\epsilon^{-1} \frac{\nabla' \cdot \mathbf{J}(\mathbf{r}', \tau)}{4\pi R} - \frac{\dot{\Pi}(\mathbf{r}', \tau)}{4\pi R} \right] dS', \nabla \cdot \dot{\mathbf{J}}'(\mathbf{r}, t) \right\rangle_\sigma = \left\langle \int_S \frac{\hat{n}' \cdot \nabla' \dot{\Phi}(\mathbf{r}', \tau)}{4\pi R} dS', \nabla \cdot \dot{\mathbf{J}}'(\mathbf{r}, t) \right\rangle_\sigma . \quad (5.53)$$

Combining the inner products and using the definition of a surface charge density in (5.32) gives (5.49). □

The differentiated TD-APIE and TD-WC-EFIE are simple to implement. They both result in symmetric matrix equations; allowing specialized storage and solution algorithms to be used. However, they do suffer from some drawbacks. First, because they are differentiated the equations exhibit DC null spaces similar to the TD-EFIE. This does not typically corrupt solutions at middle frequencies, however, at very low frequencies it may have a more substantial effect. Further, the integral operators in the TD-APIE calculate the time derivative of the vector and scalar potentials. For coupling these methods to quantum mechanical calculations, it may be more desirable to be able to calculate the vector and scalar potentials directly.

To address the drawbacks of the differentiated TD-APIE, a different modification to the equations of Theorem 6 can be derived. This gives the time domain **A**-Φ integral equation (TD-APIE).

Theorem 10. *(TD-APIE) The variational problems of Theorem 6 can be modified to result in the following* A-Φ *formulation that utilizes the same temporal test space for both equations.*

Vector Potential Equivalence Principle:
$\forall(\mathbf{A}^{\text{inc}}\times\hat{n}) \in \mathscr{H}^{\frac{5}{2}}$ *search for* $(\Pi, \mathbf{J}) \in \mathcal{H}^{\frac{1}{2}} \times \mathscr{H}^{\frac{1}{2}}$ *such that* $\forall \mathbf{J}' \in \mathscr{H}^{\frac{1}{2}}$:

$$\left\langle \int_S \left[\mu \frac{\mathbf{J}(\mathbf{r}', \tau)}{4\pi R} - \nabla \int_{-\infty}^{\tau} \frac{\Pi(\mathbf{r}', t')}{4\pi R} dt' \right] dS', \dddot{\mathbf{J}}'(\mathbf{r}, t) \right\rangle_\sigma$$
$$= \left\langle -\big(\hat{n}\times(\mathbf{A}^{\text{inc}}(\mathbf{r}, t)\times\hat{n})\big), \dddot{\mathbf{J}}'(\mathbf{r}, t) \right\rangle_\sigma . \quad (5.54)$$

Scalar Potential Equivalence Principle:
$\forall\Phi^{\text{inc}} \in H_\sigma^{\frac{5}{2}}\big(\mathbb{R}_+, H^{-\frac{1}{2}}(\nabla^2, S)\big)$ *search for* $(\Pi, \mathbf{J}) \in \mathcal{H}^{\frac{1}{2}} \times \mathscr{H}^{\frac{1}{2}}$ *such that* $\forall \mathbf{J}' \in \mathscr{H}^{\frac{1}{2}}$:

$$\left\langle \int_S \left[\epsilon^{-1} \int_{-\infty}^{\tau} \frac{\nabla' \cdot \mathbf{J}(\mathbf{r}', t')}{4\pi R} dt' - \frac{\Pi(\mathbf{r}', \tau)}{4\pi R} \right] dS', \nabla \cdot \ddot{\mathbf{J}}'(\mathbf{r}, t) \right\rangle_\sigma$$
$$= \left\langle \Phi^{\text{inc}}(\mathbf{r}, t), \nabla \cdot \ddot{\mathbf{J}}'(\mathbf{r}, t) \right\rangle_\sigma . \quad (5.55)$$

Proof. The scalar potential equivalence principle is the same as that given in Theorem 6, so no modifications are needed. The vector potential equivalence principle is found by integrating by parts temporally. In particular, the differentiated vector potential equivalence principle of (5.46) is integrated by parts. The changes in function spaces follows easily from this. □

Theorem 11. *The variational problems of Theorem 10 correspond to stable systems individually.*

Proof. This result follows easily from past arguments for the stability of the variational problems. Additionally, this equation requires no time derivatives so there is no fear of the basis functions not being smooth enough to be differentiated. □

The set of equations to be solved in Theorem 10 still have the benefit of producing a symmetric matrix system. As desired, these operators also calculate the vector and scalar potentials as opposed to the time derivatives of these quantities. The cost of this, however, is that the temporal integrals must be discretized. This will increase the computation time, but will not change the asymptotic computational complexity [22]. The temporal test space of these equations is $H_\sigma^{-\frac{5}{2}}$, which further complicates the discretization. More details related to this are discussed in Section 5.5.

5.4.2 Analysis of Past A-Φ Formulation

The function spaces and variational problems of Section 5.4.1 can now be used to understand why the original A-Φ formulation discussed in Section 4.1.2 showed such poor stability properties. The original A-Φ formulation was developed by taking an inverse Fourier-Laplace transform of the equations presented in [1,14]. The same sets of unknown functions were also used, i.e., the current density and the normal component of the vector potential.

The equations for the original A-Φ formulation are

$$\hat{n}\times\int_S\left[\mu\frac{1}{4\pi R}\mathbf{J}(\mathbf{r}',\tau)-\nabla\frac{1}{4\pi R}\Sigma(\mathbf{r}',\tau)\right]dS'=\mathbf{A}^{\text{inc}}(\mathbf{r},t)\times\hat{n} \tag{5.56}$$

$$\int_S\left[\epsilon^{-1}\frac{1}{4\pi R}\nabla'\cdot\mathbf{J}(\mathbf{r}',\tau)-\frac{1}{4\pi R}\ddot{\Sigma}(\mathbf{r}',\tau)\right]dS'=\dot{\Phi}^{\text{inc}}(\mathbf{r},t), \tag{5.57}$$

where $\Sigma=\hat{n}'\cdot\mathbf{A}$. Extending the analysis of Section 5.4.1 to this set of equations suggests the following lemma.

Lemma 4. *The equivalent variational formulation for the equations studied in Section 4.1.2 cannot lead to a stable system. The variational formulation is the following.*

Vector Potential Equation:
$\forall(\mathbf{A}^{\text{inc}}\times\hat{n})\in\mathscr{H}^{\frac{5}{2}}$ *search for* $(\Sigma,\mathbf{J})\in\mathcal{H}^{\frac{3}{2}}\times\mathscr{H}^{\frac{1}{2}}$ *such that* $\forall\mathbf{J}'\in\mathscr{H}^{\frac{1}{2}}$:

$$\left\langle\int_S\left[\mu\frac{\mathbf{J}(\mathbf{r}',\tau)}{4\pi R}-\nabla\frac{\Sigma(\mathbf{r}',\tau)}{4\pi R}\right]dS',\dddot{\mathbf{J}}'(\mathbf{r},t)\right\rangle_\sigma = \left\langle-\big(\hat{n}\times(\mathbf{A}^{\text{inc}}(\mathbf{r},t)\times\hat{n})\big),\dddot{\mathbf{J}}'(\mathbf{r},t)\right\rangle_\sigma. \tag{5.58}$$

Scalar Potential Equation:
$\forall\dot{\Phi}^{\text{inc}}\in H_\sigma^{\frac{3}{2}}\big(\mathbb{R}_+,H^{-\frac{1}{2}}(\nabla^2,S)\big)$ *search for* $(\Sigma,\mathbf{J})\in\mathcal{H}^{\frac{3}{2}}\times\mathscr{H}^{\frac{1}{2}}$ *such that* $\forall\mathbf{J}'\in\mathscr{H}^{\frac{1}{2}}$:

$$\left\langle\int_S\left[\epsilon^{-1}\frac{\nabla'\cdot\mathbf{J}(\mathbf{r}',\tau)}{4\pi R}-\frac{\ddot{\Sigma}(\mathbf{r}',\tau)}{4\pi R}\right]dS',\nabla\cdot\dot{\mathbf{J}}'(\mathbf{r},t)\right\rangle_\sigma = \left\langle\dot{\Phi}^{\text{inc}}(\mathbf{r},t),\nabla\cdot\dot{\mathbf{J}}'(\mathbf{r},t)\right\rangle_\sigma. \tag{5.59}$$

Proof. These equations cannot be discretized consistently. The first complication is related to the two unknowns requiring different basis functions.

Although this is possible to do, it overly complicates the discretization of the equations. The more significant problem is that the two equations require different temporal test spaces. Within the MOT discretization framework this cannot be achieved. As a result, using standard discretization processes cannot lead to a stable discretization of this system. □

The importance of Lemma 4 is seen clearly in the numerical results produced for this A-Φ formulation in Section 4.1.3. The same temporal basis and testing functions were used for both unknowns, violating the correct choices presented in Lemma 4. As a result, this formulation exhibited instability for a simulation with a center frequency of 200 kHz, which is an extremely poor result. As will be demonstrated in Section 5.6, the TD-APIE and differentiated TD-APIE from Section 5.4.1 are able to produce stable results at the same frequencies for which the EFIE is stable. This greatly out-performs the naive discretization suggested by a simple inverse Fourier-Laplace transform of the frequency domain equations of [1, 14].

5.5 Discretization of Variational Formulations

The focus of this section is making explicit the steps needed to discretize the variational problems introduced in Section 5.4. In particular, sample functions from some of the relevant function spaces will be presented to assist in arriving at a stable discrete scheme. Additionally, the role of the damping parameter σ in the temporal function spaces will be discussed. Finally, the discretized equations for the differentiated TD-APIE and TD-APIE are presented.

5.5.1 General Concepts

As has been previously mentioned, the spatial discretization is relatively simple since RWG functions are members of the correct function space for the current density. This makes them the easiest choice for discretizing the current density, although other functions can be used [15]. For ρ and Π, the natural choice is a pulse basis function. This is necessary for the different matrix systems to be symmetric and also allows for typical singularity

extraction methods to be applicable.

The temporal basis functions require more care since there are substantially more choices commonly used compared to the spatial discretization. To give some examples, sample functions characteristic of some of the relevant spaces are presented. The most common temporal test function used is the Dirac delta function. This is a member of the temporal function space $H_\sigma^{-\frac{3}{2}}$. The next space is $H_\sigma^{-\frac{1}{2}}$, with the simplest basis function in this space being a pulse function (e.g., it is 1 for a single time step and 0 otherwise). A typical function in the space $H_\sigma^{\frac{1}{2}}$ is a triangular function. Finally, an example function in the space $H_\sigma^{\frac{3}{2}}$ is the quadratic B-spline.

From this discussion, it is possible to easily discretize the differentiated TD-APIE or TD-WC-EFIE. A low-order basis function that can be used is a triangle function; which can be tested with a delta function. As a result, the MOT procedure can be used directly for these equations.

Discretizing the TD-APIE is a more difficult task. This is because the temporal basis space is $H_\sigma^{\frac{1}{2}}$ and the temporal test space is $H_\sigma^{-\frac{5}{2}}$. This means that the delta function is not a correct testing function, so the MOT procedure cannot be directly applied to this system. However, it is possible to form a discrete system using the MOT procedure that is equivalent to using the correct temporal basis and testing spaces [45, 53]. In particular, the basis function that should be used in the MOT procedure can be found by convolving a basis and testing function pair from the correct Sobolev spaces. Since a function in $H_\sigma^{-\frac{5}{2}}$ would look like the derivative of a delta function, it is anticipated that a basis function from $H_\sigma^{-\frac{1}{2}}$ could be used in the MOT procedure. Preliminary results doing this are promising, but more study is still needed.

There are many more functions that can be used to implement higher-order schemes. For instance, the temporal basis functions used in [53] are in $H_\sigma^{\frac{1}{2}}$ while the testing functions are in $H_\sigma^{-\frac{1}{2}}$. These functions work because these are the correct function spaces for the differentiated EFIE [15]. The basis and testing functions used in [45] are in $H_\sigma^{-\frac{1}{2}}$. The scheme in [45] works because using basis and testing functions in $H_\sigma^{-\frac{1}{2}}$ can be shown to be discretely equivalent to using a basis function in $H_\sigma^{\frac{1}{2}}$ and a testing function in $H_\sigma^{-\frac{3}{2}}$. These are the correct spaces for the original EFIE, leading to an overall stable discretization.

Another point is needed to be made related to the nesting properties of the

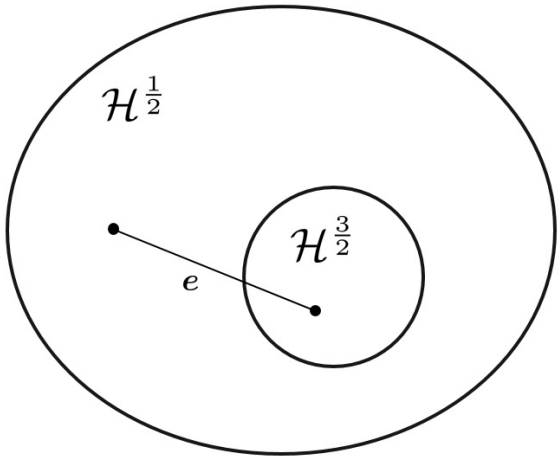

Figure 5.1: Demonstration of how using too smooth of a basis function can lead to large error, $\boldsymbol{e}$, and potentially instability for a TDIE.

Sobolev spaces. As an example, it is clear to see that $H_\sigma^{\frac{3}{2}} \subset H_\sigma^{\frac{1}{2}}$. Although this is true, if a variational formulation calls for the basis function to be an element of $H_\sigma^{\frac{1}{2}}$, it is better to use an element that is in $H_\sigma^{\frac{1}{2}}$ but is not in $H_\sigma^{\frac{3}{2}}$. The reason for this is illustrated in Fig. 5.1. If too smooth of a basis function is used, the error that may occur for projecting the actual solution in $H_\sigma^{\frac{1}{2}}$ into $H_\sigma^{\frac{3}{2}}$ may lead to instability. This is what happened for the TD-WC-EFIE when a quadratic B-spline basis function was used. Although not shown here, the same result also applies for the testing spaces. That is, $H_\sigma^{-\frac{3}{2}} \subset H_\sigma^{-\frac{5}{2}}$; and so, if the appropriate testing space is $H_\sigma^{-\frac{5}{2}}$ a testing function from $H_\sigma^{-\frac{3}{2}}$ should not be used. This has been tested numerically with the TD-APIE. A delta function was used as the testing function (an element of $H_\sigma^{-\frac{3}{2}}$) while a triangle function was used as the basis function (an element of $H_\sigma^{\frac{1}{2}}$). The results were unstable, demonstrating the need to use functions from the largest space possible, as opposed to smaller subspaces.

A final remark for discretizing the variational formulations is required for the choice of σ. For efficiency reasons, this is selected to be 0. However, the stability theorems are only technically valid for $\sigma > 0$. In practice, it has been found that if the basis and testing functions are picked from the correct function spaces and the matrix elements are accurately evaluated, the methods are stable enough to be widely used [15].

5.5.2 Discretized Equations for the Differentiated TD-APIE

For practical purposes, it is useful to perform some rescaling of the different equations in the differentiated TD-APIE. This results in a symmetric matrix system, as well as gives it a saddle point form similar to the TD-A-EFIE. The matrix system is

$$\begin{bmatrix} \mu_r \Delta t \dot{\mathbf{V}}^{(0)} & \mathbf{D}^T \mathbf{S}^{(0)} \\ \mathbf{S}^{(0)} \mathbf{D} & -\frac{\epsilon_r}{c_0^2 \Delta t} \dot{\mathbf{S}}^{(0)} \end{bmatrix} \begin{Bmatrix} (c_0 \Delta t)^{-1} \mathbf{J}^{(i)} \\ \eta_0^{-1} \boldsymbol{\psi}^{(i)} \end{Bmatrix} = \begin{Bmatrix} -\eta_0^{-1} \dot{\boldsymbol{\alpha}}^{(i)} \\ \frac{\epsilon}{c_0 \Delta t} \dot{\boldsymbol{\phi}}^{(i)} \end{Bmatrix} - \sum_{j=i-j_{max}}^{i-1} \begin{bmatrix} \mu_r \Delta t \dot{\mathbf{V}}^{(i-j)} & \mathbf{D}^T \mathbf{S}^{(i-j)} \\ \mathbf{S}^{(i-j)} \mathbf{D} & -\frac{\epsilon_r}{c_0^2 \Delta t} \dot{\mathbf{S}}^{(i-j)} \end{bmatrix} \begin{Bmatrix} (c_0 \Delta t)^{-1} \mathbf{J}^{(j)} \\ \eta_0^{-1} \boldsymbol{\psi}^{(j)} \end{Bmatrix}. \quad (5.60)$$

The different matrix elements are defined as

$$\dot{\mathbf{V}}_{mn}^{(i-j)} = \int_{S_m} \int_{S_n} \sum_{l=0}^{N_h} a_l \dot{\xi}_l^{(i-j)} \mathbf{f}_m(\mathbf{r}) \cdot \mathbf{f}_n(\mathbf{r}') \frac{P_l(\hat{R})}{4\pi R} dS' dS \quad (5.61)$$

$$\mathbf{S}_{mn}^{(i-j)} = \int_{T_m} \int_{T_n} \sum_{l=0}^{N_h} a_l \xi_l^{(i-j)} h_m(\mathbf{r}) h_n(\mathbf{r}') \frac{P_l(\hat{R})}{4\pi R} dS' dS \quad (5.62)$$

$$\dot{\mathbf{S}}_{mn}^{(i-j)} = \int_{T_m} \int_{T_n} \sum_{l=0}^{N_h} a_l \dot{\xi}_l^{(i-j)} h_m(\mathbf{r}) h_n(\mathbf{r}') \frac{P_l(\hat{R})}{4\pi R} dS' dS, \quad (5.63)$$

where the temporal convolutions are contained in

$$\xi_l^{(i-j)} = \int_{-\infty}^{\infty} P_l(k_1 t' + k_2) T\big((i-j)\Delta t - \zeta/c - t'\big) dt' \quad (5.64)$$

$$\dot{\xi}_l^{(i-j)} = \int_{-\infty}^{\infty} P_l(k_1 t' + k_2) \dot{T}\big((i-j)\Delta t - \zeta/c - t'\big) dt'. \quad (5.65)$$

In these equations, $\mathbf{f}_n$ is an RWG function associated with the nth interior edge, h_n is a pulse basis function associated with the nth triangle, and T is the temporal basis function. For this set of equations, the temporal basis function should be from $H_\sigma^{\frac{1}{2}}$ while the testing function should be from $H_\sigma^{-\frac{3}{2}}$. To satisfy this, a triangle function is used for the basis function and a Dirac delta function for testing. Other choices can be easily incorporated into

(5.64) and (5.65) if need be. Finally, the excitations may be calculated as

$$\dot{\boldsymbol{\alpha}}_m^{(i)} = \int_{S_m} \mathbf{f}_m(\mathbf{r}) \cdot \dot{\mathbf{A}}^{\text{inc}}(\mathrm{r}, i\Delta t) dS \tag{5.66}$$

$$\dot{\boldsymbol{\phi}}_m^{(i)} = \int_{T_m} h_m(\mathbf{r}) \dot{\Phi}^{\text{inc}}(\mathbf{r}, i\Delta t) dS. \tag{5.67}$$

5.5.3 Discreized Equations for the TD-APIE

The TD-APIE may be discretized in a manner similar to the TD-EFIE. The matrix system is

$$\begin{aligned}
\begin{bmatrix} \mu\mathbf{V}^{(0)} & \mathbf{D}^T\hat{\mathbf{S}}^{(0)} \\ \hat{\mathbf{S}}^{(0)}\mathbf{D} & -\epsilon\mathbf{S}^{(0)} \end{bmatrix} \begin{Bmatrix} \mathbf{J}^{(i)} \\ \boldsymbol{\psi}^{(i)} \end{Bmatrix} &= \begin{Bmatrix} -\boldsymbol{\alpha}^{(i)} \\ \epsilon\boldsymbol{\phi}^{(i)} \end{Bmatrix} \\
&- \sum_{j=i-j_{max}}^{i-1} \begin{bmatrix} \mu\mathbf{V}^{(i-j)} & \mathbf{D}^T\hat{\mathbf{S}}^{(i-j)} \\ \hat{\mathbf{S}}^{(i-j)}\mathbf{D} & -\epsilon\mathbf{S}^{(i-j)} \end{bmatrix} \begin{Bmatrix} \mathbf{J}^{(j)} \\ \boldsymbol{\psi}^{(j)} \end{Bmatrix} \\
&- \sum_{i-j_{\max}-1}^{i-p-1} \begin{bmatrix} \mathbf{0} & \mathbf{D}^T\hat{\mathbf{S}}_T^{(i-j)} \\ \hat{\mathbf{S}}_T^{(i-j)}\mathbf{D} & \mathbf{0} \end{bmatrix} \begin{Bmatrix} \mathbf{C}_{\mathbf{J}}^{(j+1)} \\ \mathbf{C}_{\boldsymbol{\psi}}^{(j+1)} \end{Bmatrix}.
\end{aligned} \tag{5.68}$$

The different matrix elements are defined as

$$\mathbf{V}_{mn}^{(i-j)} = \int_{S_m}\int_{S_n} \sum_{l=0}^{N_h} a_l \xi_l^{(i-j)} \mathbf{f}_m(\mathbf{r}) \cdot \mathbf{f}_n(\mathbf{r}') \frac{P_l(\hat{R})}{4\pi R} dS' dS \tag{5.69}$$

$$\mathbf{S}_{mn}^{(i-j)} = \int_{T_m}\int_{T_n} \sum_{l=0}^{N_h} a_l \xi_l^{(i-j)} h_m(\mathbf{r}) h_n(\mathbf{r}') \frac{P_l(\hat{R})}{4\pi R} dS' dS \tag{5.70}$$

$$\hat{\mathbf{S}}_{mn}^{(i-j)} = \int_{T_m}\int_{T_n} \sum_{l=0}^{N_h} a_l \tilde{\xi}_l^{(i-j)} h_m(\mathbf{r}) h_n(\mathbf{r}') \frac{P_l(\hat{R})}{4\pi R} dS' dS \tag{5.71}$$

$$\hat{\mathbf{S}}_{T,mn}^{(i-j)} = \int_{T_m}\int_{T_n} \sum_{l=0}^{N_h} a_l \bar{\xi}_l^{(i-j)} h_m(\mathbf{r}) h_n(\mathbf{r}') \frac{P_l(\hat{R})}{4\pi R} dS' dS. \tag{5.72}$$

The temporal integrals are given by

$$\xi_l^{(i-j)} = \int_{-\infty}^{\infty} P_l(k_1 t' + k_2) T\big((i-j)\Delta t - \zeta/c - t'\big) dt' \tag{5.73}$$

$$\tilde{\xi}_l^{(i-j)} = \int_{-\infty}^{\infty} P_l(k_1 t' + k_2) \int_{-\infty}^{\kappa - t'} T(t'') dt'' dt', \text{ for } \kappa/\Delta t - \beta \leq p \tag{5.74}$$

$$\bar{\xi}_l^{(i-j)} = \delta_{l0}\beta\Delta t, \text{ for } p \leq \kappa/\Delta t - \beta \leq (p+1), \tag{5.75}$$

where $\kappa = (i-j)\Delta t - \zeta/c$ and the support of T is $[-\Delta t, p\Delta t]$. More details related to evaluating these matrix elements can be found in Section 2.4. The vector for the recursive computation is calculated as

$$\begin{Bmatrix} \mathbf{C}_{\mathbf{J}}^{(j+1)} \\ \mathbf{C}_{\boldsymbol{\psi}}^{(j+1)} \end{Bmatrix} = \begin{Bmatrix} \mathbf{C}_{\mathbf{J}}^{(j)} \\ \mathbf{C}_{\boldsymbol{\psi}}^{(j)} \end{Bmatrix} + \begin{Bmatrix} \mathbf{J}^{(j)} \\ \boldsymbol{\psi}^{(j)} \end{Bmatrix} \int_{-\infty}^{\infty} T(t'') dt'', \; \begin{Bmatrix} \mathbf{C}_{\mathbf{J}}^{(1)} \\ \mathbf{C}_{\boldsymbol{\psi}}^{(1)} \end{Bmatrix} = \begin{Bmatrix} \mathbf{0} \\ \mathbf{0} \end{Bmatrix}. \tag{5.76}$$

Finally, the excitations may be calculated as

$$\boldsymbol{\alpha}_m^{(i)} = \int_{S_m} \mathbf{f}_m(\mathbf{r}) \cdot \mathbf{A}^{\text{inc}}(\mathrm{r}, i\Delta t) dS \tag{5.77}$$

$$\boldsymbol{\phi}_m^{(i)} = \int_{T_m} h_m(\mathbf{r}) \Phi^{\text{inc}}(\mathbf{r}, i\Delta t) dS. \tag{5.78}$$

For this set of equations, the temporal basis functions should be from $H_\sigma^{\frac{1}{2}}$ while the testing function should be from $H_\sigma^{-\frac{5}{2}}$. As discussed Section 5.5.1, the MOT procedure cannot be directly applied for these basis and testing spaces. Instead, it is applied to a basis function from $H_\sigma^{-\frac{1}{2}}$. In particular, a pulse basis function is used (i.e. it is constant from $[-\Delta t, \Delta t]$).

5.6 Numerical Results

In this section, a few numerical results are presented to highlight the stability of the TD-APIE and differentiated TD-APIE. Another simulation is also performed to demonstrate the accuracy of both formulations when the TD-EFIE is inaccurate due to low frequency effects.

Eigenvalue stability analyses are shown for two different simulations using the TD-APIE and differentiated TD-APIE, in Figs. 5.2 and 5.3, respectively. Modifications to the companion matrix are needed to perform an eigenvalue

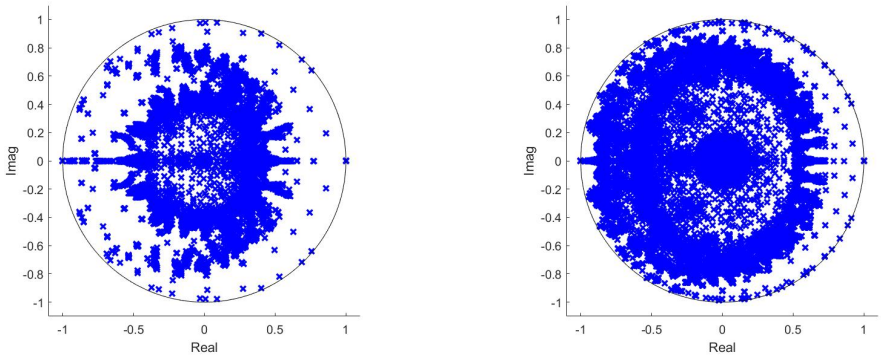

(a) (b)

Figure 5.2: Eigenvalues from the stability analysis for the TD-APIE with center frequencies of (a) 30 MHz and (b) 80 MHz.

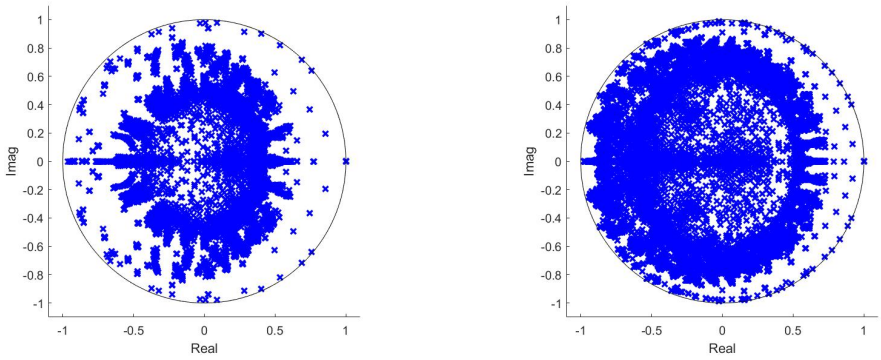

(a) (b)

Figure 5.3: Eigenvalues from the stability analysis for the differentiated TD-APIE with center frequencies of (a) 30 MHz and (b) 80 MHz.

stability analysis for the TD-APIE, however, details are presented in [22]. Both simulations are for a 1 meter radius PEC sphere that has been used in past demonstrations. The first simulation has a center frequency of 30 MHz, a bandwidth of 29 MHz, and a time step of 0.847 ns. The second simulation has a center frequency of 80 MHz, a bandwidth of 20 MHz, and a time step of 0.5 ns. The eigenvalues demonstrate that both simulations are stable. This is comparable stability to that seen using the TD-EFIE or differentiated TD-EFIE, highlighting the improvements of the proposed method compared to past A-Φ implementations. In similarity with the TD-EFIE and differentiated TD-EFIE, it is seen that the differentiated TD-APIE system also has a DC null space corresponding to the group of eigenvalues

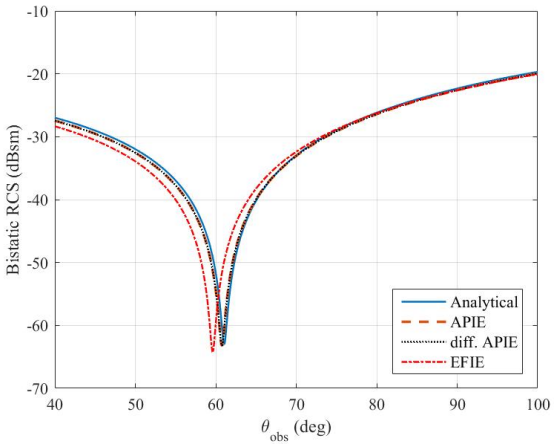

Figure 5.4: Bistatic RCS of a 1 m PEC sphere in the E-plane at 10 MHz. Calculations are performed with the Mie series, TD-APIE, differentiated TD-APIE, and TD-EFIE.

near $(1, 0i)$ (in Fig. 5.3).

The TD-APIE system has groups of eigenvalues at $(1, 0i)$ and $(-1, 0i)$, however, it is not anticipated that these are due to null spaces in the operator. Instead, it is believed that they are due to the temporal integrals in the operators. Due to these temoral integrals, it is not possible for the solution to decay completely to zero. This leads to the eigenvalues on the unit circle.

Similar results for stability have also been achieved with the TD-WC-EFIE formulation presented in Corollary 1. The results are not presented here for brevity. It is noted that the discrete system is effectively identical to the differentiated TD-APIE, making the results redundant.

Another simulation was performed for a 1 meter radius PEC sphere. For all formulations, the center frequency of the pulse was 40 MHz, the bandwidth was 40 MHz, and the time step was 0.3125 ns. The RCS results for each method are shown in Fig. 5.4. The accuracy for both the TD-APIE and differentiated TD-APIE are good. The TD-EFIE is inaccurate due to the low frequency breakdown of the operator.

CHAPTER 6

CONCLUSIONS AND FUTURE WORK

Emerging applications in the realm of quantum physics require the development of new computational electromagnetic solvers due to the limitations of conventional approaches. These limitations were discussed in detail, and a variety of methods that have been developed to overcome them in both the frequency and time domains were discussed. One of the particularly promising approaches discussed was the **A**-Φ formulation. This method does not exhibit the same low frequency breakdown phenomena of the traditional approaches. Further, because the **A** and Φ are considered more fundamental quantities in quantum physics, this formulation is ideally suited for coupling into calculations related to the emerging applications discussed.

The **A**-Φ formulation has been previously implemented successfully for a number of different computational methods. To further extend the applicability of this formulation, the goal of this thesis was to develop a set of **A**-Φ TDIEs. Initial methods developed from this formulation were found to be highly unstable. A variety of alternative approaches were discussed to try and overcome this problem of instability. This thesis culminated in the development of a set of provably stable **A**-Φ TDIEs. This was done by adopting a rigorous functional framework developed for the TD-EFIE. By extending this framework, two sets of equations were developed that could be discretized consistently to yield stable systems. The necessary steps to discretize these equations were discussed in detail, and numerical results demonstrated the validity of the theoretical analysis.

There are a few possible directions for future work related to the **A**-Φ TDIEs. Although there has been a large amount of theoretical progress related to the formulation, there is still some needed extensions. The most pressing result that needs to be further analyzed is related to discretizing the TD-APIE. In particular, the validity of using basis functions from $H_\sigma^{-\frac{1}{2}}$ and testing functions from $H_\sigma^{-\frac{3}{2}}$ needs to be determined. Although it seemed to

work for a pulse basis function, it is still uncertain whether it will also work for higher-order basis functions. This is important to determine so that the accuracy of the method can be improved.

Another useful theoretical result would be to extend the stability results of the **A**-Φ TDIEs to the TD-MFIE. It is well known within the engineering literature that the TD-MFIE is easier to stabilize than the TD-EFIE. However, the mathematical literature seems to not necessarily reflect this, and discourages the use of equations like the TD-MFIE [50, 52]. Since the MFIE can be derived from the **A**-Φ equations [14], the functional framework of the **A**-Φ TDIEs should be able to be extended to the TD-MFIE. This would be useful to make explicit the domain and range of the integral operators used in the TD-MFIE, as well as to close the gap between theory and practice (i.e., practice shows the equations are stable, but theory does not clearly show this yet).

An additional development that is needed is to extend this formulation to penetrable materials. The **A**-Φ TDIEs presented in this thesis can only be applied to PEC structures. As with the **E**-**H** formulation, penetrable scatterers require additional unknowns and equations [16]. As a result, more equations are still needed to be derived to have **A**-Φ TDIEs that can be applied to penetrable scatterers. It is likely necessary for many interesting physics applications to be able to analyze penetrable scatterers. It is hoped that the functional framework discussed in this thesis can be extended to the necessary equations for the penetrable material case. This will greatly aid in determining what equations should be used, and what basis and testing functions are appropriate.

The next main direction for future work is to begin coupling the **A**-Φ TDIEs into multiphysics calculations. One of the easiest multiphysics applications to use this in would be a Maxwell-Schrödinger system [9]. Another area that it could be used in would be atom-photon interactions [3, 10]. This requires adjusting the method so that the dyadic Green's function may be extracted from the simulation results. Once this has been accomplished, the time domain results could also be used to determine the changes in the stimulated emission rate for emitters in arbitrary electromagnetic environments over a broad bandwidth [11].

Another possible application would be for Casimir force calculations [4, 5]. To the author's knowledge, methods in the time domain for calculating

the Casimir force have relied on the use of the finite-difference time-domain method [6, 7]. There are many advantages that can be had by using TDIEs over finite-difference time-domain codes; making this another interesting area where the **A**-Φ TDIEs could be applied.

Once the **A**-Φ TDIEs have been extended to be able to calculate the Maxwell stress tensor for the Casimir force calculations, another possible application is related to optical tweezers [1]. This application is not necessarily quantum in nature, but the subwavelength nature of the typical interactions still makes the **E**-**H** formulation a poor approach.

Clearly, this work can still be extended in a large number of exciting directions. It is hoped that the breadth of possible applications for this method continues to lead to fruitful work in the future.

REFERENCES

[1] W. C. Chew, "Vector potential electromagnetics with generalized gauge for inhomogeneous media: Formulation," *Progress In Electromagnetics Research*, vol. 149, pp. 69–84, 2014.

[2] M. Fox, *Quantum Optics: An Introduction*. Oxford University Press, 2006, vol. 15.

[3] C. Cohen-Tannoudji, J. Dupont-Roc, and G. Grynberg, *Atom-Photon Interactions: Basic Processes and Applications*. Wiley, 1992.

[4] A. W. Rodriguez, F. Capasso, and S. G. Johnson, "The Casimir effect in microstructured geometries," *Nature Photonics*, vol. 5, no. 4, pp. 211–221, 2011.

[5] J. L. Xiong, M. S. Tong, P. Atkins, and W. C. Chew, "Efficient evaluation of Casimir force in arbitrary three-dimensional geometries by integral equation methods," *Physics Letters A*, vol. 374, no. 25, pp. 2517–2520, 2010.

[6] A. W. Rodriguez, A. P. McCauley, J. D. Joannopoulos, and S. G. Johnson, "Casimir forces in the time domain: Theory," *Physical Review A*, vol. 80, no. 1, p. 012115, 2009.

[7] A. P. McCauley, A. W. Rodriguez, J. D. Joannopoulos, and S. G. Johnson, "Casimir forces in the time domain: Applications," *Physical Review A*, vol. 81, no. 1, p. 012119, 2010.

[8] W. C. Chew, A. Y. Liu, C. Salazar-Lazaro, and W. E. I. Sha, "Quantum electromagnetics: A new look–Part I," *IEEE Journal on Multiscale and Multiphysics Computational Techniques*, vol. 1, pp. 73–84, 2016.

[9] C. J. Ryu, A. Y. Liu, W. E. I. Sha, and W. C. Chew, "Finite-difference time-domain simulation of the Maxwell–Schrödinger system," *IEEE Journal on Multiscale and Multiphysics Computational Techniques*, vol. 1, pp. 40–47, 2016.

[10] A. Y. Liu and W. C. Chew, "Dressed atom fields and dressed states in waveguide quantum electrodynamics," under review, 2017.

[11] P.-f. Qiao, W. E. I. Sha, W. C. H. Choy, and W. C. Chew, "Systematic study of spontaneous emission in a two-dimensional arbitrary inhomogeneous environment," *Physical Review A*, vol. 83, no. 4, p. 043824, 2011.

[12] F. P. Andriulli, A. Tabacco, and G. Vecchi, "Solving the EFIE at low frequencies with a conditioning that grows only logarithmically with the number of unknowns," *IEEE Transactions on Antennas and Propagation*, vol. 58, no. 5, pp. 1614–1624, 2010.

[13] Y.-L. Li, S. Sun, Q. I. Dai, and W. C. Chew, "Finite element implementation of the generalized-Lorenz gauged A-Φ formulation for low-frequency circuit modeling," *IEEE Transactions on Antennas and Propagation*, vol. 64, no. 10, pp. 4355–4364, 2016.

[14] Q. S. Liu, S. Sun, and W. C. Chew, "A potential based integral equation method for low-frequency electromagnetic problems," under review, 2017.

[15] E. van't Wout, D. R. van der Heul, H. van der Ven, and C. Vuik, "Stability analysis of the marching-on-in-time boundary element method for electromagnetics," *Journal of Computational and Applied Mathematics*, vol. 294, pp. 358–371, 2016.

[16] J.-M. Jin, *Theory and Computation of Electromagnetic Fields*. John Wiley & Sons, 2011.

[17] S. Rao, D. Wilton, and A. Glisson, "Electromagnetic scattering by surfaces of arbitrary shape," *IEEE Transactions on Antennas and Propagation*, vol. 30, no. 3, pp. 409–418, 1982.

[18] E. van't Wout, D. R. van der Heul, H. van der Ven, and C. Vuik, "Design of temporal basis functions for time domain integral equation methods with predefined accuracy and smoothness," *IEEE Transactions on Antennas and Propagation*, vol. 61, no. 1, pp. 271–280, 2013.

[19] P. Wang, M. Xia, J. Jin, and L. Zhou, "Time-domain integral equation solvers using quadratic B-spline temporal basis functions," *Microwave and Optical Technology Letters*, vol. 49, no. 5, pp. 1154–1159, 2007.

[20] H. A. Ülkü and A. A. Ergin, "Application of analytical retarded-time potential expressions to the solution of time domain integral equations," *IEEE Transactions on Antennas and Propagation*, vol. 59, no. 11, pp. 4123–4131, 2011.

[21] B. Shanker, M. Lu, J. Yuan, and E. Michielssen, "Time domain integral equation analysis of scattering from composite bodies via exact evaluation of radiation fields," *IEEE Transactions on Antennas and Propagation*, vol. 57, no. 5, pp. 1506–1520, 2009.

[22] A. J. Pray, N. V. Nair, and B. Shanker, "Stability properties of the time domain electric field integral equation using a separable approximation for the convolution with the retarded potential," *IEEE Transactions on Antennas and Propagation*, vol. 60, no. 8, pp. 3772–3781, 2012.

[23] P. Yla-Oijalä and M. Taskinen, "Calculation of CFIE impedance matrix elements with RWG and n×RWG functions," *IEEE Transactions on Antennas and Propagation*, vol. 51, no. 8, pp. 1837–1846, 2003.

[24] M. Burton and S. Kashyap, "A study of a recent, moment-method algorithm that is accurate to very low frequencies," *Applied Computational Electromagnetics Society Journal*, vol. 10, pp. 58–68, 1995.

[25] G. Vecchi, "Loop-star decomposition of basis functions in the discretization of the EFIE," *IEEE Transactions on Antennas and Propagation*, vol. 47, no. 2, pp. 339–346, 1999.

[26] W.-L. Wu, A. W. Glisson, and D. Kajfez, "A study of two numerical solution procedures for the electric field integral equation at low frequency," *Applied Computational Electromagnetics Society Journal*, vol. 10, no. 3, pp. 69–80, 1995.

[27] J.-S. Zhao and W. C. Chew, "Integral equation solution of Maxwell's equations from zero frequency to microwave frequencies," *IEEE Transactions on Antennas and Propagation*, vol. 48, no. 10, pp. 1635–1645, 2000.

[28] Z.-G. Qian and W. C. Chew, "Fast full-wave surface integral equation solver for multiscale structure modeling," *IEEE Transactions on Antennas and Propagation*, vol. 57, no. 11, pp. 3594–3601, 2009.

[29] F. P. Andriulli, F. Vipiana, and G. Vecchi, "Hierarchical bases for non-hierarchic 3-D triangular meshes," *IEEE Transactions on Antennas and Propagation*, vol. 56, no. 8, pp. 2288–2297, 2008.

[30] F. P. Andriulli, K. Cools, H. Bağci, F. Olyslager, A. Buffa, S. Christiansen, and E. Michielssen, "A multiplicative Calderón preconditioner for the electric field integral equation," *IEEE Transactions on Antennas and Propagation*, vol. 56, no. 8, pp. 2398–2412, 2008.

[31] M. Benzi, G. H. Golub, and J. Liesen, "Numerical solution of saddle point problems," *Acta Numerica*, vol. 14, pp. 1–137, 2005.

[32] J. Cheng, R. J. Adams, J. C. Young, and M. A. Khayat, "Augmented EFIE with normally constrained magnetic field and static charge extraction," *IEEE Transactions on Antennas and Propagation*, vol. 63, no. 11, pp. 4952–4963, 2015.

[33] N.-W. Chen, K. Aygun, and E. Michielssen, "Integral-equation-based analysis of transient scattering and radiation from conducting bodies at very low frequencies," *IEE Proceedings-Microwaves, Antennas and Propagation*, vol. 148, no. 6, pp. 381–387, 2001.

[34] F. P. Andriulli, H. Bağcı, F. Vipiana, G. Vecchi, and E. Michielssen, "Analysis and regularization of the TD-EFIE low-frequency breakdown," *IEEE Transactions on Antennas and Propagation*, vol. 57, no. 7, pp. 2034–2046, 2009.

[35] Y. Beghein, K. Cools, and F. P. Andriulli, "A DC stable and large-time step well-balanced TD-EFIE based on quasi-Helmholtz projectors," *IEEE Transactions on Antennas and Propagation*, vol. 63, no. 7, pp. 3087–3097, 2015.

[36] K. Cools, F. P. Andriulli, F. Olyslager, and E. Michielssen, "Time domain Calderón identities and their application to the integral equation analysis of scattering by PEC objects Part I: Preconditioning," *IEEE Transactions on Antennas and Propagation*, vol. 57, no. 8, pp. 2352–2364, 2009.

[37] F. P. Andriulli, K. Cools, F. Olyslager, and E. Michielssen, "Time domain Calderón identities and their application to the integral equation analysis of scattering by PEC objects Part II: Stability," *IEEE Transactions on Antennas and Propagation*, vol. 57, no. 8, pp. 2365–2375, 2009.

[38] X. Tian and G. Xiao, "Time-domain augmented electric field integral equation for a robust marching on in time solver," *IET Microwaves, Antennas & Propagation*, vol. 8, no. 9, pp. 688–694, 2014.

[39] M. M. Jia, Y. W. Zhao, and S. Sun, "Analysis and stabilization of the low-frequency time-domain augmented EFIE," *IEEE Antennas and Wireless Propagation Letters*, vol. 15, pp. 1751–1754, 2016.

[40] M. M. Jia, Y. W. Zhao, and S. Sun, "Time domain augmented EFIE based on numerical convolution technique," in *2015 IEEE International Symposium on Antennas and Propagation & USNC/URSI National Radio Science Meeting*. IEEE, 2015, pp. 1158–1159.

[41] M. M. Jia, Y. W. Zhao, H. L. Mao, and L. W. Zhao, "Stability properties of the MOT based time domain augmented electric field integral equation in solving low frequency problems," in *2015 IEEE 4th Asia-Pacific Conference on Antennas and Propagation (APCAP)*. IEEE, 2015, pp. 413–414.

[42] S. Walker, M. Bluck, and I. Chatzis, "The stability of integral equation time-domain scattering computations for three-dimensional scattering; similarities and differences between electrodynamic and elastodynamic computations," *International Journal of Numerical Modelling: Electronic Networks, Devices and Fields*, vol. 15, no. 5-6, pp. 459–474, 2002.

[43] R. S. Varga, *Geršgorin and His Circles*. Springer Science & Business Media, 2010, vol. 36.

[44] P. J. Davies and D. B. Duncan, "Averaging techniques for time-marching schemes for retarded potential integral equations," *Applied Numerical Mathematics*, vol. 23, no. 3, pp. 291–310, 1997.

[45] A. J. Pray, Y. Beghein, N. V. Nair, K. Cools, H. Bağcı, and B. Shanker, "A higher order space-time Galerkin scheme for time domain integral equations," *IEEE Transactions on Antennas and Propagation*, vol. 62, no. 12, pp. 6183–6191, 2014.

[46] Q. He, H. Gan, and D. Jiao, "Explicit time-domain finite-element method stabilized for an arbitrarily large time step," *IEEE Transactions on Antennas and Propagation*, vol. 60, no. 11, pp. 5240–5250, 2012.

[47] M. M. Jia, Y. W. Zhao, Y. Li, and S. Sun, "Study of late time stability for marching on-in-time solution of TDIE," in *2014 IEEE Antennas and Propagation Society International Symposium (APSURSI)*. IEEE, 2014, pp. 1905–1906.

[48] Y. Beghein, K. Cools, and D. De Zutter, "A temporal Galerkin discretization of the charge-current continuity equation," in *2013 International Conference on Electromagnetics in Advanced Applications (ICEAA)*. IEEE, 2013, pp. 628–631.

[49] W. C. Chew, *Waves and Fields in Inhomogeneous Media*. IEEE Press, 1995.

[50] T. Ha-Duong, "On retarded potential boundary integral equations and their discretisation," in *Topics in Computational Wave Propagation*. Springer, 2003, pp. 301–336.

[51] I. Terrasse, "Résolution mathématique et numérique des équations de Maxwell instationnaires par une méthode de potentiels retardés," Ph.D. dissertation, 1993.

[52] A. Bachelot, L. Bounhoure, and A. Pujols, "Couplage éléments finis-potentiels retardés pour la diffraction électromagnétique par un obstacle hétérogène," *Numerische Mathematik*, vol. 89, no. 2, pp. 257–306, 2001.

[53] Y. Beghein, K. Cools, H. Bagci, and D. De Zutter, "A space-time mixed Galerkin marching-on-in-time scheme for the time-domain combined field integral equation," *IEEE Transactions on Antennas and Propagation*, vol. 61, no. 3, pp. 1228–1238, 2013.

[54] E. van't Wout, H. van der Ven, D. R. van der Heul, and C. Vuik, "A provably stable MoT scheme based on quadratic spline basis functions," in *Proceedings of the 2012 IEEE International Symposium on Antennas and Propagation*. IEEE, 2012, pp. 1–2.

[55] K. Cools, F. P. Andriulli, and E. Michielssen, "A Calderón multiplicative preconditioner for the PMCHWT integral equation," *IEEE Transactions on Antennas and Propagation*, vol. 59, no. 12, pp. 4579–4587, 2011.

[56] G. C. Hsiao and R. E. Kleinman, "Mathematical foundations for error estimation in numerical solutions of integral equations in electromagnetics," *IEEE Transactions on Antennas and Propagation*, vol. 45, no. 3, pp. 316–328, 1997.